Patrick Joel da Silva

Machado-Joseph Disease: Understanding Epidemiological and Clinical Features and a Potential New Therapeutic Entity

Dissertação para obtenção ao grau de Mestre em Farmacologia Aplicada sob a orientação da Professora Doutora Cláudia Cavadas e do Professor Doutor Luís Pereira de Almeida e apresentada à Faculdade de Farmácia da Universidade de Coimbra

Setembro 2017

· U C ·

Universidade de Coimbra

Machado-Joseph Disease: Understanding Epidemiologic and Clinical Features and a Potential New Therapeutic Entity

Patrick Joel da Silva

Dissertação para obtenção ao grau de Mestre em Farmacologia Aplicada sob a orientação da Professora Doutora Cláudia Cavadas e do Professor Doutor Luís Pereira de Almeida e apresentada à Faculdade de Farmácia da Universidade de Coimbra

Setembro, 2017

UNIVERSIDADE DE COIMBRA

O trabalho aqui apresentado foi realizado nos grupos de investigação *Neuroendocrinologia e Envelhecimento* e *Vetores e Terapia Génica*, ambos do CNC - Centro de Neurociências e Biologia Celular (Universidade de Coimbra, Portugal), liderados respetivamente pela Professora Doutora Cláudia Cavadas e pelo Professor Doutor Luís Pereira de Almeida.

Este trabalho foi financiado pelo FEDER através do Programa Operacional Regional -Centro 2020, do Programa Operacional de Fatores de Competitividade (COMPETE 2020) e por Fundos Nacionais através da Fundação para a Ciência e a Tecnologia (FCT) – projetos BrainHealth2020 (CENTRO-01-0145-FEDER-000008), ViraVector (CENTRO-01-0145-FEDER-022095), CortaCAGs (POCI-01-0145-FEDER-016719 e POCI-01-0145-FEDER-007440), bem como pelos projetos EXPL/NEU-NMC/0331/2012 (FCT) e pelos SynSpread, ESMI e ModelPolyQ, no âmbito do *EU Joint Programme - Neurodegenerative Disease Research* (JPND), os dois últimos cofinanciados pelo programa H2020 da União Europeia, GA No. 643417; ainda pela *National Ataxia Foundation* (USA), pelo *American Portuguese Biomedical Research Fund* (APBRF) e pelo *Richard Chin and Lily Lock Machado Joseph Disease Research Fund*.

The work presented here was carried out at the research groups *Group of Neuroendocrinology and Aging* and *Group of Vectors and Gene Therapy*, both of CNC - Center for Neuroscience and Cell Biology (University of Coimbra, Portugal), respectively headed by Professor Doctor Cláudia Cavadas and Professor Doctor Luís Pereira de Almeida.

This work was funded by the ERDF through the Regional Operational Program Center 2020, Competitiveness Factors Operational Program (COMPETE 2020) and National Funds through FCT (Foundation for Science and Technology) - BrainHealth2020 projects (CENTRO-01-0145-FEDER-000008), ViraVector (CENTRO-01-0145-FEDER-022095), CortaCAGs (POCI-01-0145-FEDER-016719 and POCI-01-0145-FEDER-007440), as well as the EXPL/NMC/0331/2012 (FCT) and the SynSpread, ESMI and ModelPolyQ under the EU Joint Program - Neurodegenerative Disease Research (JPND), the last two co-funded by the European Union H2020 program, GA No.643417; by National Ataxia Foundation (USA), the American Portuguese Biomedical Research Fund (APBRF) and the Richard Chin and Lily Lock Machado-Joseph Disease Research Fund.

Aos meus pais.

Boas pessoas são aquelas que se colocam em último,
que renunciam às próprias tentações e necessidades,
dedicando-se unicamente em prol dos interesses de outros.

Adaptado de ***The Young Pope***.

Agradecimentos

À Professora Doutora Cláudia Cavadas por, desde logo, me ter dado a oportunidade de integrar o seu grupo de investigação e de desenvolver este trabalho. Pela voz de incentivo que nunca fez cessar, pela confiança e pela ajuda que sempre disponibilizou, facilitando a ultrapassar todas as dificuldades que se foram revelando ao longo do ano. Não podia deixar de realçar o quanto a sua alegria e boa disposição é capaz de influenciar o estado de espírito de quem a acompanha: obrigado por isso, por mostrar que todos os momentos difíceis, com o devido ânimo, podem ser ultrapassados.

Ao Professor Doutor Luís Almeida por me integrar no seu grupo de investigação e ter acreditado nas minhas capacidades. Por arranjar sempre tempo para responder a toda e qualquer dúvida e intermitência que foram surgindo ao longo do trabalho; certamente aprendi muito consigo ao longo deste ano. Por fim, agradecer o facto de em todos os momentos ter a palavra certa, de amizade e motivação, a dar, capaz sempre de impulsionar o espírito mesmo nos dias mais difíceis.

À Janete que me acompanhou desde sempre e sem a qual este trabalho nunca teria chegado a bom porto. Pela tua dedicação, pelos ensinamentos, pela disponibilidade, mesmo depois de abandonares o Centro. Pela compreensão, por acreditares e me fazeres acreditar e, acima de tudo, pelo carinho e amizade com que sempre me cuidaste.

Aos amigos que fiz no grupo de *Neuroendocrionologia e Envelhecimento* que foram, todos sem exceção, infinitamente recetivos desde o primeiro dia. Que prazer ter-vos conhecido e poder conviver convosco todos os dias. Em especial, agradecer à Marisa, à Magda, à Célia, à Laetitia e à Sara que sempre estiveram disponíveis para ajudar com o que quer que fosse, e que, inclusivamente, contribuíram ativamente neste trabalho.

A todos os elementos do grupo de *Vetores e Terapia Génica* pela amizade e acessibilidade que sempre demonstraram.

À Joana que foi, com toda a certeza, a pessoa mais tolerante e compreensiva para comigo durante este ano (não que os restantes tenham sido pouco). Pela orientação e pela dedicação. Foi muito bom aprender tantas coisas, em tão pouco tempo contigo, e sempre com tão boa disposição.

À Vera, em particular, pela ajuda e contribuição na realização do trabalho, e a todas as restantes meninas - a Sandra, a Cátia e a Margarida - do grupo de *Life Sciences and Mass*

Spectrometry, que sempre foram atenciosas comigo. Não posso esquecer o Doutor Bruno Manadas que desde o primeiro dia se mostrou disponível a ajudar.

A todos os amigos de Coimbra que me foram acompanhando ao longo destes cinco anos de percurso académico, com altos e baixos, mas que sempre estiveram presentes. Aquilo que sou hoje devo-o em grande parte a todos vós, com quantos me cruzei, convivi e partilhei tantos e tantos momentos enriquecedores e verdadeiramente inesquecíveis.

Aos amigos da Tremoceira, que espacialmente longe ou perto, estão sempre presentes na minha vida. São absolutamente infalíveis e tenho muito orgulho desta amizade que nos une, que nasceu no berço e não mais morrerá.

À Juliana, claro, que com a sua força mental me manteve sempre ciente de que tudo é possível de alcançar. Por seres tão paciente e perseverante durante este período e pelo apoio incondicional que sempre me deste e dás.

Ao Edgar, que consegue ser irmão e melhor amigo. Por seres o modelo perfeito a seguir. Por teres uma determinação que é exemplo para qualquer pessoa e aliares isso a uma humildade e simplicidade inigualável. Por tudo o que me dás a cada singelo dia de convivência partilhada. Esta tese é em grande parte tua.

Aos meus pais, os verdadeiros obreiros de tudo isto. Por tudo aquilo que são e por tudo aquilo que dão. Pelos valores que me incutiram e fizeram de mim a pessoa que sou hoje. Tenho muito orgulho nos dois, como sei que têm em mim.

A todos os que mencionei e a todos quantos a minha memória possa ter omitido, um sincero MUITO OBRIGADO.

Table of Contents

List of Acronyms

9HP	9-hole peg test
ACN	Acetonitrile
ADL	Activities of daily living
AO	Age of onset
BDNF	Brain-derived neurotrophic factor
BW	Body weight
CAG	Cytosine-guanine-adenosine trinucleotide
CCFS	Composite cerebellar functional severity score
CNS	Central nervous system
DH	Dominant hand
DRPLA	Dentatorubral-pallidoluysian atrophy
DS	Disease stage
DUB	Deubiquitinating
EQ-5D-3L	EuroQol 5-dimension 3-level version
EQ-VAS	EuroQol visual analogue scale
FA	Formic acid
Hb	Haemoglobin
HD	Huntington's disease
HSA	Human serum albumin
HSP	Hereditary spastic paraplegia
I.P.	Intraperitoneal
INAS	Inventory of non-ataxia signs
IS	Internal standard
JD	Josephin domain
LC	Liquid chromatography
LOX	Lipoxygenase
M/Z	Mass-to-charge ratio
MJD	Machado-Joseph disease

MMP	Matrix metalloproteinase
MoCA	Montreal cognitive assessment
MRM	Multiple reaction monitoring
mRNA	Messenger RNA
NDH	Non-dominant hand
NES	Nuclear export signal
NLS	Nuclear localization signal
PGC-1α	Peroxisome proliferator-activated receptor gamma coactivator 1-alpha
PHQ-9	Patient's health questionnaire
PolyQ	Polyglutamine
PSQI	Pittsburgh sleep quality index
PTGS	Prostaglandin-endoperoxidase synthase
Q	Glutamine
ROS	Reactive oxygen species
RT	Retention time
SARA	Scale for the assessment and rating of ataxia
SBMA	Spinal and bulbar muscular atrophy
SCA	Spinocerebellar ataxia
SCA3	Spinocerebellar ataxia type 3
SCAFI	SCA functional index
SIRT	Sirtuin
STAC	Sirtuin-activating compounds
Ub	Ubiquitin
UIM	Ubiquitin-interacting motifs
UPS	Ubiquitin-proteasome system

List of Figures

CHAPTER 1: Introduction

CHAPTER 2: Epidemiologic and Clinical Characterization of MJD Patients

CHAPTER 3: Pharmacokinetic Characterization of Resveratrol in Plasma and Brain Tissue of Mice

List of Tables

CHAPTER 1 – Introduction

CHAPTER 2 – Epidemiologic and Clinical Characterization of MJD Patients

CHAPTER 3 – Pharmacokinetic Characterization of Resveratrol in Plasma and Brain Tissue of Mice

Abstract

Machado-Joseph disease (MJD), also known as spinocerebellar ataxia type 3, is a rare neurodegenerative disease. Among all autosomal dominantly inherited ataxias, it is the most frequent one, globally affecting 1.5 per 10^5 individuals. MJD is determined by an abnormal number of repeats of the CAG trinucleotide (above a threshold of 55 repeats) in the coding region of the causative gene, *ATXN3*, causing the resulting protein, ataxin-3, to contain a toxic polyglutamine expanded tract that triggers a series of pathogenic mechanisms, leading to a progressive neurodegeneration of several brain regions, particularly the cerebellum. The number of the CAG trinucleotide repeats is determinant for the age of onset of the first symptoms – usually gait ataxia, – as well as for progression and severity of disease. Other signs and symptoms, such as dysmetria, dysphagia, dysarthria, nystagmus and ophthalmoparesis/ophthalmoplegia, among others, are also frequent in patients with MJD, contributing to a gradual deterioration of their quality of life. Presently, there is no therapy instituted to cure or even slow the progression of this fatal disease.

The general purpose of this thesis was to narrow the gap between the disease and a possible therapy, creating a groundwork for further and more in-depth works to explore its application in MJD patients.

First, we studied a group of MJD patients, from which we evaluated epidemiological, clinical and psychological variables, taking advantage of scales and questionnaires, in order to obtain a standardized characterization for future clinical studies. Results here presented confirm that cerebellar function is highly compromised in these patients, being also verified a high frequency of oculomotor symptoms and pyramidal signs. With this work, it was possible to characterize a cohort of patients that may constitute a relevant group for a future clinical trial designed for the evaluation of a novel therapeutic approach to MJD.

Second, we performed a preclinical study in mice with the goal of further understanding how systemic and cerebral concentration levels of a compound and its major metabolites, which had previously been shown to be effective in a MJD mouse model, evolved. Results show that the compound, administered intraperitoneally, is rapidly metabolized, being found at low systemic concentrations shortly after administration. Additionally, and contrarily to its metabolites, concentration levels in brain tissue decreased rapidly, even failing to be detected 30 minutes after administration. Thence, further studies are required toward finding the best formulation and route of administration for the

compound here explored, so that it can be established as a new therapeutic approach for MJD.

Resumo

A doença de Machado-Joseph (DMJ), também conhecida por ataxia espinocerebelosa do tipo 3, é uma doença neurodegenerativa rara. De entre todas as ataxias autossómicas dominantes, é a mais frequente, afetando à escala global 1.5 a cada 10^6 indivíduos. A DMJ é determinada pela existência de um número anormal de repetições do trinucleotídeo CAG (acima de 55) na região codificante do gene causal, *ATXN3*, originando uma proteína resultante, ataxina-3, com um trato expandido de poliglutaminas tóxico que desencadeia uma série de mecanismos patogénicos, levando à neurodegenerescência progressiva de várias regiões do cérebro, nomeadamente o cerebelo. O número de repetições do trinucleotídeo CAG é determinante na idade de aparecimento dos primeiros sintomas – geralmente ataxia da marcha, – bem como na progressão e severidade da doença. Outros sinais e sintomas, como dismetria, disfagia, disartria, nistagmo e oftalmoparesia/oftalmoplegia, entre outros, são também frequentes nos doentes de DMJ, contribuindo para uma gradual deterioração da qualidade de vida destes. Presentemente, não existe nenhuma terapia instituída que permita curar ou mesmo retardar a progressão desta doença fatal.

Esta tese teve como objetivo geral estreitar a distância entre a doença e uma possível terapêutica, criando uma base para que outros trabalhos mais aprofundados possam explorar a sua aplicação em doentes da DMJ.

Em primeiro lugar, estudámos um grupo de doentes de DMJ, aos quais avaliámos variáveis epidemiológicas, clínicas e psicológicas, recorrendo a escalas e a questionários, de modo a obter uma caracterização padronizada para futuros estudos clínicos. Os resultados aqui apresentados confirmam que a função cerebelosa está altamente comprometida nos doentes, verificando-se também uma frequência elevada de sintomas oculomotores e sinais piramidais. Com este trabalho foi possível criar um coorte de doentes que podem constituir um grupo relevante para um futuro ensaio clínico desenhado para avaliar uma nova abordagem terapêutica para a DMJ.

Em segundo lugar, realizámos um estudo pré-clínico em murganhos com o objetivo de perceber como evoluem os níveis de concentração sistémicos e cerebrais de um composto, e dos seus principais metabolitos, que tinha sido previamente demonstrado ser eficaz num modelo de roedores de DMJ. Os resultados mostram que o composto, administrado por via intraperitoneal, é rapidamente metabolizado, encontrando-se em baixas concentrações sistémicas pouco tempo depois de administrado. Além disso, e

contrariamente aos seus metabolitos, os níveis de concentração no tecido cerebral decrescem rapidamente, deixando mesmo de ser detetado 30 minutos após administração. Por este motivo, novos estudos são necessários com o intuito de encontrar a melhor formulação e via de administração para o composto aqui explorado, de maneira a que se possa vir a estabelecer como uma nova abordagem terapêutica para a DMJ.

CHAPTER 1
Introduction

1.1 Spinocerebellar Ataxias

Spinocerebellar ataxias (SCA) are a wide and heterogeneous group of progressive neurodegenerative disorders, frequently with late onset, that, in some cases, can lead to total incapacitated states and, ultimately, be fatal. Few irregularities aside, SCAs are numbered according to the order of its genetic locus discovery (Storey, 2014).

All known SCAs result from mutations in specific and unrelated genes. Those mutations fall into four mechanisms: (1) exonic cytosine-adenosine-guanine (CAG) trinucleotide repeat, resulting in translated proteins with abnormally expanded polyglutamine (polyQ) tracts; (2) non-coding repeats; (3) point mutations and (4) large duplications or deletions (Storey, 2014).

As this work focuses on Machado-Joseph Disease (MJD), also referred to as SCA3, and considering that this specific disease is the outcome of an expanded CAG repeat, this thesis will further focus in the first mentioned mechanism resulting phenotypes, excluding all the others and respective SCAs.

1.1.1 Polyglutamine-Expanded Spinocerebellar Ataxias

PolyQ SCAs, similarly to the other three known polyQ diseases – Huntington's Disease (HD), Spinal and Bulbar Muscular Atrophy (SBMA) and Dentatorubral-Pallidoluysian Atrophy (DRPLA), – are caused by an abnormal expanded stretch of the coding CAG trinucleotide in a causative gene resulting in the translation of a mutant protein with an elongated glutamine tract (Zoghbi and Orr, 2000). To this date, six SCA phenotypes have been described exclusively resulting from this mutational mechanism: SCA1 (Orr et al., 1993), SCA2 (Imbert et al., 1996; Pulst et al., 1996; Sanpei et al., 1996), SCA3/MJD (Takiyama et al., 1993; Kawaguchi et al., 1994), SCA6 (Zhuchenko et al., 1997), SCA7 (Lindblad et al., 1996) and SCA17 (Nakamura et al., 2001). Besides polyglutamine tract expansion, gene products share no homology with each other. Detailed information about the involved genes and respective proteins, their endogenous functions, the number of normal and pathological CAG repeats, and also the prominently affected brain areas for each are provided in Table 1.1.1.

In order to become pathogenic, the glutamine tract has to reach a certain threshold of CAG repeats according to the respective affected gene (see Table 1.1.1). Beyond that

threshold, the number of repeats seems to determinate both age of onset, progression and severity of each condition. In this context, it is observed a significant inverse correlation between extension of the stretch and age of onset (Kawaguchi et al., 1994; Maruyama et al., 1995; Sasaki et al., 1995; Zoghbi and Orr, 2000). On the other hand, longer polyQ tracts are more toxic (or at least result in greater neuronal toxicity) leading to faster disease progression and more severe phenotypes, thus suggesting a positive correlation between the number of repeats and severity, while the same happens between number of repeats and rate of progression for each condition (Zoghbi and Orr, 2000).

Table 1.1.1 Features of polyQ expanded SCAs.

Disease	Gene	Coding protein	Putative endogenous function	CAG repeat		Prominently affected brain structures
				Normal	Pathological	
SCA1	ATXN1	Ataxin-1	Transcription regulator	6-44	39-91	Cerebellum and brainstem
SCA2	ATXN2	Ataxin-2	RNA transport, metabolism and translation regulator	13-32	32-500	Cerebellum, pons, medulla oblongata and spinal cord
MJD	ATXN3	Ataxin-3	Transcription regulator, DUB activity	10-51	55-89	Cerebellum and brainstem
SCA6	CACNA1A	Voltage-dependent P/Q-type calcium channel subunit alpha-1A	Calcium channel activity	3-20	20-33	Cerebellum
SCA7	ATXN7	Ataxin-7	Transcription regulator	4-35	36-460	Cerebellum and brainstem
SCA17	TBP	TATA-box-binding protein	Transcription regulator	25-44	47-63	Cerebellum

Data displayed in the table was consulted and adapted from Shao and Diamond, 2007; Seidel et al., 2012; Storey, 2014. Uniprot.org and omim.org online databases were also consulted.

Consensus on what lies between the glutamine expansion and the pathogenesis is yet to be reached. However, a multitude of altered mechanisms featured transversally in polyQ diseases have been observed and described, somehow brightening the understanding of these diseases. They are, as reviewed in (Shao and Diamond, 2007; Takahashi, Katada and Onodera, 2010; Weber et al., 2014): (1) aberrant protein conformation leading to a loss of endogenous functionality and increased propensity to aggregate and form insoluble

oligomeric structures; (2) generation of toxic proteolytic-cleavage resultant fragments of the expanded protein within the host cell; (3) interaction between mutant proteins and transcription factors, resulting in transcriptional perturbation; (4) mitochondrial dysfunction and impaired cell metabolism; (5) degradation of cellular protein quality control – both autophagy and proteasome system are impaired in polyQ diseases, resulting in proteotoxic stress; (6) dysregulation of intracellular Ca^{2+} homeostasis. Pathogenic mechanisms will be approached, in detail, in section 1.2.4, regarding MJD pathogenesis.

The formation of oligomeric mutant protein aggregates seems to be central in polyQ pathologies considering that it is commonly found in all of them, whether in cellular nuclei - SCA1, SCA7, SCA17, – in cytoplasm – SCA2, SCA6, – or in both – SCA3 (Gatchel and Zoghbi, 2005). Several studies have been aimed at identifying and understanding the precise content of aggregates and subjacent toxic mechanisms, once their role beyond disease pathogenicity still remains elusive. Additionally to the mutated proteins, these aggregates are also reported to sequester other cellular elements, namely components of the Ubiquitin-Proteasome System (UPS) and unspecific surrounding proteins (Wang et al., 2000; Donaldson et al., 2003). The loss of function of sequestered proteins may be a considerable mechanism leading to pathogenesis and neurodegeneration.

1.1.2 Machado-Joseph Disease

1.1.2.1 The ATXN3 Gene

MJD comes up as a consequence of an unstable expansion of the CAG tract localized in the coding region of *ATXN3* gene, mapped to chromosome 14q32.1 (Takiyama et al., 1993; Kawaguchi et al., 1994). The *ATXN3* gene – previously named MJD, MJD1 or SCA3 gene, – spans about 48 kbp in size and was first disclosed being comprised of 11 exons, whereas the CAG stretch was found to be in exon 10 (Ichikawa et al., 2001) (Figure 1.1.1.a).

Healthy individuals carry alleles ranging from 10 to 51 CAG triplets, while MJD patients' alleles are encompassed between 55 and 89 repeats. Amidst normal non-causing and expanded disease-causing alleles, few intermediate-length alleles have been reported (Maciel et al., 2001; van Alfen et al., 2001; Gu et al., 2004; Padiath et al., 2005; Takahashi et al., 2016). However, since the report of such cases are remarkably rare and the clinical manifestations are so varied among them – reported cases are either uncharacteristic with MJD presentation or not associated with disease onset (Maciel et al., 2001), – it remains

hard to predict implications adjacent to expansions that lie between normal and pathologically-expanded alleles.

Similarly to what happens in other polyQ diseases, the CAG tract length is inversely correlated with age of onset (AO) (Kawaguchi et al., 1994; Maruyama et al., 1995; van de Warrenburg et al., 2002). Moreover, expanded tracts are unstable and tend to expand upon vertical transmission, originating cases where children present first symptomatology at younger ages than their parent(s) did/do, a phenomenon that preferentially occurs after paternal transmission, known as anticipation (Takiyama et al., 1995; Durr et al., 1996; Igarashi et al., 1996).

1.1.2.2 Ataxin-3, the Gene Product

Concerning the gene translated product, *ATXN3* gene encodes ataxin-3, a protein predominantly found in cytoplasm and nuclear matrices, involved in several cellular mechanisms, namely in gene transcription and in the metabolism of proteins. Structurally, non-expanded human ataxin-3 is composed of 339 amino acid residues plus a variable stretch of Q residues, resulting in a molecular weight rounding 42 kDa for normal individuals. While many protein isoforms may exist since there are several described *ATXN3* transcripts (Bettencourt et al., 2010), only two of them have been extensively studied (Harris et al., 2010).

The protein contains a globular catalytic N-terminal positioned Josephin domain (JD) and, in the flexible C-terminus, ubiquitin-interacting motifs (UIMs) (Masino et al., 2003; Harris et al., 2010). Moreover, it has been characterized the existence of a nuclear localization signal (NLS273), which determines the transportation into the nucleus (Tait et al., 1998; Albrecht et al., 2004; Antony et al., 2009), and also two functional nuclear export signals (NES77 and NES141), involved in cytoplasmic retention of the protein (Antony et al., 2009) (Figure 1.1.1.b).

What differs between the two addressed isoforms is the number of UIMs: one possess two UIM domains, therefore being called 2UIM ataxin-3; while the other splice variant has an extra UIM domain in the variable C-terminal region, being named 3UIM ataxin-3 (Goto et al., 1997; Harris et al., 2010). Both variants are expressed in brain, although 3UIM ataxin-3 is clearly the predominant isoform found there (Harris et al., 2010).

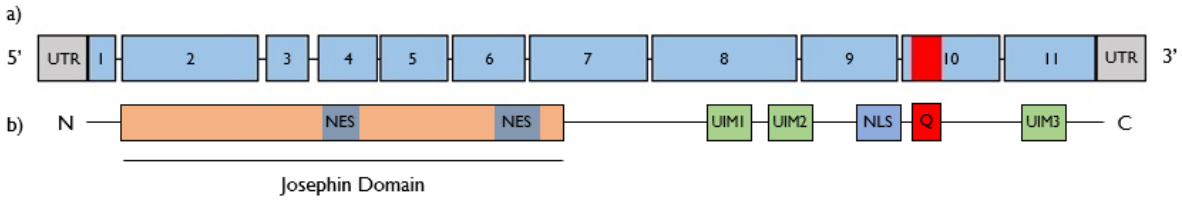

Figure 1.1.1 Schematic representation of ATXN3 gene and ataxin-3 protein. a) *ATXN3* gene comprises 11 exons (blue squares). The CAG tract (in red) is located in exon 10: above a threshold of 55 repeats individuals will develop MJD. b) Ataxin-3 protein possesses an N-terminal Josephin Domain (JD) and a flexible C-terminal. The protein contains two nuclear export signals (blue squares within JD), a nuclear localization signal (blue square at C-terminus), a polyQ tract (in red) and three or two ubiquitin-binding motifs (green squares), according to the respective isoform. In b), the most predominant 3UIM isoform is represented.
UTR: untranslated region; NES: nuclear export signal; UIM: ubiquitin-interacting motifs; NLS: nuclear localization signal; Q: glutamine tract.

1.1.2.2.1 Localization

Yet inducing neuronal damage in restricted brain areas when mutated, ataxin-3 is a ubiquitously expressed protein, being found not only in neuronal tissues, including areas spared by disease, but also in non-neuronal tissues (Paulson et al., 1997a; Wang et al., 1997; Trottier et al., 1998).

Concerning its subcellular localization, ataxin-3 has a heterogeneous distribution. At first, studies pointed that it would preferentially be detected within nucleus and cytoplasm (Paulson et al., 1997a; Tait et al., 1998; Trottier et al., 1998). Later, Pozzi and colleagues confirmed that besides being found in nuclear and cytoplasmic matrices, ataxin-3 is also present inward mitochondria (Pozzi et al., 2008).

Many factors are related and somehow explain the unspecific distribution and organelle translocation of the protein. The existence of a functional NLS sequence within ataxin-3 has been shown to be directly involved in the promotion of the protein's active importation into nucleus (Macedo-Ribeiro et al., 2009). Nuclear exportation may occur through chromosomal maintenance 1 (also known as exportin 1) dependent and independent pathways: the dependent pathway involving the protein's NES motifs, whereas independent pathway depends on the protein's conformational folding (Macedo-Ribeiro et al., 2009). Proteotoxic stresses, particularly heat-shock and oxidative, are also a factor lying behind nuclear trafficking of ataxin-3 (Reina, Zhong and Pittman, 2010).

1.1.2.2.2 Biological Functions

Although ataxin-3 biological function yet remains to be fully clarified, its involvement in numerous cellular pathways has been explored.

Evidence suggests that ataxin-3 plays an important role regulating UPS, cleaving and editing ubiquitin (Ub) chains of substrates destined for degradation (Doss-Pepe et al., 2003). Summarily, UPS is a clearance mechanism central to cells appropriate functionality, being the main mechanism for the turnover of most short-lived, damaged and misfolded proteins in eukaryotic cells (Hershko and Ciechanover, 1998). However, not every protein carrying an Ub-chain is automatically recognized by the proteasome complex and degraded, as this is a complex and much regulated event. Ataxin-3, being defined as a deubiquitinating enzyme, is apparently one of those regulatory proteins, interacting with both E3 ubiquitin-ligases and consequent substrates, regulating the ubiquitination conditions previously to proteasome presentation (Winborn et al., 2008; Durcan et al., 2011; Scaglione et al., 2011; Liu et al., 2016).

The protein's deubiquitinating activity derives from the catalytic triad structure (cysteine 14, histidine 119 and asparagine 134) present in Josephin domain, which is characteristic of cysteine proteases (Nicastro et al., 2005). Moreover, within JD, two Ub-binding sites have also been reported (Mao et al., 2005; Nicastro et al., 2009) which, along with the mentioned C-terminal UIMs, are relevant to bind polyUb-chained substrates. In fact, the presence of UIMs conducts ataxin-3 to bind and cleave preferentially long polyUb chains, with four or more Ub molecules, whilst substrates with less than four may have little affinity or even be unable to bind ataxin-3 (Burnett, Li and Pittman, 2003; Winborn et al., 2008; Nicastro et al., 2009). Supporting these findings, *in vitro* studies where a mutant catalytically inactive form of ataxin-3 was employed, resulted in a robust accumulation of polyUb substrates in the cell, to a similar extent observed when the proteasome was pharmacologically inhibited (Berke et al., 2005). Another study comprising ataxin-3 knock-out mice resulted in abnormal accumulation of polyUb proteins, whereas monoUb proteins showed no significant results (Schmitt et al., 2007).

Ataxin-3 is also linked to the regulation of gene transcription and expression. This regulation is stated to occur both in a deubiquitinating (DUB) activity-dependent manner – UPS regulates chromatin as well as other components of transcription machinery (Costa Mdo and Paulson, 2012), – and in a DUB activity-independent manner through two distinct mechanisms, (1) binding directly to cAMP-response element binding protein (CBP), p300 and

p300/CBP-associated factor (PCAF) coactivators and repressing their transcriptional activity (Li et al., 2002) and (2) interacting with transcriptional corepressors histone deacetylase 3 (HDAC3) and nuclear receptor corepressor (NCoR) (Li et al., 2002; Evert et al., 2006).

1.1.2.3 Neuropathological Features

Neuropathological studies established that neurodegeneration affects: (1) the cerebellum, presenting an accentuated atrophy of hemispheres, vermis and dentate nucleus with a considerable loss of the Purkinje cell layer; (2) the brainstem: all structures – pons, midbrain and medulla oblongata, – are implicated in disease condition; (3) basal ganglia: the dorsal striatum (caudate nucleus and putamen) is prominently degenerated; (4) substantia nigra; (5) thalamus, although the limbic nuclei remain spared; (6) the spinal cord, namely anterior horn cells and Clarke's column and (7) cranial nerves III to XII (Paulson, 1993; Rub, Brunt and Deller, 2008; Schulz et al., 2010; Scherzed et al., 2012). Hippocampus, basal forebrain, amygdala, hypothalamus, habenula, raphe nuclei and parabrachial nuclei are apparently spared by the disease (Rub, Brunt and Deller, 2008). The impairment of a wide spectrum of neural systems - namely visual, auditory, somatosensory, vestibular and oculomotor, - happens as a direct result of the widespread neuronal loss that afflicts such diversity of brain structures (Rub et al., 2003a; Rub et al., 2003b; Rub et al., 2004; Rub et al., 2006; Rub et al., 2007; Hoche et al., 2008).

Early on, a similar pattern between ataxin-3 insoluble inclusions' localization and neurodegeneration was described (Schmidt et al., 1998), being suspected a possible causative relationship between the presence of aggregates and observed neuronal loss. This hypothesis has however been disputed since inclusions were proven to exist in both affected and unaffected structures of the brain (Yamada et al., 2001; Yamada et al., 2004). Moreover, inclusions distribution also seems to be related with the polyQ tract expansion, as patients carrying longer polyQ tracts present wider distribution patterns for the inclusions (Yamada et al., 2008). Considering all the available data, it remains undetermined the real involvement of inclusion bodies over the disease context.

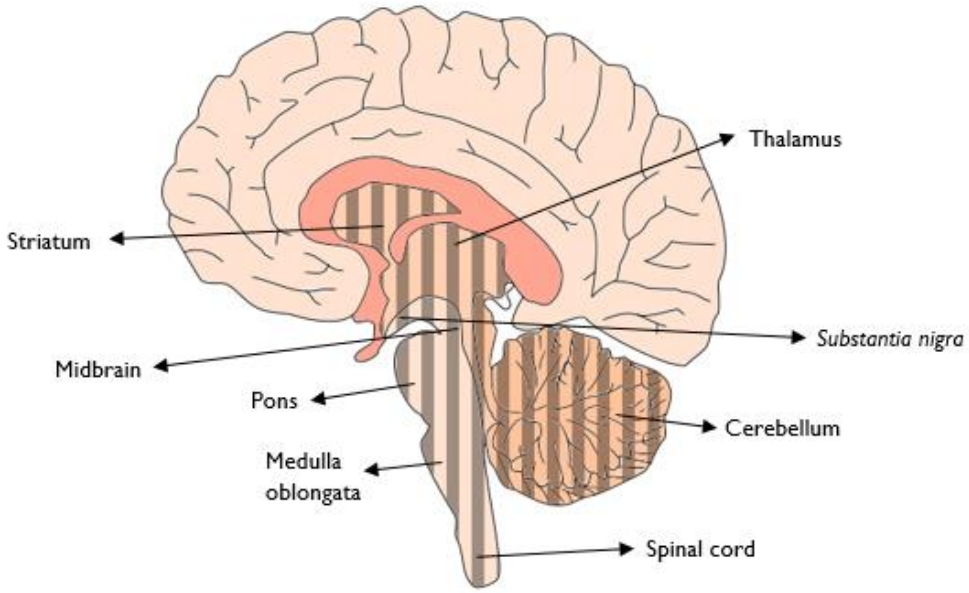

Figure 1.1.2 Main affected brain regions in MJD. Neurodegeneration in MJD is widespread, afflicting mostly the cerebellum, brainstem, *substantia nigra*, striatum and thalamus (regions marked with stripes). Adapted from Taroni and DiDonato, 2004.

1.1.2.4 Pathogenesis

To this date, cellular and molecular events underlying MJD pathogenesis remain poorly understood. An expansion of the polyQ tract motivates an abnormal 3-dimensional shape of the protein, altering its biological behaviour – through both a toxic gain and loss of functions, – and also interfering with its localization, since expanded ataxin-3 is preferentially found within neuronal nuclei (Perez et al., 1998; Bichelmeier et al., 2007). Both these factors reportedly result in a consistent death of neuronal populations over several suggested pathogenesis mechanisms. Importantly, each mechanism explored in this subchapter is by no means mutually exclusive as they all are described to occur.

1.1.2.4.1 PolyQ Tract Expansion, Aberrant Conformation and Aggregates Formation

Transversally to all polyQ diseases, a mutated disease-causing protein with an expanded glutamine tract misfolds, acquiring an aberrant conformation and, ultimately, aggregating and generating inclusion bodies. These inclusions can be found in both cytoplasm – called neuronal cytoplasmic inclusions (NCIs), – and nucleus – neuronal intranuclear

inclusions (NIIs), – of neuronal cells, and within axons of several fibre tracts (Seidel et al., 2010), representing a hallmark of MJD pathogenesis. However, the inherent toxicity of such inclusions is still questionable, being even suggested that they are the result of protective cellular mechanisms, in order to manage the acquired toxic behaviour of misfolded disease proteins, in this case expanded ataxin-3 (Arrasate et al., 2004; Invernizzi et al., 2012). It is known that this inclusions carry not only the mutant ataxin-3, but also sequester other crucial proteins involved in several cellular mechanisms/pathways, spoiling their activity and impairing normal neuronal functionality (Donaldson et al., 2003).

Underneath the aggregation process, it is assumed to occur an α-helix to β-sheet ataxin-3 conformational shift (Nagai et al., 2007). In fact, it has been demonstrated that properly folded α-helix polyQ monomers are not toxic to cell, whereas misfolded β-sheet polyQ monomers and oligomers are (Nagai et al., 2007). This transition to a toxic conformation precedes mutant ataxin-3 assembly into inclusion complexes and cytotoxic amyloid-like fibrils, similarly to what happens in other amyloidopathies (Scherzinger et al., 1997; Bevivino and Loll, 2001; Chen et al., 2002; Nagai et al., 2007).

1.1.2.4.2 The "Toxic Fragments Hypothesis"

Since early, it has been suggested that proteolytic cleavage-resulting protein fragments are of major importance regarding polyQ diseases pathogenesis (Wellington et al., 1998). The proteolytic cleavage of expanded ataxin-3, mediated by caspases and calcium-dependent calpain proteases (Berke et al., 2004; Haacke, Hartl and Breuer, 2007), generates smaller, yet more toxic and aggregate-prone, C-terminal fragments, containing the expanded glutamine tract (Goti et al., 2004). The functional properties of those fragments are still uncertain but apparently they play an important role over inclusion bodies formation, enhancing ataxin-3 aggregation, which results in increased cytotoxicity and cell death (Ikeda et al., 1996; Paulson et al., 1997b; Goti et al., 2004; Jung et al., 2009). The presence of fragments in MJD patients and in MJD animal models brains, in contrast with the absence in healthy human brains (Goti et al., 2004), also corroborates the importance of them over MJD pathology, consistently to what happens in other polyQ disorders where the abundance of a cleavage fragment is associated with pathogenesis (Merry et al., 1998; Mende-Mueller et al., 2001; Wellington et al., 2002).

1.1.2.4.3 Impairment of Clearance Mechanisms

Bearing in mind that ataxin-3 holds an important role over clearance mechanisms, a translocation to the nuclear matrix, as well as conformational changes, may restraint interaction with substrates, leading to both UPS and autophagy dysfunctionality. The impairment of both these mechanisms motivate misfolded proteins to accumulate, form oligomers and, ultimately, deposit in the form of aggregates (Ross and Poirier, 2005), which may be enough to disrupt cellular homeostasis and lead to neurodegeneration, as observed in brains of MJD patients.

The assumption of mutant ataxin-3 being involved in the dysregulation of UPS is however questioned, since DUB activity between normal and expanded ataxin-3 was shown not to be significantly different (Burnett, Li and Pittman, 2003). Thereby, it is hypothesized that, as expanded ataxin-3 remains functional and still exhibits polyUb-chain binding propensity, the interaction with other proteins may be incorrect and unstable, not resulting in a proper cleavage/arrangement of ubiquitin substrates, causing disturbances over proteins turnover (Burnett, Li and Pittman, 2003).

Macroautophagy (henceforward referred to simply as autophagy), on its turn, seems to be strictly involved in the degradation of misfolded aggregate-prone proteins, particularly those which result from a polyQ tract elongation, as ataxin-3 does (Ravikumar, Duden and Rubinsztein, 2002; Menzies et al., 2010). Although being so, the mutant form of ataxin-3, as previously noted, preferentially localizes within neuronal nucleus, while autophagy can only remove cytoplasmic aggregates, since it is essentially a cytoplasmic mechanism (reviewed in (Mizushima, 2007)). In this framework, ataxin-3 clearance by means of autophagy is defective, contributing to a greater extent of the mutant protein aggregation.

Additionally, inclusion complexes reportedly recruit other crucial macromolecules, namely autophagy and proteasome-related proteins (Nascimento-Ferreira et al., 2011). Since they remain sequestered within inclusions bodies, their activity is inhibited, disrupting normal protein homeostasis.

1.1.2.4.4 Dysregulation of Transcription

Endogenous ataxin-3 holds activity over transcription regulation, an important and equally sensitive function, over which cellular fate revolves. Mutated ataxin-3 seems to have a compromised interaction with transcription factors and co-activators, being suggested that dysregulation of transcription may be a relevant pathogenesis mechanism. Accordingly, it has been demonstrated in MJD cell lines, animal models and in MJD patients' brains a significant upregulation of mRNA and protein expression of several inflammatory mediators, namely interleukin-1 receptor antagonist (IL-1ra), interleukin-1β (IL-1β), interleukin-6 (IL-6), cytokine-inducible transcription factors C/EBP-related transcription factor beta and delta (C/EBPβ and C/EBPδ) and the cytokine stromal cell-derived factor 1 (SDF-1), thus supporting the involvement of an inflammatory process in MJD (Evert et al., 2001; Evert et al., 2003). Also, membrane-associated constituents, such as matrix metalloproteinase-2 (MMP-2) and amyloid β-protein (Aβ), known to be involved in other diseases of the central nervous system, appear to be upregulated in MJD cell lines and disease brains, suggesting the involvement of erratic gene transcription in MJD pathogenesis (Evert et al., 2001; Evert et al., 2006).

Contrarily, several genes involved in glutamatergic neurotransmission, intracellular calcium signalling/mobilization or MAP kinase pathways, $GABA_{A/B}$ receptor subunits, heat shock proteins and transcription factors regulating neuronal survival and differentiation are downregulated in MJD (Chou et al., 2008). One of those transcriptional factors is the brain-derived neurotrophic factor (BDNF) (Evert et al., 2003). As BDNF is a factor related with nerve and glial cells growth and viability (Murer, Yan and Raisman-Vozari, 2001), and because it seems to be downregulated in MJD cell lines (and within MJD human brains, especially in dentate nucleus), a loss of important neurotrophic support in disease-affected neurons is suggested and, therefore, a linkage between neurodegeneration and a decrease of BDNF transcription is hypothesized (Evert et al., 2003).

The inability to promote FOXO4-mediated superoxide dismutase 2 (SOD2) under oxidative stress conditions, which occurs in cells expressing non-expanded ataxin-3, is another evidence of transcriptional dysregulation caused by the mutation of the protein (Araujo et al., 2011).

1.1.2.4.5 Mitochondrial Dysfunction

Despite being known a relevant implication of mitochondrial dysfunction over several neurodegenerative diseases (Johri and Beal, 2012), little data exists reporting the significance of such organelle defective functionality over MJD pathogenesis. In this context, mitochondrial involvement in MJD pathology is described to occur over three distinct mechanisms: (1) expanded ataxin-3 activates mitochondrial apoptotic pathways, through upregulation of Bax protein (apoptosis inducer) and downregulation of Bcl-xL (anti-apoptotic protein) (Chou et al., 2006); (2) reduction of antioxidant enzymes activity followed by increased mitochondrial DNA damage (Liu et al., 2003; Liu et al., 2008; Yu et al., 2009) and (3) impairment of mitochondrial complex II (Laco et al., 2012).

As the imbalance of anti/pro-apoptotic proteins is obviously nefarious to cell survival, also the impairment of the detoxifying cellular machinery and the expected increase of reactive oxygen species production, due to mitochondrial complex II spoilage, seem to be relevant cumulative pathogenic mechanisms in MJD.

1.1.2.4.6 Dysregulation of Intracellular Ca^{2+} Homeostasis

Neuronal function and survival is strikingly dependent on Ca^{2+} homeostasis and a perturbation on this ion's intracellular concentration may be sufficient to cause neuronal death (Orrenius, Zhivotovsky and Nicotera, 2003). Although available data linking disruption of intracellular Ca^{2+} homeostasis to MJD pathology is very limited, there is mounting evidence that such mechanism dysregulation plays an important role over other neurodegenerative disorders (reviewed in (Bezprozvanny, 2009)) and, assuming that many of those disorders share common pathogenesis mechanisms, it is presumable that abnormal Ca^{2+} signalling plays a part on the complex MJD pathogenic paradigm.

Chen and colleagues observed a significant improvement in a motor coordination assay and a significantly decrease in neuronal loss in pontine nuclei and *substantia nigra* regions in mice fed with 5 mg per kg of body weight of dantrolene, a general Ca^{2+} signalling stabilizer (Chen et al., 2008). These results establish a connection between deranged intracellular Ca^{2+} homeostasis and neurodegeneration. They also demonstrate that calcium-signalling stabilizers can potentially represent a therapeutic window for MJD patients (Chen et al., 2008).

1.1.2.5 Clinical Frame

1.1.2.5.1 Clinical Presentation

MJD clinical presentation is directly related with the progressive impairment of several neuronal systems during the role of disease. Given that, following the gradual atrophy of cerebellum - which displays activity over equilibrium, movement and posture, - it is observed a progressive gait and limb ataxia in patients. Indeed, gait disorders are the initial symptoms in about two thirds of all SCA patients and the most common ones throughout all SCAs (Globas et al., 2008; Lo et al., 2016). Besides cerebellar ataxia affecting patients' gait, speech and balance, MJD patients also manifest oculomotor, pyramidal, extrapyramidal and brainstem signs, reflecting the damage to which such neural systems are subjected to throughout disease's progression.

Progressive ataxia, hyperreflexia, nystagmus and dysarthria are the early prominent symptoms of the disease (Matilla-Duenas, 2012). Subsequently to disease's evolution, a multitude of other features develop, including dystonia, dysphagia, temporal and facial atrophy, tongue atrophy and fasciculations, bulging eyes, slow saccades, ophtalmoparesis (that can evolve to ophtalmoplegia) and diplopia (Lima and Coutinho, 1980; Sudarsky and Coutinho, 1995; Matilla-Duenas, 2012). Additionally, other non-motor symptomatology have been reported, namely sleep disorders (Schols et al., 1998; Friedman, Fernandez and Sudarsky, 2003), vestibular dysfunction (Yoshizawa et al., 2004), cognitive, executive and affective disturbances (Zawacki et al., 2002; Cecchin et al., 2007b; Braga-Neto et al., 2012), and dysautonomia, including orthostatic hypertension, urinary incontinence and thermoregulation disturbances (Yeh et al., 2005).

Along with the disease progression, it gets to a severe point where gait autonomy is absent and the patients are unable to walk without help, confined to a wheelchair or bedridden (Jardim et al., 2001b). Camey and colleagues published a long-term cohort study taking advantage of the Markov chain method to assess gait ataxia progression rate in years, to finally define severity of gait ataxia in five stages, from milder to worse: no ataxia to death. Results of the study trace the mean times to reach stages 2, 3 and 4 (stage 2: moderate gait autonomy preserved; stage 3: inability to walk without help; stage 4: patient being wheelchair-bound or bedridden) were 5.4, 10.8 and 19.4 years, respectively. Mean time from no ataxia to death was 29 years (Camey et al., 2010). Similar results were found in Klockgether and colleagues' publication, diverging only in mean time from no ataxia to death, which was reported to be 37 years (Klockgether et al., 1998).

Since MJD's clinical presentation, AO and disease progression is very pleomorphic between individuals, the phenotype is segregated into three subtypes – MJD type I, type II and type III, – in order to better divide probands homogenously (Coutinho and Andrade, 1978) (Table 1.1.2). Besides these subtypes, there are another two very rare MJD manifestations which are proposed by a few authors as type IV and type V (Suite, Sequeiros and McKhann, 1986; Sakai and Kawakami, 1996).

Table 1.1.2 MJD subtypes characterization.

MJD subtype	Mean AO	Description	Characterising symptomatology
Type I or "Type Joseph"	24 years	The most severe subtype with a rapid disease progression. Reportedly, patients with larger CAG repeats belong to this subtype.	Severe dystonic and pyramidal signs and gait and limb ataxia.
Type II or "Type Thomas"	40 years	The most frequent subtype.	Mostly pyramidal and cerebellar deficits. Extrapyramidal signs are not frequent, but when present are very tenuous.
Type III or "Type Machado"	47 years	The subtype with the less severe manifestation.	Cerebellar ataxia and peripheral neuropathy are the major manifestations.

Displayed data was adapted from Coutinho and Andrade, 1978; Paulson, 1993; Bettencourt and Lima, 2011.

1.1.2.5.2 Diagnosis

As MJD pathology involves the dysfunction of a multitude of neuronal systems, a cornucopia of signs and symptoms are exhibited by patients. Although vast, nearly none of them is unique and characteristic for this disease, existing a clinical overlap as most of the features are shared with other similar diseases. For this reason, it is hard and highly inappropriate to perform a diagnosis regarding only clinical criteria.

The establishment of a differential diagnosis is dependent on molecular genetic testing, which focuses on detecting the abnormal CAG trinucleotide expansion in the causative *ATXN3* gene. The diagnosis is suspected and a molecular genetic testing is encouraged if one individual (1) already exhibits cerebellar ataxia and pyramidal signs

associated with a dystonic-rigid extrapyramidal syndrome or peripheral amyotrophy; (2) exhibits minor but specific clinical signs of the disease and/or (3) has familial history (Lima and Coutinho, 1980; Paulson, 1993). Clinical characterization is performed with the help of different scales, such as SARA (Scale for the Assessment and Rating of Ataxia), INAS (Inventory of Non-Ataxia Signs) and/or ICARS (International Cooperative Ataxia Rating Scale), among many others.

Presently, prenatal diagnosis and preimplantation genetic diagnosis techniques are available for use by at-risk families (Sequeiros et al., 1998; Drusedau et al., 2004).

1.1.2.5.3 Disease Treatment and Management

Although the increasing interest in understanding disease's pathogenic mechanisms, an effective pharmacological treatment to fully treat this ultimately fatal disease is still unavailable. To this date, we are lacking a pharmacological approach to reverse or even reduce the rate of disease's progression. The treatment methods used are exclusively supportive since no medication has proven to slow the course of disease (D'Abreu et al., 2010). Symptomatic pharmacological therapeutics are used to alleviate some of the clinical signs, particularly spasticity (Freeman and Wszolek, 2005), dystonia (Wilder-Smith et al., 2003; Nandagopal and Moorthy, 2004) and muscle cramps (Kanai et al., 2003). Depression, sleep disturbances, fatigue and other extrapyramidal signs can also be controlled using supportive medication (Paulson, 1993; D'Abreu et al., 2010). Besides pharmacological treatment, physical exercise, physiotherapy, speech therapy and occupational therapy are consensual approaches among medical community, as the progression of the disorder remain inexorable (Ilg et al., 2014).

Bearing in mind that there is no medicinal product approved for the treatment of MJD and currently in-use methods do nothing but mildly improve symptoms (as the patients' condition slowly but relentlessly deteriorates), advances have been made in the field of therapy research, in the last decade. Indeed, numerous therapeutic strategies have been explored (revised in (Weber et al., 2014)), including (1) preventing proteolytic cleavage, in order to decrease toxic fragments formation; (2) inhibiting nuclear shuttling of ataxin-3; (3) hindering protein aggregation; (4) improving protein folding; (5) increasing degradation of misfolded proteins, both through proteasomal, lysosomal and autophagic pathways; (6) rescuing mitochondrial functionality and (7) promoting calcium homeostasis.

1.1.2.6 Prevalence

Along with the development of novel genetic techniques and, consequently, a more precise diagnosis, the number of epidemiological and prevalence studies increased significantly. In contrast, before genetic diagnosis methods were available, the number of such studies was very limited, since even a correct diagnosis was very hard to establish, in part explaining the significant uncertainty about global epidemiology and distribution of SCAs (and MJD) remaining until present days. Recently, a comprehensive systematic review on worldwide prevalence of hereditary ataxias (and spastic paraplegia) was published, recognizing MJD as the most prevalent among all SCA phenotypes and somehow clarifying a long-time remaining mystery that had become SCAs global prevalence (Ruano et al., 2014). Table 1.1.3 summarizes absolute frequencies and prevalence of MJD per 100,000 people in some selected studies.

Table 1.1.3 MJD frequency and prevalence in few studied countries/regions.

Country (Region)	Population	Absolute Frequency	Prevalence per 100,000 people	Reference
Brazil (Rio Grande do Sul)	10,000,000	178	1.78	Jardim et al., 2001
The Netherlands	15,893,950	134	0.84	van de Warrenburg et al., 2002
Singapore	3,500,000	31	0.86	Zhao et al., 2002
Japan	126,900,000	760[a]	0.60[a]	Tsuji et al., 2008
Japan (Hokuriku District)	3,107,347	170[a]	5.45[a]	Shibata-Hamaguchi et al., 2009
Portugal	10,322,000	322	3.1	Coutinho et al., 2013

[a] values are estimated based on data reported in respective articles.

Focusing in Portugal, Coutinho and colleagues studied, with depth, the prevalence and distribution of hereditary cerebellar ataxia (HCA) and hereditary spastic paraplegia (HSP) (Coutinho et al., 2013). Their published epidemiological study reports a prevalence of 5.6 per 100,000 individuals for all SCAs, when pooled together. MJD is the most frequent phenotype and alone affects 322 individuals from 102 families, resulting in a prevalence of 3.1 per 100,000 people (Coutinho et al., 2013). Regarding distribution, it clearly varies geographically, being more prevalent in the Tagus River Valley area and obviously in Azores Islands, particularly in Flores Island where the highest worldwide prevalence occurs (1:239)

(Bettencourt et al., 2008; Bettencourt and Lima, 2011; Coutinho et al., 2013). Figure 1.1.3 illustrates regional prevalence of MJD in mainland Portugal, and in Azores and Madeira archipelagos.

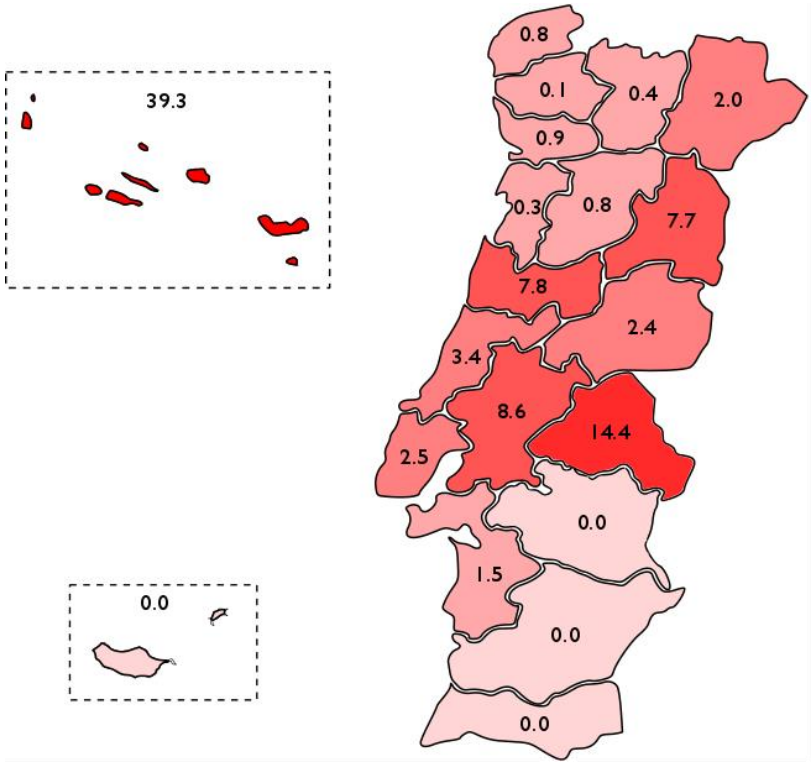

Figure 1.1.3 Regional prevalence of MJD in Portugal territory (per 10^5 population). Azores archipelago presents one of the highest regional prevalence worldwide (estimated in 39.3 per 10^5 population). In Portugal mainland, the Tagus River Valley area (Lisboa and Santarém), but also Portalegre, Guarda, Coimbra and Leiria are the districts where MJD is mostly prevalent. Adapted from Coutinho et al., 2013.

Obtained information from databases on rare diseases was limited to a report series from *Orphanet*, published on March 2016 (can be consulted here: *http://www.orpha.net/orphacom/cahiers/docs/GB/Prevalence_of_rare_diseases_by_decreasing_prevalence_or_cases.pdf*). Here, MJD is estimated to affect 1.5 per 10^5 individuals worldwide. SCA2 and SCA1 are also estimated to affect a similar proportion of individuals. The remaining considered SCA phenotypes, having a much more limited frequency, are presented neither by their prevalence nor incidence, which would be residual, but by the number of published familiar cases or by the number of published singular cases. Interestingly, SCA6, which is one of the most frequent phenotypes, is not addressed in this report series.

1.2 Resveratrol

Resveratrol is a polyphenolic phytochemical from stilbene family that can be found in root, skin and seeds from a variety of plant species (Burns et al., 2002). As some of them are edible (eg. grapes, berries, peanuts, pistachios), a spontaneous consumption of the compound is expected to occur, in a regular diet regimen.

Resveratrol is biosynthesized by plants in response to biotic and abiotic stresses, like wounding, pathogen attack or UV irradiation (Dixon and Paiva, 1995). The biosynthesis process results as a branch from the complex phenylpropanoid pathway, which under specific enzyme catalysis gives rise to a plethora of metabolites of major importance to plants, such as lignins, chalcones, flavonoids and stilbenoids (Sparvoli et al., 1994).

Although compound's first isolation and characterization being made only in 1940 by Takaoka, from the root of *Veratum grandiflorum*, the interest in its therapeutic benefits goes way back in time: *Polygonum cuspidatum*, the richest source of resveratrol, has been a very used herb in East Asiatic traditional medicine since ancient times (Chung et al., 1992; Paul et al., 1999). In the late 80's and early 90's, scientific community regained interest in the molecule as the red wine consumption – and therefore resveratrol intake, – eventual contribution towards decreasing incidence of cardiovascular disease was speculated, a phenomenon then named "The French Paradox" (Renaud and de Lorgeril, 1992). Later, in 1997, Jang and colleagues postulated that resveratrol had cancer chemopreventive properties, showing activity over all three major stages of carcinogenesis – initiation, promotion and progression, – expanding its therapeutic potentiality and, with that, bringing again the interest to furtherly research the compound (Jang et al., 1997).

Since then, resveratrol has been extensively studied and emerged as a very interesting new chemical entity, exhibiting activity over a multitude of molecular mechanisms and pathways that are central to innumerable pathologies. This chapter will discuss, with depth, compound's physical and chemical characteristics, pharmacokinetic properties, biological activity. A brief overlook on its application in clinical trials will also be given.

1.2.1 Physicochemical Characteristics

Resveratrol, or 3,4',5-trihydroxystilbene, is a polyphenol belonging to the stilbene family. Structurally, it is a diarylethene – two phenol rings, carrying three hydroxyl substitutions, two in meta positions (3 and 5) and one para-positioned (4'), are bounded by a carbon-carbon double bound (Figure 1.2.1). It is considered a phytoalexin, owing that to its low molecular weight (228.25 $g.mol^{-1}$), its antioxidant properties and by being *de novo* biosynthesised by plants.

Resveratrol occurs naturally in two geometrical *trans*- (E) and *cis*- (Z) isoforms (structures are depicted in Figure 1.2.1). The *trans*-isomer is the most predominant and the most stable natural form (Trela and Waterhouse, 1996). However, under solar light or UV irradiation, even for a short period of time, an almost complete *trans*-to-*cis* isomerization is reported to occur (Trela and Waterhouse, 1996; Vian et al., 2005). Since *trans*-resveratrol is seen as the most biologically active form (Rius et al., 2010), this photosensitivity has to be taken in special account.

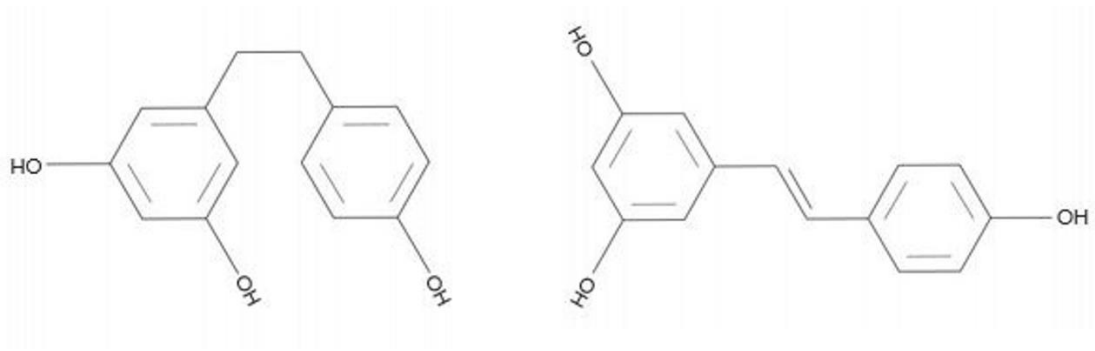

Figure 1.2.1 Chemical structures of* cis-** ***(on the left) and* trans-*resveratrol (on the right).

Another hurdle to the compound's usage is its very low water-solubility (≈0.13 mM at normal pressure and temperature conditions), making it almost totally insoluble in water (Amri et al., 2012). Of note, water-solubility is of major importance in drug absorption and, therefore, in bioavailability. Nevertheless, resveratrol is considered a Biopharmaceutical Class System class II drug, essentially due to its membrane permeability (Amri et al., 2012). On the other hand, resveratrol, similarly to other stilbenoids, is soluble in organic solvents such as ethanol, dimethyl sulfoxide (DMSO) and dimethylformamide (DMF).

Table 1.2.1 Physicochemical properties of **trans-*resveratrol*.**

IUPAC name	5-[(E)-2-(4-hydroxyphenyl)ethenyl]benzene-1,3-diol
Chemical formula	$C_{14}H_{12}O_3$
Molecular weight	228.25 $g.mol^{-1}$
Melting point	254 °C
Solubility in water	≈0.13 mM
Solubility in organic solvents	≈200 mM (in ethanol), ≈70 mM (in DMSO)
logP	3.1
Rule of five	Yes

Data here presented was adapted from Amri et al., 2012. Drugbank.ca and pubchem.ncbi.nlm.nih.gov were also consulted.

1.2.2 Pharmacokinetic Properties

The past decade's increase of interest on resveratrol aid to further understand not only the compound's biological activity, which will be addressed later, but also its pharmacokinetic properties, as numerous pharmacokinetic studies have been performed, in both animal models and humans. Considering that most of the research done so far has been conducted in animal models, many times exploring effects from concentrations which are now known to be very hard (if not impossible) to reach in human systemic circulation – and because of that those results have to be carefully interpreted and extrapolated, – it becomes even more important to perform pharmacokinetic and dose-response studies in humans, toward (1) the establishment of pharmacokinetics and pharmacodynamics profiles, (2) understanding safety and toxicity adjacent to its use, (3) develop suitable and improved novel formulations, (4) defining optimal dosages and (5) addressing efficacy and possible therapeutic results, in order to finally clarify the usefulness of resveratrol.

In this subchapter, resveratrol's pharmacokinetic properties will be reviewed. Also, strategies to overcome its low bioavailability will be addressed.

1.2.2.1 Bioavailability

Since resveratrol was pointed out as a potential novel therapeutic entity evidencing very robust results in cancer, neurodegenerative, cardiovascular and metabolic diseases, discussion turned over to compound's pharmacokinetics, and particularly its bioavailability.

Unfortunately and contrarily to its enormous therapeutic potential, resveratrol's bioavailability upon oral intake (the most common and accepted route of administration), yet showing high interindividual variability (Nunes et al., 2009), is very low in humans, whether it is administered dissolved or suspended in juice/wine/ethanol (Soleas, Yan and Goldberg, 2001a, 2001b; Goldberg, Yan and Soleas, 2003; Walle et al., 2004; Vitaglione et al., 2005), or taken as a solid form in capsules/tablets (Boocock et al., 2007a; Vaz-da-Silva et al., 2008; Almeida et al., 2009).

From the current understanding of resveratrol's bioavailability, few conclusion can be drawn, as reviewed in (Cottart et al., 2010): (1) upon resveratrol ingestion through wine consumption, the free form is either not detected or obtained serum levels are very low (Vitaglione et al., 2005); (2) when resveratrol is administered at doses of approximately 25 mg, plasma concentrations of resveratrol-aglycone are always below 10 $\mu g.L^{-1}$ (Soleas, Yan and Goldberg, 2001b, 2001a; Goldberg, Yan and Soleas, 2003; Walle et al., 2004), while administration of higher doses results in higher plasma concentrations, up to 530 $\mu g.L^{-1}$ for a 5 g resveratrol administration (Boocock et al., 2007a); (3) reveratrol's time to reach peak plasma concentrations is apparently related with the administration dosage, as peak plasma concentrations are reached in the first 30 minutes for low doses, whereas it takes more time (ranging from 1 to 1.5h) to obtain peak concentrations for higher doses (Boocock et al., 2007a).

To further understand why resveratrol has such limited bioavailability, it is interesting to explore the various physiological and non-physiological factors that influence its entry and disposition within systemic circulation and its availability at the target tissue after administration.

1.2.2.1.1 High Absorption Rate and Extent

Upon oral intake, resveratrol is absorbed at intestinal level. The first clues about human intestinal absorption rate were obtained through Caco-2 membrane models, using human intestinal cell lines (Kaldas, Walle and Walle, 2003; Li et al., 2003). In both studies, resveratrol was extensively absorbed by Caco-2 monolayers, supposedly through a passive diffusion mechanism (Kaldas, Walle and Walle, 2003; Li et al., 2003). Worth noticing, absorption of resveratrol in the presence of efflux transporters inhibitors (verapamil for

glycoprotein-p and MK-571 for MRP) was not significantly affected, suggesting that such efflux pumps are not involved in resveratrol's transport (Li et al., 2003).

Subsequent human pharmacokinetic studies demonstrated that resveratrol is rapidly and highly absorbed *in vivo* as well: Golderg and colleagues were the first to administer resveratrol in humans, reporting a rapid absorption – the highest recorded serum level was observed at the first time-point (30 minutes) (Goldberg, Yan and Soleas, 2003); meanwhile Walle's group, in the following year, administered ^{14}C-labeled resveratrol orally, demonstrating that, at least, 70% of the total orally taken resveratrol was absorbed and reached plasma (Walle et al., 2004).

1.2.2.1.2 Rapid and Extensive Metabolism

Despite being well-absorbed upon oral intake, the molecule's plasma concentrations are incredibly low. This happens because resveratrol is rapidly and extensively metabolized, particularly by phase II drug-metabolizing enzymes (sulfotransferases – SULTs, and UDP-glucuronosyltransferases – UGTs), giving rise to sulfate and glucuronic metabolites which, inversely to the aglycone form, display high plasma concentrations.

First reports regarding resveratrol metabolism in rodents showed that *trans*-resveratrol-3-*O*-glucuronide and *trans*-resveratrol-3-sulfate were the most abundant metabolites, whilst unconjugated resveratrol was not found either in mouse or rat's systemic circulation (Yu et al., 2002). Similar coetaneous results were described by Marier and colleagues, where resveratrol-glucuronide incredibly displayed 7- and 46-fold higher AUCs than the parent compound after intravenous and *per os* administration in rats, respectively (Marier et al., 2002). It was then hypothesized that enterocytes at intestinal lumen would play a role in presystemic metabolism of resveratrol. This was later corroborated by Caco-2 monolayer experiments using human intestinal epithelial cells, as resveratrol phase II conjugation was reported to occur (Kaldas, Walle and Walle, 2003; Li et al., 2003; Maier-Salamon et al., 2006).

Obtained results from *in vivo* human studies are consistent with reported data in rodents: resveratrol has little systemic availability, suffering from an avid presystemic and hepatic metabolism, whilst its conjugated metabolites are much more abundant (Boocock et al., 2007a). In their published paper, Boocock and colleagues identified six metabolites: two monosulfates, one disulfate, two monoglucuronides and one glucuronide-sulfate, being

resveratrol-3-sulfate the predominant metabolite (Boocock et al., 2007a; Boocock et al., 2007b). Other metabolites, such as reduced dihydro-resveratrol conjugates and other polar products, are also described in the literature (Rotches-Ribalta et al., 2012). Interestingly, sulphated forms are more abundant than glucoronated ones in humans, contrasting with what is found in animal studies (Wenzel and Somoza, 2005).

Contrarily to what would be expected, many authors envision the plasmatic abundancy of resveratrol conjugated forms as a positive factor since (1) conjugated forms seem to hold biological activity (Calamini et al., 2010; Hoshino et al., 2010; Lu et al., 2013), (2) human deconjugating enzymes, such as β-glucuronidases and sulfatases, may enhance resveratrol-aglycone concentration at target sites (Patel et al., 2013) and (3) through enterohepatic circulation, resveratrol conjugated forms contribute to a greater and longer systemic exposure of resveratrol, enhancing its bioavailability (Marier et al., 2002).

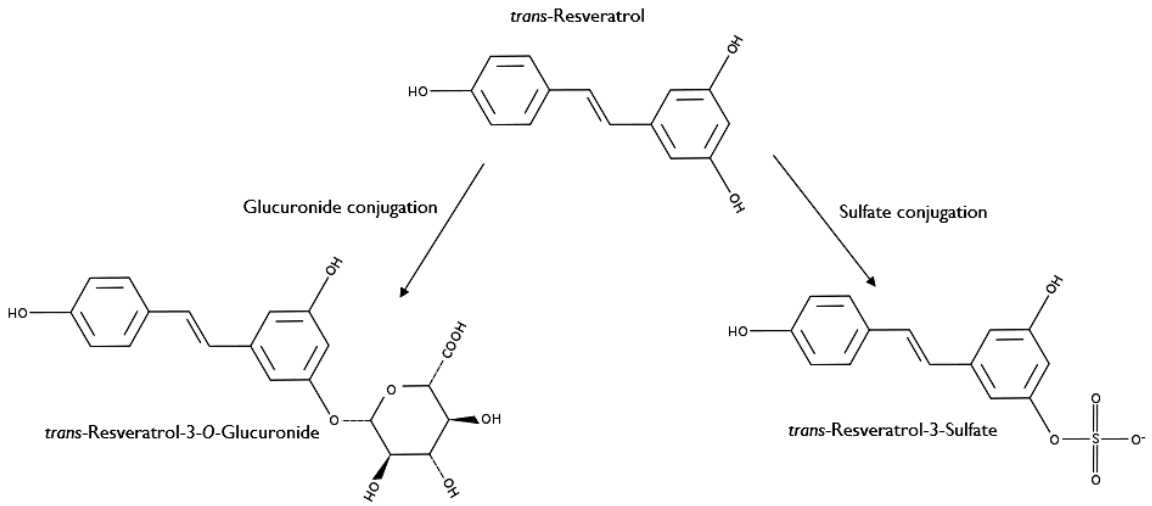

Figure 1.2.2* Trans-*resveratrol and predominant metabolites.

1.2.2.1.3 High Affinity to Bind Plasmatic Proteins

Since resveratrol has a very low aqueous solubility, in order to remain at high concentrations at serum, it must display affinity to bind plasmatic carriers. In this context, resveratrol was shown to be bound (>90%) in a non-covalent manner to human plasma lipoproteins (Burkon and Somoza, 2008). Lu and colleagues investigated the binding properties of resveratrol to human serum albumin (HSA) and haemoglobin (Hb), concluding that resveratrol is capable of bounding and forming complexes with both, yet affinity of HSA

toward resveratrol being larger than that of Hb (Lu et al., 2007). Considering concentrations of HSA and Hb in plasma (40 $g.L^{-1}$ and 140 $g.L^{-1}$, respectively), one can deduce that both proteins play important roles acting as resveratrol transporters, delivering it to cell membrane receptors, but also as reservoirs for the compound.

1.2.2.1.4 Rapid Excretion

Also contributing for the low bioavailability of resveratrol is its rapid elimination, through both urine and faeces. Boocock and colleagues' paper exposes resveratrol (and conjugated forms) very short plasmatic half-lives and residence time upon single oral intake (doses varying from 0.5 to 5 g): resveratrol-3-sulfate half-life ranges from 3.2 to 11.5 hours, whereas glucuronide and the aglycone forms' half-lives are encompassed between 2.9 to 10.6 hours and 2.9 to 8.9 hours, respectively (Boocock et al., 2007a). Moreover, for the lowest dose (0.5 g), 77% of total resveratrol species suffered urinary excretion within 4 hours after intake, clearly demonstrating the rapid excretion to which resveratrol is subject (Boocock et al., 2007a).

1.2.2.1.5 Other Non-Physiological Factors

Besides above mentioned physiological factors directly involved, other non-physiological factors are also implicated in resveratrol's bioavailability. Few studies have explored the impact of food matrix on resveratrol absorption and bioavailability: food is reported to delay resveratrol absorption rate, although not affecting its extension (Vaz-da-Silva et al., 2008). On its turn, high-fat food concomitantly to resveratrol intake either delayed resveratrol absorption (la Porte et al., 2010) or, contrastingly, did not affect resveratrol bioavailability (Vitaglione et al., 2005). Also, the intake of alcohol and other polyphenols, namely quercetin, didn't seem to affect resveratrol absorption extent (la Porte et al., 2010).

Interestingly, resveratrol pharmacokinetics apparently exhibit circadian variations, displaying higher bioavailability when administrated in the morning (Almeida et al., 2009).

1.2.2.2 Safety and Tolerability

Before advancing to human testing, it is necessary to conduct studies in animals in order to estimate relevant toxicological parameters, namely NOAEL (no-observed-adverse-effect level), and then, bearing that knowledge, safely extrapolate drug dosages to further clinical assessment.

With that in mind, Juan and colleagues orally administrated on Sprague-Dawley rats 20 mg/day of trans-resveratrol per kg of body weight (bw) during 28 days, the corresponding amount of 1.4 g/day for a human weighing 70 kg (Juan, Vinardell and Planas, 2002). Apart from a mild increase in testicular and brain weight and in serum levels of aspartate transaminase (AST) enzyme, haematology, clinical chemistry and histopathology showed resveratrol had no harmful effects, proving its safeness at such dose (Juan, Vinardell and Planas, 2002). Later, Crowell and colleagues explored the toxicological effects of 300, 1000 and 3000 mg/day per kg of bw gavage-administered resveratrol in rats for 4 weeks (Crowell et al., 2004). Most of the reported adverse events consisted of nephrotoxicity and were observed in rats given the highest dose. Also, two rats (out of the 40 included in that dose's study arm) eventually ended up dying. Only animals treated with 300 mg/day per kg of bw (corresponding amount of 3.4 g/day for a human with a standard 70 kg of weight[1]) showed no adverse effects (Crowell et al., 2004). Williams and colleagues extensively explored resveratrol toxicity reviewing a battery of *in vitro* and *in vivo* studies, including an interesting three-month study in rats using doses up to 750 mg/day per kg of bw (Williams et al., 2009). That specific study demonstrated that resveratrol was safe to use at such dosage, since no adverse events were described to occur nor other relevant toxicological changes in clinical chemistry, histopathology and haematology were reported. Furthermore, resveratrol exhibited no mutagenic properties, was not-genotoxic and didn't induce any adverse reproductive effect, leaving authors to conclude that the compound is well-tolerated and non-toxic (Williams et al., 2009).

In humans, the number of studies assessing resveratrol tolerability and safety are limited. Yet, for what is known, it doesn't seem to be causative of significant adverse events. Upon single oral intake of doses ranging from 0.5 to 5 g by healthy volunteers, no serious adverse event was reported to occur (Boocock et al., 2007a). In the follow-up study, participants were given the same dose but for 29 straight days (Brown et al., 2010). 28 out of the 44 study subjects experienced at least one adverse event while on the study. The

[1] Calculations were made based on Nair and Jacob, 2016.

majority of reported events were gastrointestinal, namely diarrhoea, nausea and abdominal pain. Interestingly, none of those symptoms were observed in individuals consuming 0.5 or 1.0 g of resveratrol (Brown et al., 2010). Similarly, in another trial where individuals were given 2.0 g of resveratrol twice a day for two periods of eight days, 6 out of 8 participants experienced mild diarrhoea (la Porte et al., 2010). Besides that, it wasn't observed any other clinically significant alteration (la Porte et al., 2010).

Putative resveratrol interactions with other drug's pharmacokinetics are also of interest when assessing its potential toxicity. In this respect, resveratrol has been shown to inhibit cytochrome P450 3A4 (CYP3A4) activity *in vitro* (Chan and Delucchi, 2000; Piver et al., 2001). Chow and colleagues evaluated the resulting effects on drug-metabolizing enzymes of a four-week long intervention with resveratrol (1.0 g/day) in healthy volunteers (Chow et al., 2010). Findings suggest that resveratrol inhibits the activity of CYP3A4, CYP2D6 and CYP2C9, while inducing CYP1A2 activity (Chow et al., 2010). Since those isoenzymes, namely CYP3A4, hold important activity over innumerable drugs' metabolism, it is expected that the intake of resveratrol may reduce metabolic clearance, increasing the bioavailability to higher plasma concentrations than expected, hence increasing the risk of toxicity of these other drugs. On the contrary, drugs suffering from CYP1A2 first-passage metabolism may see its bioavailability stand below therapeutic levels as its clearance is enhanced, when taken concomitantly with resveratrol.

Altogether, and although still lacking data on long-term administration, resveratrol seems to be well-tolerated by humans. Despite this, its use (even as a supplement) must be taken in care since it may interfere with several other drugs pharmacokinetics, increasing the risk of occurring adverse events.

1.2.2.3 Novel Strategies to Improve Human Applicability

In recent years, research has focused on novel strategies either to improve biological activity, to reduce cytotoxicity or to overcome the poor pharmacokinetics of resveratrol that compromises its applicability in clinical studies. Aiming that, many novel formulations have been explored, attempting to enhance resveratrol aqueous solubility, protect it from first-passage extensive metabolism, sustain release the compound or even target its release to specific sites of action (reviewed in Amri et al., 2012). Table 1.2.2 summarizes strategies

employed to increase resveratrol bioavailability, maximize its biological effects, and/or minimize toxicity.

Alternatively, other routes of administration, such as buccal (mouth retention) (Asensi et al., 2002) or intranasal delivery (nose-to-brain delivery) (Hao et al., 2016), intended to transpose the extensive pre-systemic metabolism and to target-deliver the compound, are drawing the attention of the scientific community.

1.2.3 Biological Properties

Interest in resveratrol's biological properties began when the *French Paradox* had it boom in France, intimately linking resveratrol intake through wine consumption to the low incidence of cardiovascular disease observed in the French population (Renaud and de Lorgeril, 1992; Renaud et al., 1998). Later, Jang and colleagues discovered and published in *Science* the compound's anticancer properties and it resulted as a turning point in resveratrol research (Jang et al., 1997). Since that time, the number of publications increased exponentially and resveratrol emerged as a very promising natural compound owning several potential therapeutic features, acting as a multifaceted antioxidant, anti-inflammatory, anti-ageing, anti-atherosclerotic and anti-carcinogenic agent, exhibiting benefits in cancer, cardiovascular, metabolic and neurologic diseases, both in *in vitro* and in *in vivo* disease models. Such profusion of biological effects results essentially from the variety of resveratrol's molecular targets – prostaglandin-endoperoxidase synthase (PTGS, also known as cyclooxygenases, COXs) and lipoxygenases (LOXs), kinases, sirtuins, DNA polymerases, among others, – combined to its capacity to modulate different pathways in the micromolar range (Pirola and Frojdo, 2008).

Although all biological properties are of tremendous interest, here we will focus on the potential neuroprotective effects of resveratrol, over which it might interfere with the pathogenesis of neurodegenerative diseases.

1.2.3.1 Resveratrol: A Neuroprotective Agent

The molecular basis of neurodegenerative disorders encompasses a multitude of dysregulated mechanisms and pathogenic features (as explored for MJD in section 1.1.2.4). Interestingly, resveratrol holds direct activity over a few of those pathogenic features, among

which are oxidative stress and neuroinflammation, and modulates numerous cellular pathways of the SIRT1 axis, since SIRT1 is a molecular target of resveratrol's activity (Howitz et al., 2003). For this reasons, resveratrol is considered an intriguing and very compelling compound for research in neurodegenerative diseases.

Table 1.2.2 Developed formulations aiming at improve resveratrol's stability, solubility, delivery and activity.

Pharmaceutical Form/Vehicle	Results	Reference
Cyano-functionalized porous polymeric microspheres	Improved stability – antioxidant activity was preserved for 5 weeks	Nam et al., 2005
Ultrafine fibres encapsulation	Sustained drug release – drug release was smooth with no burst release	Huang et al., 2006
Yeast cell encapsulation	Improved aqueous solubility – encapsulated Resv showed 2-3 times higher water-solubility Improved stability – yeast cells protected resveratrol from oxidative and photo degradation Improved antioxidant activity – DPPH radical-scavenging activity was significantly enhanced	Shi et al., 2008
Liposome incorporation	Decreased cytotoxicity – incorporation within liposomes supressed Resv toxicity at 100 μM Sustained drug release – liposome formulation enables prolonged intracellular delivery Improved metabolic activity – a significant increase in metabolic activity was seen in cells treated with liposome-incorporated Resv contrasting with free-Resv	Kristl et al., 2009
HP-CD and β-CD complexation	Improved aqueous solubility – formation of inclusion complexes with CDs overcome the limited water solubility of Resv	Lu et al., 2009
Vanillin cross-linked chitosan microspheres	Improved stability – microspheres prevented Resv degradation under both irradiation and heat exposure Sustained drug release – drug release from microspheres was initially rapid but then followed by a plateau	Peng et al., 2010
Lipid-core nanocapsules loading	Improved stability – no physical changes were observed after 1, 2 and 3 months of storage Improved drug delivery – higher Resv concentrations in brain, liver and kidney compared with free-Resv Decreased gastrointestinal damage – lesion indexes in the animals treated with Resv-loaded nanocapsules were significantly lower than those observed in free-Resv group	Frozza et al., 2010
Liposome incorporation	Improved stability – liposome incorporation prevented Resv from suffer trans-to-cis isomerization	Coimbra et al., 2011
Glyceryl behenate-based SLN	Improved brain delivery – SLN can significantly increase brain concentration of Resv	Jose et al., 2014

Resv: resveratrol; HP-CD: hydroxypropyl-β-cyclodextrin; β-CD: β-cyclodextrin; SLN: solid-lipid nanoparticles.

1.2.3.1.1 Direct Antioxidant and Free-Radical Scavenging Properties

Physiological cellular processes spontaneously generate free radicals that are essential for life but also can cause cellular damage, damaging cell structures and altering their functionality (Birben et al., 2012). In fact, in almost all neurodegenerative diseases (and in the natural ageing process as well) neuronal cells, which are particularly vulnerable, are overexposed to excessive and nonessential free radicals (Simonian and Coyle, 1996). Accordingly, this toxic oxidative stress, that eventually leads to cell death and neurodegeneration, is suggested to be a major pathogenic mechanism in the etiology of a variety of late onset diseases (Tellone et al., 2015). With this in mind, natural compounds bearing antioxidant properties – phytoalexins, such as resveratrol, – were always of great interest as potential pharmacological therapies limiting reactive oxygen species (ROS) production and rescuing nervous tissue from oxidative stress damage, hence preventing neurodegeneration.

Consistent evidence prove resveratrol displays antioxidant activity *in vitro* through a quadruple effect: (1) directly scavenging hydroxyl, superoxide and metal-induced radicals (Acquaviva et al., 2002; Leonard et al., 2003), (2) inhibiting ROS generation by prooxidant enzymes activity (Chow et al., 2007; Yao et al., 2015), (3) upregulating antioxidant enzymes, namely superoxide dismutase, heme oxygenase-I, glutathione peroxidase-I, glutathione-S-transferase, glutathione reductase, thioredoxin and catalase (Kaga et al., 2005; Spanier et al., 2009; Valdecantos et al., 2010; Xia et al., 2010; Liu et al., 2012), and (4) inhibiting phosphodiesterases (PDEs), leading to a boost in cAMP levels, which on its turn activates a signalling pathway culminating in an increase in mitochondrial biogenesis (Park et al., 2012). Correspondingly, resveratrol treatment in *in vivo* models was found to increase resistance to oxidative stress and ameliorate the damage caused by it (Ye et al., 2010; Chen, Rezaizadehnajafi and Wink, 2013). Figure 1.2.3 sums up all resveratrol's antioxidant properties.

Besides this convincing antioxidant activity, few studies also demonstrated resveratrol exhibits prooxidant activity (Ahmad, Clement and Pervaiz, 2003; Dudley et al., 2009), being suggested that resveratrol acts either as an antioxidant or a prooxidant depending on its redox status, concentration and the cell type over which it might display its effect (de la Lastra and Villegas, 2007).

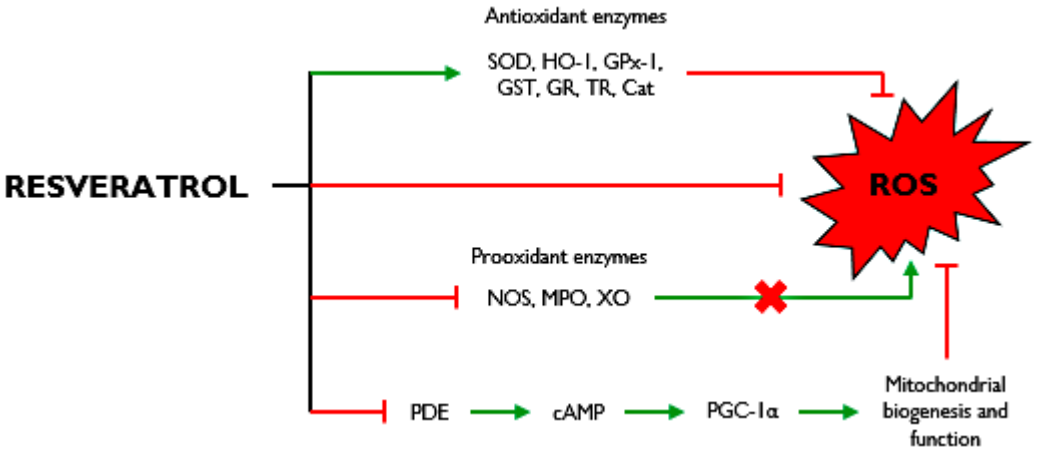

Figure 1.2.3 Targets and mechanisms underlying resveratrol's antioxidant properties. Representation based on reports by Leonard et al., 2003; Acquaviva et al., 2002; Yao et al., 2015; Chow et al., 2007; Spanier et al., 2009; Kaga et al., 2005; Xia et al., 2010; Liu et al., 2012; Valdecantos et al., 2010; Park et al., 2012.
SOD: superoxide dismutase; HO-1: heme oxigenase-1; GPx-1: glutathione peroxidase-1; GST: glutathione-S-transferase; GR: glutathione reductase; TR: thioredoxin; Cat: catalase; NOS: NADPH oxidase; MPO: myeloperoxidase; XO: xanthine oxidase; PDE: phosphodiesterase; cAMP: cyclic adenosine monophosphate; PGC-1α: peroxisome proliferator-activated receptor gamma coactivator 1-alpha; ROS: reactive oxygen species.

1.2.3.1.2 Resveratrol against Neuroinflammation

If in one hand the immune response in the CNS may be a crucial compensatory mechanism regarding limiting lesion and promoting repair and neuronal homeostasis, on the other hand, when in excess, it can also be detrimental and contribute to neuronal damage and trigger neurodegeneration (Amor et al., 2014). Therefore, it is diffusely accepted that excessive and chronic neuroinflammation represents a key feature in CNS pathologies and particularly in neurodegenerative ones.

Resveratrol has been shown to play a role over neuroinflammation since it strongly inhibits inducible NO synthase (iNOS), enzyme involved in immune response and in the generation of reactive nitrogen species (Tsai, Lin-Shiau and Lin, 1999; Lu et al., 2010). Moreover, resveratrol downregulates other cytokines and key signalling molecules participating in the pro-inflammatory response, such as interleukin-6 (IL-6), monocyte chemoattractant protein-I (MCP-I), and tumour necrosis factor alpha (TNF-α) (Bi et al., 2005; Lu et al., 2010).

Additionally, resveratrol is shown to inhibit PTGS and LOXs *in vitro* (IC_{50}: 2.5 μM for 5-lipoxigenase, 20 μM for cyclooxygenase activity of PTGS and 15 μM for its peroxidase activity) (MacCarrone et al., 1999). Since both enzymes are direct and critically involved in

proinflammatory mediation (Aggarwal et al., 2006), such inhibitory effect of resveratrol consequently attenuates neuroinflammation.

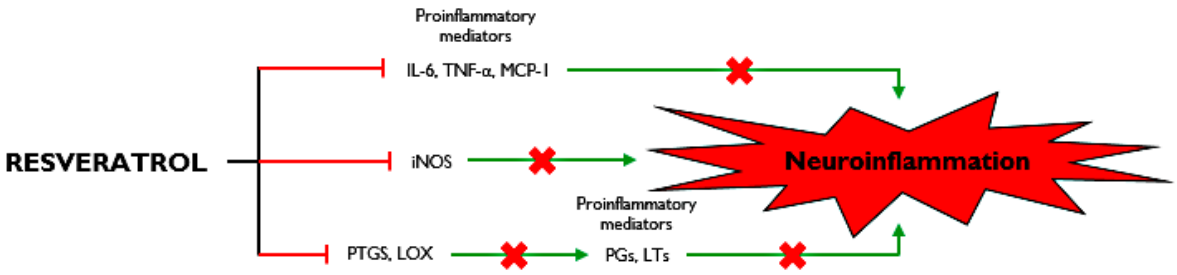

Figure 1.2.4 Targets over which resveratrol restrains neuroinflammation. Representation based on reports by Tsai et al., 1999; Lu et al., 2010; Bi et al., 2005; Lu et al., 2010; MacCarrone et al., 1999.
IL-6: interleukin-6; TNF-α: tumour necrosis factor-alpha; MCP-1: monocyte chemoattractant protein-1; iNOS: inducible NO synthase; PTGS: prostaglandin-endoperoxide synthase; LOX: lipoxygenases; PGs: prostaglandins; LTs: leukotrienes

1.2.3.1.3 SIRT1-Dependent Activity

Sirtuin-1, one of the seven reported existing sirtuins in mammals (SIRT1 through SIRT7) (Frye, 2000), is a NAD^+-dependent histone and non-histone proteins deacetylase (Imai et al., 2000) with activity over DNA transcription, mitochondria biogenesis, apoptosis, inflammatory pathways and autophagy (Haigis and Sinclair, 2010; Chalkiadaki and Guarente, 2012). Knowing the importance of SIRT1 in neurodegenerative diseases (Kim et al., 2007; Jiang et al., 2011; Montie, Pestell and Merry, 2011; Jeong et al., 2012; Cunha-Santos et al., 2016; Guo et al., 2016), molecules able to activate/upregulate SIRT1 are expected to demonstrate important therapeutic action.

Early in this century, Howitz and colleagues performed a screen of compounds reporting a group of molecules that pharmacologically activated sirtuins, designated as Sirtuin-Activating Compounds (STACs) (Howitz et al., 2003). Most of discovered STACs were natural polyphenols, namely quercetin, piceatannol, butein and resveratrol. The most potent and non-toxic compound discovered in that screen was resveratrol, increasing approximately by tenfold SIRT1's activity (Howitz et al., 2003). Apparently, this SIRT1 activation by resveratrol occurs through a direct allosteric activation in the N-terminal domain of the protein (Hubbard et al., 2013; Cao et al., 2015).

Following Howitz and colleagues discovery, many results were published highlighting the potential of resveratrol acting as a SIRT1 activator, mimicking transcriptional changes induced by caloric restriction (Barger et al., 2008; Park et al., 2009) and increasing longevity and/or delaying age-related deterioration both in yeast (Morselli et al., 2009) and in animal models, such as worms (Wood et al., 2004; Zarse et al., 2010), flies (Bauer et al., 2004; Wood et al., 2004) and fish (Valenzano et al., 2006; Yu and Li, 2012). Despite these findings, no study has yet demonstrated resveratrol-mediated lifespan extension in wild-type, healthy mammals. Regarding metabolically compromised mammals, resveratrol supplementation shifts the physiology of mice on a high-calorie diet towards that of mice on a standard diet, reducing by 31% the risk of death caused by excessive-calorie feeding, modulating longevity pathways and improving motor function, insulin sensitivity, organ pathology, PGC-1α activity and mitochondrial biogenesis (Baur et al., 2006). Later published studies unravelled that such life-extending and mitochondrial-related effects are due to resveratrol's direct activation of SIRT1-AMPK axis, thereby modulating numerous downstream pathways and proteins (Lagouge et al., 2006; Um et al., 2010; Price et al., 2012).

Although still remaining to be completely understood, few mechanisms over which SIRT1 mediates neuroprotection have been suggested (Figure 1.2.5). Those include (1) the decrease of pro-inflammatory markers, through the upstream inhibition of NF-kB gene expression (Yeung et al., 2004), (2) the activation of autophagy, in virtue of the deacetylation and activation of autophagy-related proteins (Lee et al., 2008), and (3) the activation of PGC-1α signalling pathway, resulting in an improvement in mitochondrial functionality and biogenesis (Nemoto, Fergusson and Finkel, 2005; Lagouge et al., 2006).

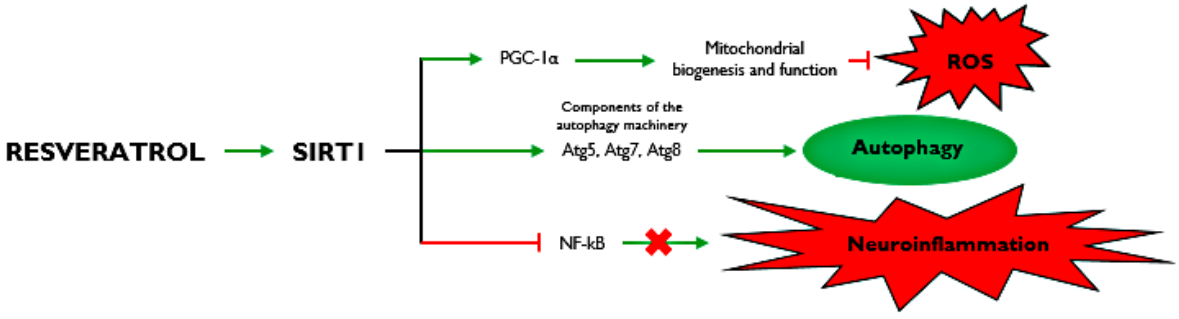

Figure 1.2.5 Downstream pathways involved in neuroprotection induced by resveratrol and mediated by SIRT1. Representation based on findings reported by Nemoto et al., 2005; Lagouge et al., 2006; Lee et al., 2008; Yeung et al., 2004.
PGC-1α: peroxisome proliferator-activated receptor gamma coactivator 1-alpha; Atg: autophagy protein; NF-kB: nuclear factor kappa-light-chain-enhancer of activated B cells.

1.2.3.2 Resveratrol Efficacy in MJD Mouse Model

Taking into account the importance of SIRT1 and the capacity of resveratrol to activate it, Cunha-Santos and colleagues recently investigated whether resveratrol would alleviate MJD phenotype (Cunha-Santos et al., 2016). Published data showed that a therapy based on the resveratrol-mediated SIRT1 activation dramatically improved motor performance and reduced neuropathology in animal models of MJD disease. Moreover, in transgenic MJD resveratrol-treated mice, SIRT1 mRNA levels were re-established to similar levels of those exhibited by controls. Altogether, results suggest that resveratrol is highly promising to treat MJD patients (Cunha-Santos et al., 2016).

1.2.4 Resveratrol in Clinical Trials

Accumulating preclinical data demonstrating thrilling biological properties have led resveratrol to take a step forward in scientific research, crossing the existing limbo between preclinical and clinical research that is very strict and for many compounds inconceivable.

A review of the clinical studies database *clinicaltrials.gov*, through July 2017, reveals that resveratrol is present in a total of 129 studies, spanning from interventional to observational in type, from not yet recruiting to completed in status and, regarding the phase, from early 1 to phase 4. Excluding observational studies (3 studies) plus the ones that were withdrawn or which the status is unknown for the last 2 years (19 studies), and including only those which resveratrol is studied as a single-agent (not in a mixture of compounds) (27 studies), remain 80 studies that are distributed as represented in Figure 1.2.6.

The clinical trials described at Figure 1.2.6 are mostly distributed in phases I and II, where corresponding studies include a short number of participants and the primary goal is to address pharmacokinetic parameters and the safety of the drug. Many of the studies here included are those previously reviewed in Subchapter 1.2.2.

Another conclusion that can be drawn inspecting the present charts is the fact that number of the trials aimed at investigating the potential role of resveratrol in the management of CNS conditions, metabolic syndrome, cancer and cardiovascular diseases is very similar (as observed by the orientation of the primary endpoints). This clearly demonstrates that the compound's implementation as a pharmacological agent is envisioned

with high interest for the treatment of various conditions: from diabetes type 2 to several types of cancer, but also neurologic diseases including neurodegenerative ones.

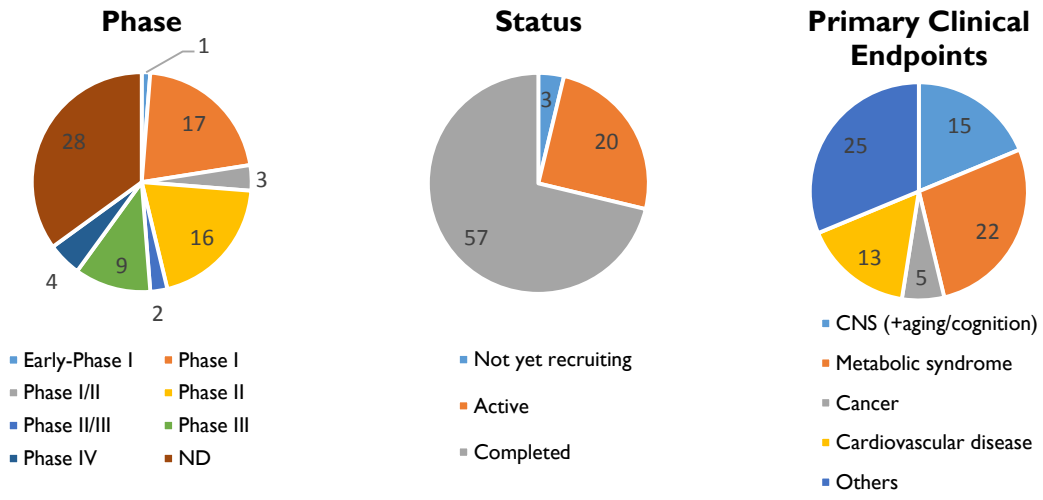

Figure 1.2.6 Characterization of clinical trial with resveratrol. Distribution by phase, status and primary clinical endpoints (by class of disease). Data obtained from *clinicaltrials.gov* on July, 2017.

Importantly, despite the increasing interest, reflected by the number and variety of published studies with and about the molecule, resveratrol was not yet approved to be used as a drug for any given disease by either EMA or FDA, or any other health authority.

1.2.4.1 Clinical Efficacy of Resveratrol in Neurodegenerative Diseases

Available data involving resveratrol efficacy towards the treatment of neurodegenerative diseases is very limited considering that, from all the registered clinical trials, only 4 of them are directed to this very specific group of diseases - one for Friedreich Ataxia (NCT01339884), one for Alzheimer's disease (NCT01504854), one for Hereditary Spastic Paraplegia (NCT02314208) and one for Huntington's disease (NCT02336633).

Nevertheless, results for the study in Alzheimer's disease have already been published, demonstrating that resveratrol significantly decreases the levels of matrix metalloproteinase-9 (MMP-9), an enzyme that plays a central role in several neurologic pathologies including neurodegenerative ones (reviewed in Vafadari, Salamian and Kaczmarek, 2016), in cerebrospinal fluid, promoting integrity maintenance of the blood-brain barrier and limiting the infiltration of proinflammatory agents into the brain, thereby decreasing neuroinflammation status. Despite these promising molecular outcomes, no

significant improvements were achieved when explored cognitive and functional variations from baseline after 52 weeks of treatment, comparing to placebo (Moussa et al., 2017).

No other results are available as, of the remaining three before mentioned studies, two continue active and the one in Huntington's disease have only recently been completed. In this regard, to accompany any eventual development on these, and on others possible upcoming trials, are of major interest towards understanding the real potentiality of resveratrol efficacy in the context of neurodegenerative diseases.

1.3 Aim of Study and Objectives

As this thesis earlier revisited, resveratrol has continuously been proven to be effective over several mechanisms involved in neurodegenerative diseases, including many participating in MJD pathogenesis. Additionally, a recent publication by Cunha-Santos and colleagues clearly demonstrated that transgenic MJD mice, when given resveratrol, exhibited both improved motor performance and reduced neuropathology (Cunha-Santos et al., 2016). Along with this, when tested in humans, the compound has been shown to be well-tolerated. Altogether, resveratrol turns out to be an exciting and very promising novel pharmacological approach for MJD, a condition for which there is still no treatment.

Aware of this, this thesis aimed at approximate the research work that is being continually done in the field of MJD to the patients affected by the disease, i.e., in one hand to fill the existing gap between research and clinic and, on the other, somehow clear the way to an eventual implementation of a clinical trial with resveratrol in MJD patients, which has never been done before.

To serve this purpose, this thesis has two main specific objectives:

1. To perform a detailed epidemiologic and clinical characterization of MJD patients followed in *Centro Hospitalar* e *Universitário de Coimbra – CHUC* (Chapter 2);
2. To characterize resveratrol's bioavailability in mice upon experimental conditions previously established by Cunha-Santos and colleagues that demonstrated to have efficacy in alleviating behaviour deficits in mice models of MJD (Chapter 3).

Ultimately, in this thesis we expect to accomplish a detailed clinical and epidemiological characterization of the disease and also to develop an analytical method for resveratrol assay and pharmacokinetic characterization in animals, opening the way for future therapy of MJD patients.

CHAPTER 2
Epidemiologic and Clinical Characterization of MJD Patients

2.1 Methods

2.1.1 Subjects

All patients included in this study are followed in the Neurology Department of *Centro Hospitalar* e *Universitário de Coimbra – CHUC* and have been enrolled in the *European SCA-3/MJD Initiative (ESMI)* project. Only subjects with genetically confirmed MJD (by a repeat expansion in the causative *ATXN3* gene) were admitted. Previous to inclusion and any data collection, patients have signed an informed consent.

Data was collected and compiled for a total of 20 patients. As, by the time this study was executed, the number of control subjects was very low (n=2), we excluded the assessment of those subjects.

This assessment was approved by the Ethic Commission of the Faculty of Medicine of the University of Coimbra.

2.1.2 Data Acquisition

In order to limit the bias, all data obtained from the probands was acquired through a standardized examination and interview procedure. Moreover, this examination and interview procedure was always performed by the same clinicians of the Neurology Department of *CHUC*.

The clinical assessment included a physical evaluation, a scrutiny about other comorbidities and habitual medication, and an inquiry about the accomplishment of daily living activities (ADL). SARA, INAS and MoCA (Montreal Cognitive Assessment) scales/tests scores were measured. If the patients, by any mean, were unable to take part in the interview or unable to evoke/answer any question, those same questions were inquired to whom they were accompanied by.

Additionally, an external assessment was carried out to rate patient's performance in both SCAFI (SCA Functional Index) and CCFS (Composite Cerebellar Functional Severity Score) scales. Furthermore, a series of self-rating questionnaires were also obtained from each patient. Those who were too debilitated and unable to fill the questionnaires were asked for the respective answers while the document was completed by the investigator in charge.

2.1.2.1 Clinical Scales

When able, patients were subjected to a five clinical scale assessment. These scales are validated and widely used, providing relevant information about the level of physical and mental impairment. Moreover, because such scales are not definite, they are very useful towards understanding the evolution of each patient, by comparing scores obtained at different time-points.

2.1.2.1.1 SARA Scale

SARA scale evaluates patient's performance in 8 different items: gait, stance, sitting, speech disturbance, finger chase, nose-finger test, fast alternating hand movements and heel-shin slide. Each item is individually scored, yielding a total score that ranges between 0, *no ataxia*, to 40, *severe ataxia* (Schmitz-Hubsch et al., 2006).

2.1.2.1.2 INAS

Contrarily to SARA, INAS scale provides information about non-ataxic signs. It consists of 30 items which are encompassed in 16 variables: hyperreflexia, areflexia, extensor plantar response, spasticity, paresis, amyotrophy, fasciculations, myoclonus, rigidity, chorea/dyskinesia, dystonia, resting tremor, sensory symptoms, urinary dysfunction, cognitive dysfunction and brainstem oculomotor signs. A semi-quantification of non-ataxia signs and symptoms can be assessed by evaluating the presence or absence of each of the considered variables. Hence, to higher INAS counts corresponds a higher number of non-ataxic signs exhibited by one patient, therefore indicating a higher degree of extra-ataxia debilitation.

2.1.2.1.3 MoCA Test

MoCA test evaluates cognitive functionality of the subjects by assessing different cognitive domains: visuoconstructional skills, executive functions, language, memory, attention, concentration, calculation, conceptual thinking and orientation. A final score is obtained by the sum of each individual item, for a possible maximum of 30 points. Scores

above 26 are considered normal, whereas scores below 26 reflect a decline in cognitive skills.

2.1.2.1.4 SCAFI Test

SCAFI test measures the time taken to perform 3 functional tests: the 8 meter walk at maximum speed (determines functional mobility, gait and vestibular function), the 9-hole peg test (evaluates hand and fingers dexterity) and the *PATA* rate (measures the speech performance). All tests are quantitative: the 8 meter walk and the 9-hole peg test are timed and the *PATA* rate is counted. Values obtained for the 8 meter walk test and for the 9-hole peg test are inversely correlated with the patient's mobility and finger dexterity function. For the *PATA* rate test, to a greater number of repetitions corresponds a better speech performance. All tests were performed in duplicate therefore presented scores are, in fact, the mean of the two trials.

2.1.2.1.5 CCFS

CCFS evaluates only 2 variables, the 9-hole peg test and a click test, where the patient using his index finger presses alternatively two mechanical counters 10 times. Both tests are timed and a final score is yielded applying a defined equation (du Montcel et al., 2008). Higher values (more time needed to perform the tests) implicate a worse functional condition.

2.1.2.1.6 ADL

ADL scale evaluates the ability of an individual to perform a series of basic daily-life activities important to live independently. The 9 items taken into account are: speech performance, swallowing, use of cutlery, dressing, personal hygiene, frequency of falling, walking, sitting and bladder functionality. Matching with patient's ability, items are valuated from 0 to 4, to a maximum score of 36. Patients with lower ADL final scores live a more independent life, contrary to those with higher scores, which are more disabled and demand a greater need of daily assistance.

2.1.2.2 Self-Rating Questionnaires

A series of questionnaires was given to patients concerning a self-evaluation on their own physical and mental health status, quality of life and sleep quality. The nature of these questionnaires allow us (1) to figure how the disease afflicts patients in each of the inspected domain; (2) to explore differences between patients in different stages of disease and (3) to assess how patients cope with disease, especially psychologically. In this framework, the questionnaires somehow give us additional information that cannot be obtained through a standardized clinical examination, complementing our grasp on the impact of this disease in the lives of patients.

Importantly, all questionnaires were previously validated and adequate to employ in these patients.

2.1.2.2.1 Patient's Health Questionnaire

Patient's Health Questionnaire (PHQ-9) is a brief self-administrated instrument very useful in the diagnosis of depression, while measuring its severity in an at-risk population (e.g. those who suffer from a life-limiting disease such as MJD). It comprises 9 questions regarding how often the patient have been bothered, on the 2 previous weeks, by the situations mentioned in each of the items. Answers given are scored from 0, *not at all*, to 3, *nearly every day*, and are summed up to a maximum of 27 points. The severity of depression can be established from the obtained score: 1-4, minimal; 5-9, mild; 10-14, moderate; 15-19, moderately severe; 20-27, severe depression (Kroenke, Spitzer and Williams, 2001).

2.1.2.2.2 Pittsburgh Sleep Quality Index

Pittsburgh Sleep Quality Index (PSQI) addresses patients' sleep quality within the past month. It contains 19 self-rated questions plus 5 questions rated by the bed partner/roommate, if available. Anyway, only the 19 self-rated questions account for scoring. To do so, those 19 questions are divided in 7 component scores – subjective sleep quality, sleep latency, sleep duration, habitual sleep efficiency, sleep disturbances, use of sleeping medication and daytime dysfunction, – each ranging from a score of 0 to 3, where 0 corresponds to *no difficulty*, while 3 indicates *severe difficulty*. A final global score results from the sum of all 7 components and is comprehended between 0 and 21 points. A PSQI score

of 5 or less is considered as *good sleep quality*, whereas scores greater than 5 are associated with *poor sleep quality* (Buysse et al., 1989).

2.1.2.2.3 EuroQol 5-Dimension 3-Level version

EuroQol 5-Dimension 3-Level version (EQ-5D-3L) is a two-part instrument, consisting of a descriptive system plus a visual analogue scale (EQ-VAS). The descriptive system comprises 5 dimensions – mobility, self-care, usual activities, pain/discomfort and anxiety/depression, – and, for each, the patients are asked to indicate the level (*no problems*, *some problems*, *extreme problems*) that suits better their health status. 1-digit number (*1*, *2* or *3*) expresses the respective health status for each dimension. Combining the 5 dimensions a 5-digit number is obtained (e.g., *11223*) which represents the patient's global health state, for a total of 243 health states. The EQ-VAS quantitatively registers the patient's self-rated global health status, at the time of completion, on a vertical visual analogue scale from 0 (*worst imaginable health state*) to 100 (*best imaginable health state*). For this assessment, it was only considered the EQ-VAS score.

2.1.3 Other Data

Additional epidemiologic and clinical information – city of birth, weight and height, alleles' length, etc., – was obtained by checking patients' clinical files or by directly asking the patients and/or the partners/caregivers.

Age of onset was defined as the age of appearance of the first symptom of the disease (usually disturbance in gait). Disease duration was determined as the time elapsed between AO and age at examination, rounded to years.

Disease stage was determined in accordance with the literature: stage 1, ataxic but independent; stage 2, permanently dependent on walking aids; stage 3, permanently dependent on wheelchair (Klockgether et al., 1998).

2.1.4 Statistical Analysis

Variables were tested for normal distribution using D'Agostino-Pearson omnibus normality test. To test for linear relationship between variables, we took advantage of

parametric Pearson's and nonparametric Spearman correlation tests, depending whether variables were normally or non-normally distributed, respectively.

Disease stage's intergroup comparisons for SARA, INAS, ADL and CCFS were calculated by one-way Analysis of Variance (ANOVA) followed by a Newman-Keuls *post hoc* analysis.

Reported p-values are two-tailed and were considered statistically significant when lower than 0.05.

Results are expressed as mean ± standard deviation.

All statistical analysis was conducted using GraphPad Prism version 6.00 for Windows (GraphPad Software, La Jolla, California, USA).

2.2 Results and Discussion

2.2.1 Demographic Data

A demographic assessment of the probands was established concerning their naturality. City of birth was known for 18 out of the 20 patients and their geographic distribution (depicted in Figure 2.2.1) was as follows: 6 were born in Coimbra district (2 in Montemor-o-Velho, 1 in Figueira da Foz, 1 in Coimbra, 1 in Miranda do Corvo and 1 in Penela); 4 in Guarda district (3 in Gouveia and 1 in Guarda); 2 in Bragança district (both in Bragança); 2 in Porto district (both in Porto); 2 in Azores archipelago (1 in Santa Cruz das Flores, Flores Island, and 1 in Ponta Delgada, São Miguel Island); 1 in Viseu district (Viseu); and 1 in Lisboa district (Sacavém). Despite this assessment been made, putative genealogical confluences between probands were not investigated.

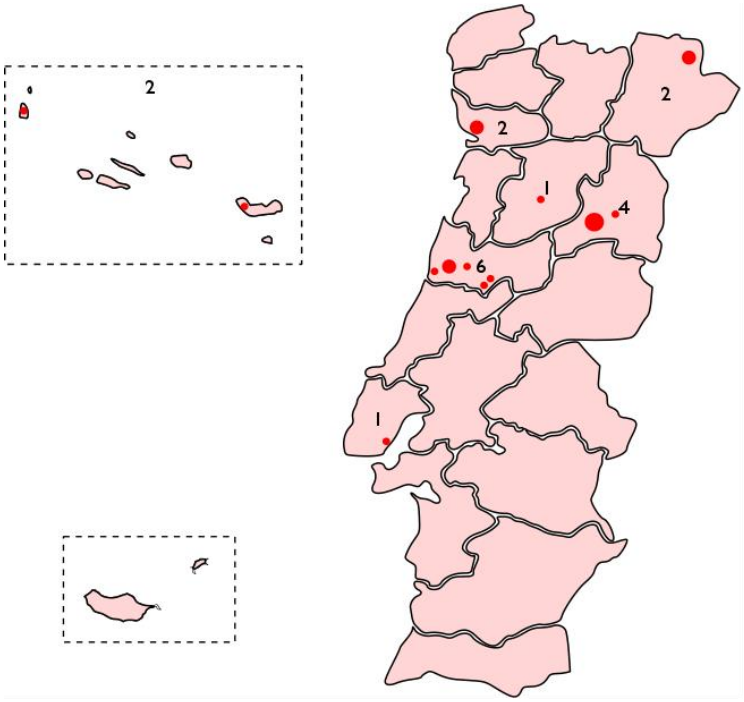

Figure 2.2.1 Geographic distribution of probands enrolled in the study.

2.2.2 Epidemiological Assessment

A total of 20 patients, 11 male and 9 female, were enrolled with mean age of 50.8 ± 11.6 years (mean ± SD), ranging from 28 to 73 years old. Age of disease onset (AO) was available for 17 out of the total 20 patients and ranged between 14 and 58 years of age. AO mean was calculated at 39.5 ± 10.9 years, which is in agreement with results published in other similar studies (Klockgether et al., 1998; Coutinho et al., 2013; Gonzalez-Zaldivar et al., 2015).

The size of the expanded *ATXN3* allele was known for 18 probands. Mean value was of 72.8 ± 3.7 CAG repeats, ranging from 63 to 81. The most common expansion tract was of $(CAG)_{75}$, with an absolute frequency of 5 (25% of total). Regarding the unexpanded allele length, which was only known for 9 out of the total subjects with calculated mean of 21.8 ± 5.0, ranging from 14 to 27 repeats (Figure 2.2.2).

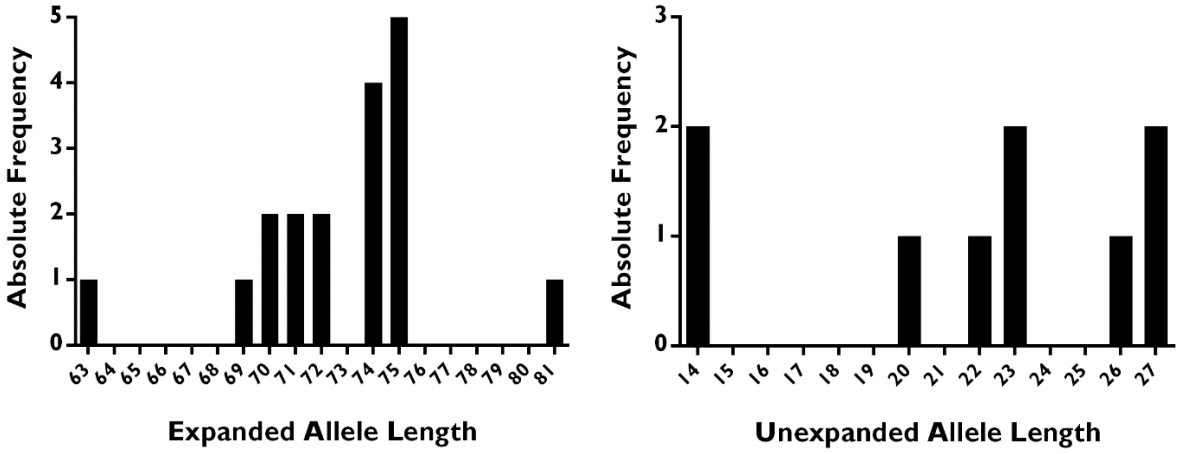

Figure 2.2.2 Absolute frequency distribution of expanded (on the left) and unexpanded allele (on the right) length.

Disease duration was another variable addressed in this study. Time span of disease was comprised between 3 and 24 years. Mean disease duration was verified at 10.6 ± 5.4 years.

Table 2.2.1 features all epidemiologic data acquired in the context of our study.

Table 2.2.1 Epidemiologic characterization of the cohort of MJD patients.

	Epidemiologic Parameters					
	Age	**Age of Onset**	**Disease Duration**	**Expanded Allele Size**	**Unexpanded Allele Size**	**BMI**
Mean ± SD	50,8 ± 11,6	39,5 ± 10,9	10.6 ± 5.4	72.8 ± 3.7	26 ± 3.6	22.7 ± 3.75
Range	28-73	14-58	3-24	63-81	14-27	16.2-29.3
n	20	17	17	18	9	16

Values for age, age of onset and disease duration are given in years; for allele's size, in number of CAG repeats; and for BMI, in $kg.m^{-2}$. BMI: body mass index; SD: standard deviation; n: sample size.

2.2.2.1 Age of Onset and Number of CAG Repeats Are Closely Correlated

Congruently to what has been reported in the literature (Kawaguchi et al., 1994; Maruyama et al., 1995; Sasaki et al., 1995), our data (Figure 2.2.3) also show a significant inverse correlation between the expanded allele length and the age of onset (ρ= -0.8925, $p<0.0001$, n=17). With this, we demonstrate that the number of CAG repeats in the *ATXN3* gene accounts for about 80% in the variability of the AO in patients (r^2=0.7966). In this

context, probands with larger expanded tracts will reach earlier a symptomatic stage of the disease.

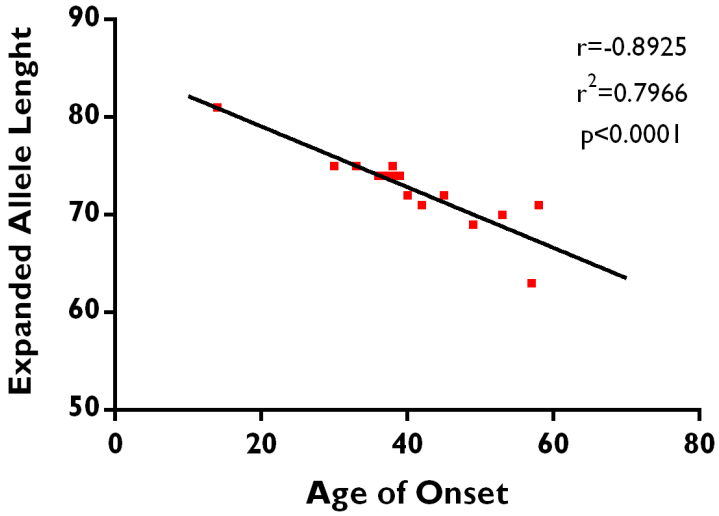

Figure 2.2.3 Age of onset plotted against size of the expanded allele. n=17; r and p-value were determined by Pearson's correlation test. Plotted line was determined by linear regression analysis. Equation for linear regression line is: *Y= -0.3109X + 85.29*, where X is the AO and Y is the expanded allele length.

2.2.3 Clinical Assessment

Clinical assessment was divided into two parts: firstly, it was discriminated the clinical manifestations profile of each patient; secondly, taking advantage of several scales (to further detail consult topic 2.1.2.1), it was evaluated probands' functional and cognitive status. In order to better comprehend and interpret obtained results, considering the lack of a control group without disease, probands were categorized in 3 groups, accordingly to their clinical phenotype (disease stage, DS), as previously noted (Klockgether et al., 1998).

2.2.3.1 Clinical Manifestations Profile

During medical physical examination process, a listing of the disease's most recurring signs and symptoms was checked out for in each patient.

Collected results demonstrated that cerebellar functionality is tremendously affected, since gait ataxia, dysmetria of both upper and lower limbs, dysarthria, dysdiadochokinesia and dysphagia were exhibited by almost every proband in study, independently of their clinical phenotype (Table 2.2.2). In fact, every proband revealed at least 2 cerebellar features (gait ataxia was manifested by the whole study population) and 10 (out of the 18 patients whose data was available) displayed all the 6 investigated cerebellar characteristics.

Pyramidal signs frequency was more irregular within the probands. Babinski sign (or flexor plantar reflex) was the most frequent sign, being manifested by 69% of the patients. At the other end, hyperreflexia of the lower limbs affected only 3 of the 17 evaluated patients, highly contrasting with hyperreflexia of the upper limbs featured by more than half of the patients. Pyramidal signs features might be associated with disease progression, considering that, for many of the assessed criteria (eg. Babinski sign, paresis), greater relative frequencies were observed in patients from later phases of disease.

Regarding ophthalmologic evaluation, nystagmus was found in all probands. Also, ophtalmoparesis and slow saccades were commonly found, totalizing frequency percentages of 72 and 67, respectively. Despite frequent, these ophthalmological features do not seem to compromise vision efficiency, as only 2 patients presented impaired visual acuity.

Of note, our outcomes for clinical core features, particularly values for cerebellar features and nystagmus, match previous reports (Schols et al., 1995; Soong et al., 1997; Jardim et al., 2001a).

Each evaluated sign and symptom, as well as their respective absolute and relative frequencies are reproduced in Table 2.2.2.

2.2.3.2 Scale-Based Clinical Evaluation

To take advantage of scales and tests while performing a clinical assessment is of great interest towards establishing relationships between clinical phenotype and independent disease-related variables by reason of, from its use, one is allowed to obtain quantifiable values for a patient clinical presentation/characterization.

Levels for cerebellar-related impairment were determined by SARA scale scores. In global study population, SARA scores were dispersed, ranging from 5, which corresponds to a minor ataxic impairment, to 37, severe ataxia. The pool of patients encompassed in disease stage (DS) 1 group, had a combined mean SARA score of 9.6 ± 3.8 (range: 5-16.5). As expected, levels for cerebellar ataxia impairment were consistently and significantly greater for patients in more advanced disease stages (Figure 2.2.4): DS2 group mean score was 18.7 ± 8.1 (range: 11.5-31), whereas for DS3 pool of patients, a mean score of 27.7 ± 9.5 (range: 18-37) was observed.

Table 2.2.2 Absolute and relative frequencies of MJD clinical symptoms and signs.

	Disease Stage 1	Disease Stage 2	Disease Stage 3	Global
Cerebellar Features				
Gait Ataxia	9/9 (100%)	5/5 (100%)	3/3 (100%)	18/18 (100%)
Dysmetria (UL)	8/9 (89%)	5/5 (100%)	3/3 (100%)	17/18 (94%)
Dysmetria (LL)	8/9 (89%)	5/5 (100%)	3/3 (100%)	17/18 (94%)
Dysarthria	8/9 (89%)	5/5 (100%)	3/3 (100%)	17/18 (94%)
Dysdiadochokinesia	7/9 (78%)	3/5 (60%)	3/3 (100%)	14/18 (78%)
Dysphagia	6/9 (67%)	4/4 (100%)	3/3 (100%)	14/17 (82%)
Pyramidal Signs				
Hyperreflexia (UL)	6/9 (67%)	4/5 (80%)	1/3 (33%)	11/18 (61%)
Areflexia (UL)	3/9 (33%)	0/5 (0%)	1/3 (33%)	4/18 (22%)
Hyperreflexia (LL)	2/8 (25%)	1/5 (20%)	0/3 (0%)	3/17 (18%)
Areflexia (LL)	2/8 (25%)	0/5 (0%)	1/3 (33%)	4/18 (22%)
Babinski Sign	4/8 (50%)	4/4 (100%)	3/3 (100%)	11/16 (69%)
Spasticity	4/9 (44%)	2/4 (50%)	1/3 (33%)	7/17 (41%)
Paresis	1/9 (11%)	0/5 (0%)	3/3 (100%)	5/18 (28%)
Other Movement Impairment				
Myoclonus	0/8 (0%)	0/5 (0%)	0/3 (0%)	1/17 (6%)
Dyskinesia	0/9 (0%)	0/5 (0%)	0/3 (0%)	0/18 (0%)
Dystonia (Trunk)	4/9 (44%)	1/5 (20%)	0/3 (0%)	5/18 (28%)
Dystonia (UL)	0/9 (0%)	1/5 (20%)	0/3 (0%)	1/18 (6%)
Dystonia (LL)	2/9 (22%)	5/5 (100%)	0/3 (0%)	7/18 (39%)
Resting Tremor	0/9 (0%)	0/5 (0%)	1/3 (33%)	1/18 (6%)
Ophthalmologic Findings				
Nystagmus	9/9 (100%)	5/5 (100%)	3/3 (100%)	18/18 (100%)
Ophtalmoparesis	4/9 (44%)	5/5 (100%)	3/3 (100%)	13/18 (72%)
Slow Saccades	6/9 (67%)	3/5 (60%)	2/3 (67%)	12/18 (67%)
Impaired Visual Acuity	0/6 (0%)	1/5 (20%)	0/3 (0%)	2/15 (13%)
Other Abnormalities				
Urinary Dysfunction	2/9 (22%)	3/5 (60%)	1/3 (33%)	6/18 (33%)
Episodic Vertigo	3/9 (33%)	0/5 (0%)	1/3 (33%)	4/17 (24%)

UL: upper limbs; LL: lower limbs.

Mean score for INAS scale was 5.6 ± 2.0 (range: 2-8) for whole study population. Here, again, significant differences were observed between the respective INAS scores for disease stages 1 and 3 (Figure 2.2.4): mean INAS score for DS 1 group was 4.5 ± 1.5 (range: 2-6); DS 2 group scored 5.8 ± 2.2, which was not statistically different from the other two groups; while probands categorized in DS 3 had a mean INAS score of 7.7 ± 0.6 (range: 7-8).

ADL scale gives useful information regarding probands' dependency and physical disability. Alike SARA and INAS, obtained mean scores for ADL scale were progressively higher with disease progression: 4.8 ± 2.9 (range: 1-10), 13 ± 6.6 (range: 6-23) and 20.3 ± 11.0 (range: 13-33) for DS 1, 2 and 3, respectively.

Global mean score for MoCA test was 26.0 ± 3.59. In this specific parameter, scores were very uniform, ranging from 23 to 29 with the exception of a MoCA score of 14, which should be a definite outlier (ROUT method, Q=0.1%): the proband was illiterate and that critically limited the individual's ability to resolve the test.

Regarding functional tests, mean scores for CCFS test were statistically different between groups 1 and 3 ($p \leq 0.01$) and between groups 2 and 3 ($p < 0.05$). As this test addresses cerebellar functionality, such findings corroborate that cerebellar performance degrades along the progression/stage of the disease. In respect to the other functional test, SCAFI, each four evaluated parameters were individually analysed and final scores can be consulted in Table 2.2.3, along with all retrieved data from clinical scales.

2.2.3.2.1 Impact of Disease-Related Variables over Clinical Scores

Although being expected that more debilitated probands – those in later disease stages, – feature a worse performance in the various clinical parameters comparatively to less affected ones; it remains intriguing to appraise which disease-related independent variables are more relevant regarding the clinical facet of the disease and, how these variables can help to predict clinical scores. In this regard, we evaluated the existence of any correlation between clinical parameters and several disease-related variables: *disease stage*, *disease duration*, *expanded allele size* or *age of onset* (results for the correlation array is depicted in Table 2.2.4).

Table 2.2.3 Clinical characterization of the probands.

		Disease Stage 1			Disease Stage 2			Disease Stage 3			Global		
		n	Mean ± SD	Range	n	Mean ± SD	Range	n	Mean ± SD	Range	n	Mean ± SD	Range
Clinical Scales/Tests	SARA	9	9.6 ± 3.8	5-16,5	5	18.7 ± 8.1	11.5-31	3	27.7 ± 9.5	18-37	18	16.2 ± 9.5	5-37
	INAS	8	4.5 ± 1.5	2-6	5	5.8 ± 2.2	3-8	3	7.7 ± 0.6	7-8	17	5.6 ± 2.0	2-8
	MoCA	9	27.1 ± 1.2	25-29	5	27.4 ± 2.1	24-29	2	19.0 ± 7.1	14-24	17	26.0 ± 3.59	14-29
	ADL	9	4.8 ± 2.9	1-10	5	13 ± 6.6	6-23	3	20.3 ± 11.0	13-33	17	9.9 ± 8.3	1-33
	CCFS	9	2.513 ± 0.158	2,301-2,771	4	2.658 ± 0.151	2.489-2.847	2	2.986 ± 0.105	2.911-3.06	17	2.62 ± 0.217	2.301-3.06
	8MW	9	9.7 ± 4.2	5.6-19.3	3	14 ± 3.7	10.7-18.0	0	-	-	13	10.7 ± 4.17	5.6-19.3
SCAFI	9HP DH	9	34.3 ± 6.7	21.8-46.4	5	72.8 ± 64.6	34.4-187.9	3	196.4 ± 132.5	46.8-299.0	20	85.5 ± 100.9	21.8-361.5
	9HP NDH	9	37.1 ± 4.9	27.3-43.2	4	54.4 ± 19.1	32.0-77.5	2	188.9 ± 185.9	57.4-320.3	17	60.8 ± 68.1	27.3-320.3
	PATA	9	22.7 ± 3.3	18-29	5	22.6 ± 8.0	10-30	2	17.5 ± 0.7	17-18	19	21.2 ± 4.7	10-30

Values for 8MW, 9HP DH and 9HP NDH is in seconds, and for PATA, in number of *pata* word repetitions per 10 seconds. 8MW: 8-meter walk; 9HP DH: 9-hole peg test (dominant hand); 9HP NDH: 9-hole peg test (non-dominant hand).

As foreseen, our results show that *disease stage* is correlated with most of clinical scale scores, particularly those for SARA and ADL scales ($p \leq 0.001$), but also with the 9-hole peg (dominant hand performance) and CCFS tests ($p \leq 0.01$) (Table 2.2.4). Noteworthy, it does not seem to exist any relationship between patients' speech performance and clinical phenotype ($p > 0.05$).

Similar results were achieved when *disease duration* was plotted against scales scores. Correlations with SARA and ADL scores were again of great significance ($p \leq 0.001$). Moreover, results suggest that an eventual decline in patient's cognitive (MoCA test) and functional (9HP DH and CCFS tests) abilities may be associated with *disease's duration* ($p \leq 0.01$). Remarkably, speech performance (PATA scores) is significantly affected by *disease duration* variable ($p = 0.222$).

Table 2.2.4 Independent variables versus clinical scales correlation array.

				SCAFI						
		SARA	MoCA	8MW	9HP DH	9HP NDH	PATA	CCFS	INAS	ADL
Disease Stage	**ρ**	0.7699	-0.5746		0.6921	0.6318		0.7352	0.6198	0.7464
	p-value	0.0003	0.0199	ns	0.0021	0.0115	ns	0.0018	0.0104	0.0006
	n	17	16		17	15		15	16	17
Disease Duration	**ρ**	0.76	-0.6642		0.7049		-0.5665	0.7599	0.526	0.7841
	p-value	0.0004	0.005	ns	0.0016	ns	0.0222	0.001	0.0364	0.0002
	n	17	16		17		16	15	16	17
EAS	**ρ**	0.5134								0.5084
	p-value	0.0351	ns	ns	ns	ns	ns	ns	ns	0.0443
	n	17								16
Age of Onset	**ρ**									-0.4965
	p-value	ns	ns	ns	ns	ns	ns	ns	ns	0.0426
	n									17

EAS: expanded allele size; ρ: Pearson's correlation coefficient; n: paired sample size; ns: not statistically significant ($p>0.05$).

Furthermore, results evidence that the *size of the expanded allele* might also condition SARA and ADL scores, whereas patients' *age of onset* did only correlate with ADL scale (Table 2.2.4). Other independent variables, such as the *size of unexpanded allele* and *BMI* (data not displayed), have apparently no influence in MJD progression and neither are influenced by it (data not shown).

Altogether, by plotting outcomes for functional and cognitive scales/tests against *disease stage* independent variable resulted in an expected inversely correlations, as scores were consecutively lower for patients in later stages of disease (Figure 2.2.5). This is easily understood considering that disease stage is *a priori* determined by the level of probands' physical debilitation, as defined by Klockgether and colleagues (Klockgether et al., 1998). Separately, *disease duration* variable was also disclosed as having a vast impact over multiple clinical scale scores, which at the outset of this study would not be so predictable to be disclosed. Indeed, results suggest that physical ability (SARA and ADL scores) (Figure 2.2.6) but also hand dexterity (CCFS and 9HP DH) and cognitive functionality (MoCA) are highly associated with the number of years of disease progression ($p<0.001$ for all, when plotted against *disease duration*). Inversely, our results failed to confirm the existence of a relationship between the *size of the expanded allele* and any of the clinical but ADL and SARA

scores, as previously mentioned. Nevertheless, considering that AO is determined by the *expanded allele size*, one can admit that the size of the allele is, yet indirectly, influent over the clinical aspects of disease.

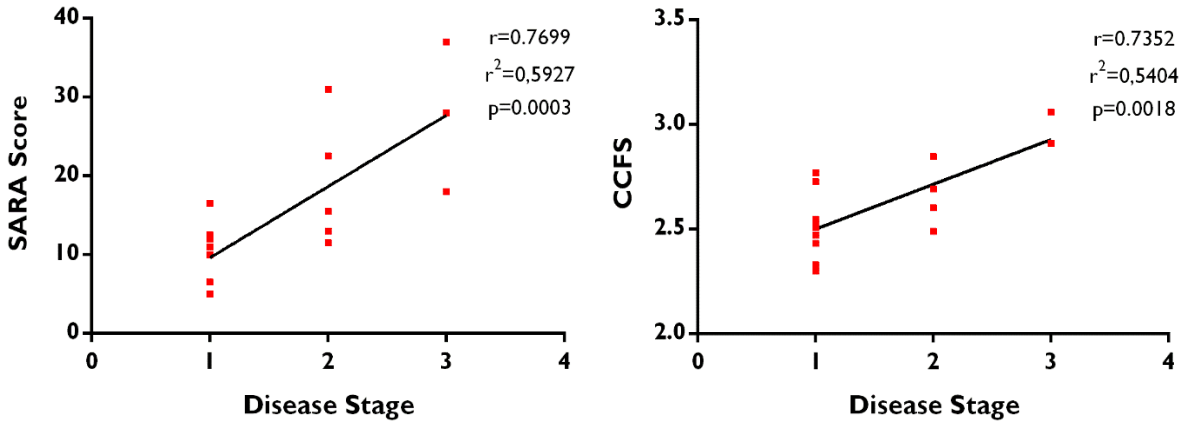

Figure 2.2.4 Disease stage plotted against SARA (on the left) and CCFS scores (on the right). n=17/15; r and p-value were determined by Pearson's correlation test. Plotted line was determined by linear regression analysis. Equations for linear regression lines are: *Y= 9.039X + 0.5833* and *Y= 0.214X + 2.287*, where X is the disease stage level and Y is the SARA score and the CCFS score, respectively.

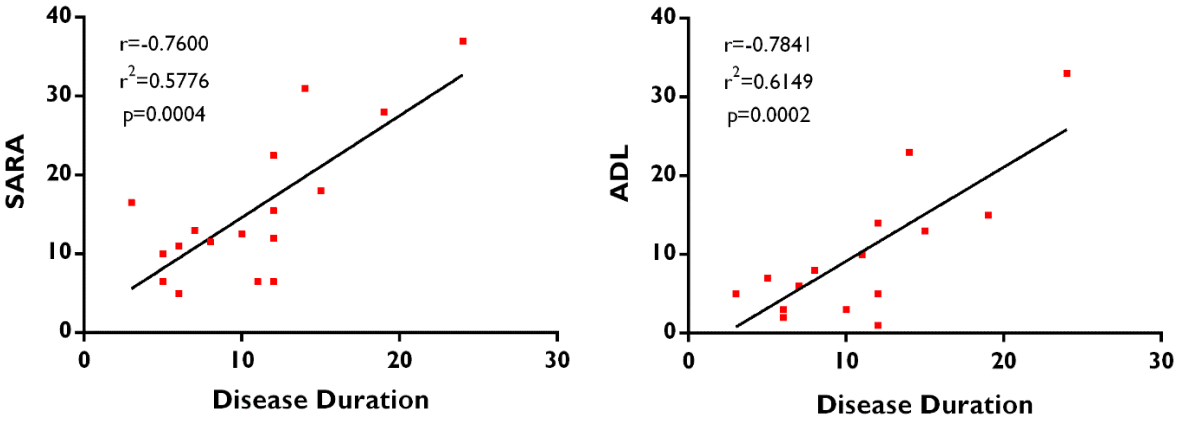

Figure 2.2.5 Disease duration plotted against SARA (on the left) and ADL scores (on the right). n=17; r and p-value were determined by Pearson's correlation test. Plotted line was determined by linear regression analysis. Equations for linear regression lines are: *Y= 1.291X + 1.722* and *Y= 1.194X - 2.776*, where X is the disease duration (in years) and Y is the SARA score and the ADL score, respectively.

2.2.4 Analysis of Self-Rating Questionnaires

In order to explore psychological health state, sleep quality and self-perceived health state, we employed three self-rated questionnaires.

The results for PHQ-9, which allowed us to assess depression severity, were utterly distinct, ranging from 1, *minimal depressed*, to 24, *severely depressed*. Mean score for global study population was 9.7 ± 7.4. Assorting the probands by severity levels of depression, most of them were minimal (n=6) or mildly depressed (n=6) (Figure 2.2.7).

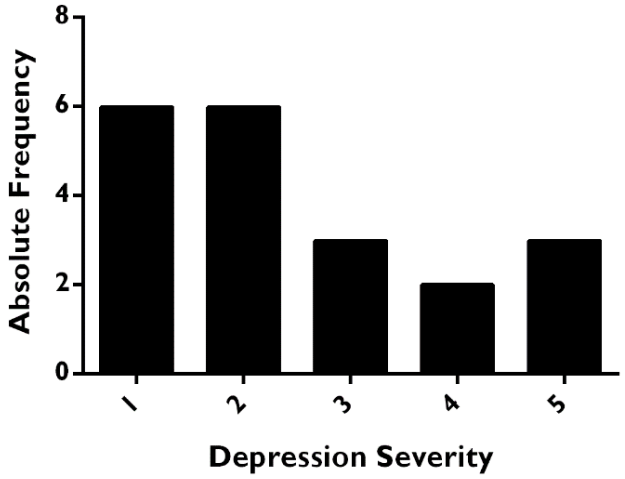

Figure 2.2.6 Probands' depression severity frequency distribution (n=20). 1: minimal depression; 2: mild depression; 3: moderate depression; 4: moderately severe depression; 5: severe depression.

Scores from the other two questionnaires - employed to evaluate probands' self-perception of their sleep quality and health state - were also of a great inconsonance, ranging both from very low to very high results. PSQI mean score for whole study population was 8.1 ± 4.6, ranging from 2 to 17. Scores for this particular questionnaire were indeed very distinct, as only 5 out of the 20 subjects (25%) were considered as having a *good sleep quality* (PSQI < 5). All results obtained from the self-rating questionnaires assessment are provided in Table 2.2.5.

Table 2.2.5 Self-rating questionnaires analysis.

		Disease Stage 1			Disease Stage 2			Disease Stage 3			Global		
		n	Mean ± SD	Range	n	Mean ± SD	Range	n	Mean ± SD	Range	n	Mean ± SD	Range
Self-rating Questionnaires	PHQ-9	9	6.3 ± 5.1	1-17	5	13.2 ± 8.5	2-23	3	18.3 ± 5.5	13-24	20	9.7 ± 7.4	1-24
	PSQI	9	7.8 ± 5.3	2-17	5	9.0 ± 5.4	2-15	3	8.7 ± 2.5	6-11	20	8.1 ± 4.6	2-17
	EQ-VAS	9	71.7 ± 18.2	40-90	5	45.6 ± 19.3	13-65	3	52.3 ± 28.0	20-70	20	63.5 ± 22.4	13-95

2.2.4.1 Influence of Disease-Related Variables on Questionnaire Scores

The plotting of questionnaires scores against disease-related variables revealed only a few putative relationships between them (Table 2.2.6).

Table 2.2.6 Correlation array of disease-related variables versus questionnaire scores.

		PHQ-9	PSQI	EQ-VAS
Disease Stage	**ρ**	0,6323	ns	ns
	p-value	0,0065		
	n	17		
Disease Duration	**ρ**	ns	ns	ns
	p-value			
	n			
EAS	**ρ**	ns	0,5924	ns
	p-value		0,0096	
	n		18	
Age of Onset	**ρ**	ns	ns	ns
	p-value			
	n			

EAS: expanded allele size; ρ: Pearson's correlation coefficient; n: paired sample size.

Data suggests that PHQ-9 scores, i.e. patients' depression severity, is correlated with their own clinical phenotype ($\rho=0.6323$, $p\leq0.01$), indicating that those in later stages of disease are the ones more depressed (Figure 2.2.8). In fact, all three probands corresponding

to the most advanced stage of disease – stage 3, – were classified either as *moderately severe depressed* or *severely depressed*. Of note, results also showed that depression scores seem to be correlated with physical disability/dependency (addressed by ADL scores) (ρ= 0.5170, p=0.0336, n=17, data not shown), similar to what was previously reported by Cecchin and colleagues (Cecchin et al., 2007a). Furthermore, none of the other disease-related variables presented a relationship with the severity of depression (p>0.05).

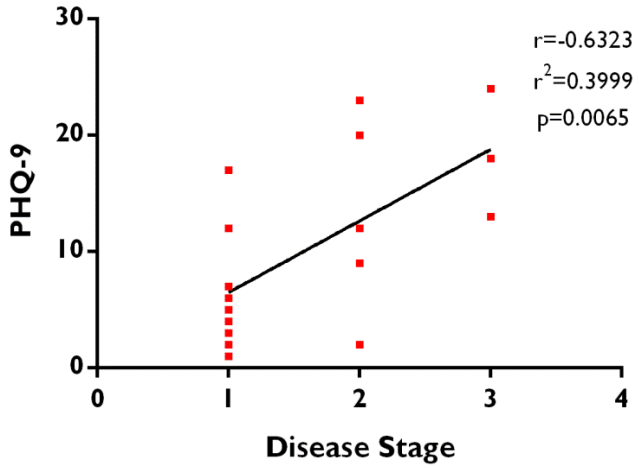

Figure 2.2.7 Disease stage plotted against PHQ-9 score. n=17; r and p-value were determined by Pearson's correlation test. Plotted line was determined by linear regression analysis. Equation for linear regression line is: *Y= 6.155X + 0.333*, where X is the disease stage and Y is the PHQ-9 score.

Concerning sleep quality, results fluctuated between very high and very low scores even among patients in similar stages of disease, therefore it was hard to establish any linking pattern between PSQI scores and other variables. Nevertheless, and somehow unexpected, scores for this questionnaire were apparently correlated with the length of the expanded allele (ρ=0.5924, p=0.0096, n=18, Figure 2.2.9). Despite nothing been published in this context, sleep disorders are of multifactorial etiology and, to eventually establish a connection between *ATXN3* allele length and sleep disorder (or predisposition to them), other aspects would need to be put in question; particularly the existence of other confounding variables, such as the age and the presence of sleep-disrupting symptomatology.

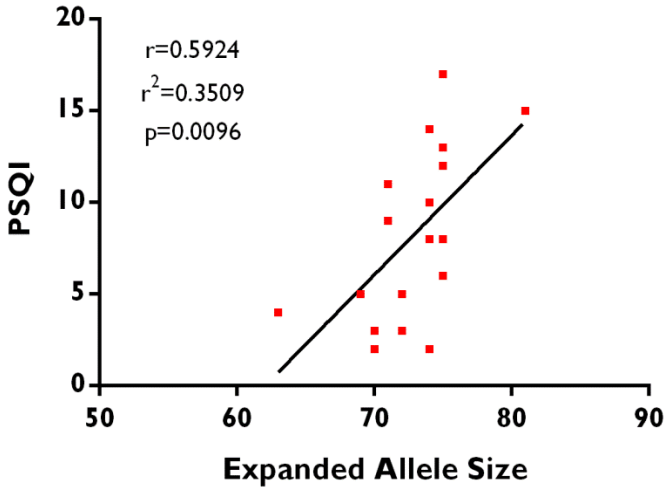

Figure 2.2.8 Expanded allele size plotted against PSQI score. n=18; r and p-value were determined by Pearson's correlation test. Plotted line was determined by linear regression analysis. Equation for linear regression line is: *Y= 0.7601X – 47.15*, where X is the expanded allele size and Y is the PSQI score.

EQ-VAS scores were also of great variance, yet a tendency for patients in earlier disease stages to self-rate their health status higher than other patients (ρ=-0.4385, p=0.0783, n=17, data not shown).

2.2.4.2 Self-Rating Questionnaires Scores Are Conditioned by the Level of Depression Severity

After realizing that clinical and questionnaires scores were not closely related, we sought for a potential interrelationship between the three domains that were self-rated by the study subjects: severity of depression, sleep quality and health state.

Notably, strong correlations were found, particularly involving the level of depression severity: between depression severity and PSQI scores, a strong and very significant correlation was observed (ρ=0.7101, p=0.0005); meanwhile EQ-VAS scores were also correlated with the level of depression severity, although less significantly (ρ=-0.5731, p=0.0083) (Figure 2.2.10).

Contrarily to these findings, no relationship was found between PSQI and EQ-VAS scores (p>0.05).

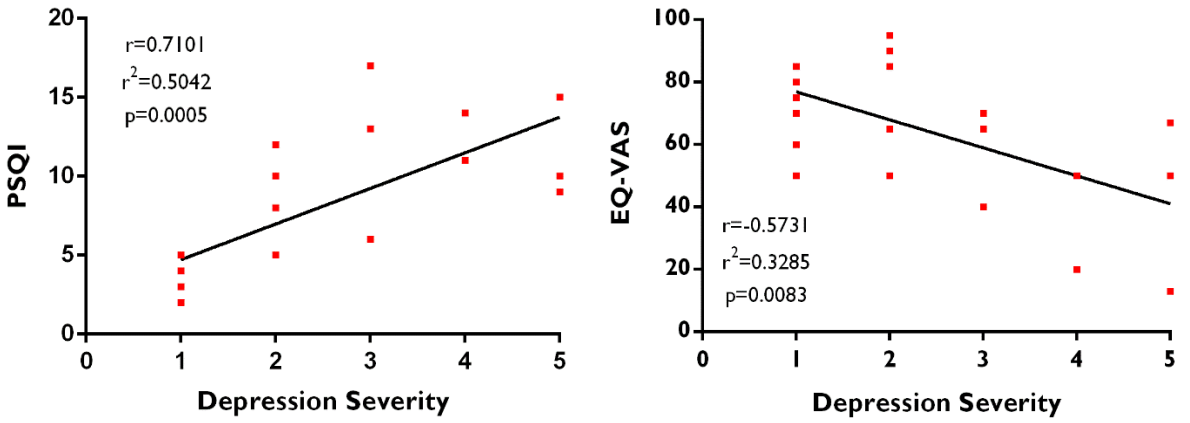

Figure 2.2.9 Depression severity plotted against PSQI (on the left) and EQ-VAS (on the right) scores. n=20; r and p-value were determined by Pearson's correlation test. Plotted line was determined by linear regression analysis. Equations for linear regression lines are: *Y= 2.256X + 2.459* and *Y= -8.974X + 85.94*, where X is the level of depression severity and Y is the PSQI score and the EQ-VAS score, respectively.

2.3 Conclusion

Machado-Joseph Disease is the most common autosomal dominantly-inherited spinocerebellar ataxia worldwide. Therefore it is fundamental to explore genetic, epidemiological, clinical and psychological characteristics underlying this untreatable and ultimately fatal disease. These efforts will improve investigators and physicians' strategies to deal with several aspects of the disease, from diagnosis to disease management. Hereupon, in the present thesis, we performed an extensive epidemiologic, clinical and psychological characterization of a cohort of MJD patients that are currently being followed at *CHUC*.

In conclusion, this study documented the existence of a strong inverse correlation between the expanded allele length and the age of symptoms onset. Other statistically significant correlations were found, suggesting that variables such as *disease stage* and *disease duration* are determinant concerning patients' clinical evolution. Worth mentioning, mood disorder (addressed by level of depression severity) apparently compromises sleep quality of the probands, yet the vice-versa might also be true. Furthermore, results make clear that cerebellar function is utterly affected, as all probands exhibited cerebellar features upon medical examination. Moreover, visual impairments are also of great frequency, particularly nystagmus. We expose several correlations between disease-related variables and clinical characteristics of the disease. Furthermore, we scrutinized psychological parameters of the disease and sought for eventual relationships that could explain differences between patients.

Generally, this study, based on results obtained from baseline medical examination and interview procedures, creates a background for this specific study population and will be useful towards the understanding of disease evolution.

Altogether, most of the results here presented and discussed are consistent with previous reports. Importantly, many of these, particularly the results obtained from the self-rating questionnaires, although granting essential information, have to be carefully interpreted as given answers are highly susceptible of being biased by many external variables. Also, in this study, when comparing and plotting values, we did not take into account confounding variables such as gender, age, taken medication, comorbidities, among others, which obviously can influence/distort results.

CHAPTER 3

Quantification of *Trans*-Resveratrol and Conjugated Metabolites in Plasma and Brain Tissue of Mice by HPLC-MS/MS Methodology

3.1 Methods

3.1.1 Experimental Methodology

3.1.1.1 Chemical and Reagents

- Resveratrol, purity: >99%. Sigma-Aldrich®.
- Dimethyl sulfoxide (DMSO). Sigma-Aldrich®.

3.1.1.2 Animals

A C57Bl/6-background transgenic MJD mouse model – generated by expressing the N-terminal-truncated human ataxin-3 with 69 glutamine repeats (69Q) and an N-terminal hemagglutinin (HA) epitope driven by a L7 promoter specifically in cerebellar Purkinje cells, – and their wild-type littermates were obtained from backcrossing heterozygous males with C57Bl/6 females, in accordance with what was previously set up in our group (Nascimento-Ferreira et al., 2013). The colony from where these animals were obtained is established at the animal holding facility of the Center for Neurosciences and Cell Biology of University of Coimbra. Genotyping was performed by PCR analysis of DNA collected from ears.

Until the start of study procedures, animals were kept in a room with monitored temperature and humidity conditions and maintained under the conventional 12h light/dark cycle photoperiod. Water and food were available *ad libitum*.

3.1.1.3 Animal Randomization, Treatment and Sample Collection

Animals were randomly distributed into four groups (n=5/6), corresponding to the four time-points *a priori* established for our analysis. All mice were weighted and administered intraperitoneally (i.p.) a single resveratrol (10 mg/kg) injection. The vehicle was DMSO diluted in a saline solution (25:75, v/v) and the dose volume was approximately 50 µL, adjusted to each mouse body weight. After administration, mice were anesthetized and sacrificed at 2.5, 5, 10 and 30 minutes (the four time-points) post-dosing. Blood samples were collected by cardiac puncture and plasma was obtained by centrifugation (1500g, 10 minutes, room temperature). Brain was excised and washed from superficial contaminating blood residues with a saline solution, snap-frozen in liquid nitrogen and then stored at -80

°C until analysis. An additional control group (n=2) was treated only with vehicle, whereas afterward procedures were equal to those who received resveratrol.

3.1.1.4 Compounds Extraction from Plasma and Brain

Analytes were isolated from plasma by a protein precipitation method. To 10 µL of plasma sample, 100 µL of 70% ACN was added and vortexed. Then, to help proteins aggregate, the resulting sample was centrifuged at 14,000 x g for 20 minutes at room temperature. The supernatant was collected into a vial.

Concerning brain samples preparation, after weighing, a previously prepared solution of 5 mM ammonium acetate in 60% ACN was added in a proportion of 9/1 (volume/brain weight) and homogenised by grinding. From the previous homogenised brain, only 100 µL was used to perform a similar centrifugation to that used for plasma samples. At last, supernatant was collected into a vial.

3.1.2 Analytical Methodology

3.1.2.1 Standards and Reagents

Standards:

- *Trans*-resveratrol, purity: 98%. Toronto Research Chemicals, Inc.®;
- *Trans*-resveratrol-(4-Hydroxyphenyl-$^{13}C_6$), purity: 98%. Sigma-Aldrich®;
- *Trans*-resveratrol-3-*O*-β-D-glucuronide, purity: 97.23%. Toronto Research Chemicals, Inc.®;
- *Trans*-resveratrol-3-sulfate Sodium Salt, purity: 96.76%. Toronto Research Chemicals, Inc.®.

Reagents:

- Acetonitrile (ACN), LC grade. Fischer Chemical®;
- Water, LC grade. Fischer Chemical®;
- Formic Acid (FA), LC grade. Amresco®;
- Methanol (MeOH), LC grade. Fischer Chemical®;
- Ammonium Acetate, LC grade, VWR International®.

3.1.2.2 Liquid Chromatography Coupled to Tandem Mass Spectrometry (LC-MS/MS): A Brief Explanation of the Methodology

Liquid chromatography coupled to tandem mass spectrometry (LC-MS/MS) is an analytical chemistry technique that combines the capabilities of the individual techniques that constitute it, by so allowing to a more definite identification and quantitative determination of compounds that have similar chromatographic retention characteristics but different mass spectra (Ardrey, 2003).

In liquid chromatography, substances are physically separated depending on their affinity towards the used stationary phase and compound identification is based on the time they take to elute from the chromatographic column or, in the other way around, on their retention time (RT). In reversed-phase chromatography (a widely used chromatographic mode based on the hydrophobicity of compounds) the stationary phase is a nonpolar matrix and the mobile-phase is a polar solvent (the most common solvents used are acetonitrile, water, methanol) (Ardrey, 2003), and therefore the interaction between analytes and stationary phase has a predominantly hydrophobic (apolar) character. Thereby, the more polar the analyte is, the little its RT will be. In any case, RTs can be controlled by applying elution gradients to the mobile-phase composition as the separation progresses, instead of using an isocratic delivery where the mobile composition remains unaltered for the entire analysis.

In mass spectrometry, the analytes, transferred by an inlet system, are firstly ionized in an ionization chamber, either in positive or negative ionization modes, resulting in protonated, $[M+H]^+$, and deprotonated molecular ions, $[M+H]^-$, respectively (Dass, 2007). Resulting molecular ions are separated by a mass analyser according to their mass-to-charge ratio (m/z) using static or dynamic electric and magnetic fields, either alone or in combination (Hoffmann and Stroobant, 2007), before reaching the detector that produces a current proportional to the number of ions arriving, measuring and amplifying it (Dass, 2007). At last, the data system records, processes and displays the data of the analysis. Importantly, the whole analysis is operated under a vacuum system allowing ions produced in the ionization chamber to freely run without interacting with air (or other species) molecules (Dass, 2007). Figure 3.1.1 schematically represents this methodology.

In this thesis, the analytical technique used for the quantification of resveratrol and its metabolites in plasma and brain matrices was LC-MS/MS.

What differs between basic mass spectrometry and tandem mass spectrometry (MS/MS) is that the last has one additional step involving mass analysis (referred to as mass spectrometry 2, MS2) which, in conjugation with a ion fragmentation occurring in between the two mass analysis stages, improves both the selectivity and sensitivity of the method.

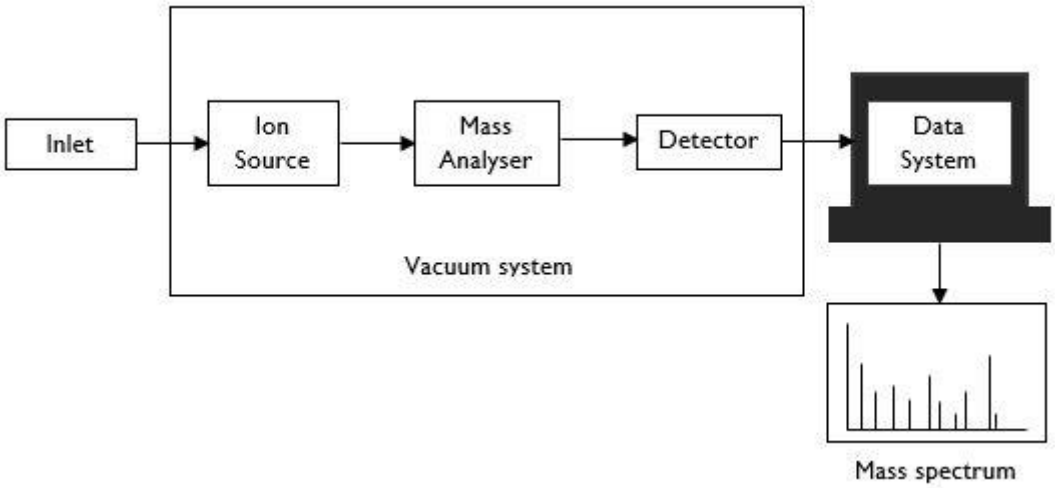

Figure 3.1.1 Schematic representation of the basic components of a mass spectrometer. The inlet system transfers the sample into the ion source, which converts the neutral sample molecules into gas-phase ions. The mass analyser separates and mass-analyses the ionic species and the detector measures and amplifies the ion current of mass-resolved ions. At last, the data system records, processes, stores and displays data to the mass spectrometer user. Adapted from (Dass, 2007).

Summarily, the concept of MS/MS involves two mass spectrometry systems, in this case two quadrupole analysers, Q1 and Q3. The first quadrupole analyser (MS1/Q1) selects a precursor ion with the desired m/z from the stream of ions obtained from the ion source; then, in an intermediate collision cell (quadrupole 2, q2), the fragmentation of the previously mass-selected ion occurs; after that, the resulting fragments are transmitted to the second MS system (MS2/Q3), which performs another mass analysis and again a m/z ion selection, prior to fragments reaching the detector (Dass, 2007) (Figure 3.1.2).

As this technology permits the detection and quantification of compounds, even if at residual concentrations in biological matrices, with extraordinary specificity and very strong sensitivity, it has become a convenient and very popular tool in the field of bioanalysis, namely in proteomics, metabolomics, forensics and drug development studies.

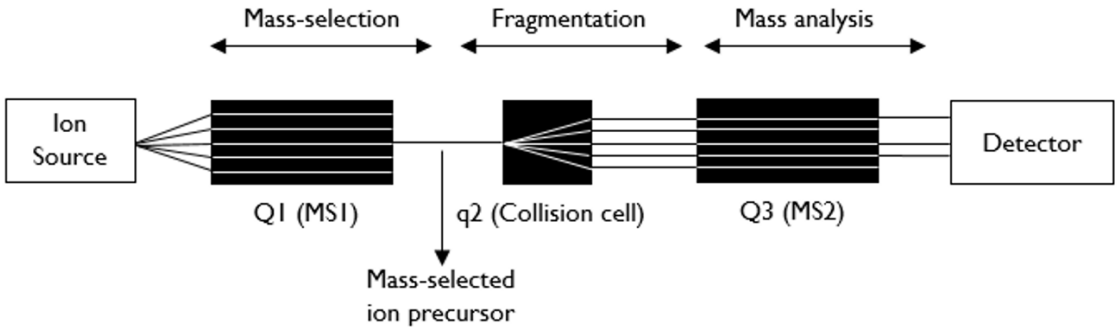

Figure 3.1.2 Basic principles of tandem mass spectrometry. Schematic representation adapted from (Ardrey, 2003; Dass, 2007).

3.1.2.3 Instrumental Conditions

The LC-MS/MS assay was performed on a LC Nexera system (Shimadzu) equipped with a CTC PAL autosampler (Eksigent) coupled to a hybrid triple quadrupole/linear ion trap 4000 mass spectrometer (ABSciex). Data acquisition was performed by Analyst® version 1.6.2 (ABSciex).

3.1.2.3.1 Liquid Chromatography

HPLC analysis consisted in a reversed-phase chromatographic separation carried out using a Phenomenex® Kinetex F5 2.6 µm (50 x 2.1 mm, 100 Å) column set at 40 °C. Security Guard™ cartridge Polar-RP (4 x 2 mm) was also used to protect the column by trapping contaminants and particulates.

In order to achieve an efficient separation of the analytes, an elution gradient composed of 0.1% formic acid in H_2O (phase A) and 0.1% formic acid in acetonitrile (phase B) was developed, as represented in Table 3.1.1. The flow rate was maintained at 250 $\mu L.min^{-1}$ and the injection volume was 10 µL. Total running time for each sample was 8 minutes.

Between samples a blank (ACN) was injected with a gradient (see Table 3.1.1) in order to perform cleaning and re-equilibration steps of the column. In addition, between different batches, three blanks (ACN) were introduced, with the same running program of the sample.

Table 3.1.1 Elution gradient used for chromatographic analysis.

Running program	Time (min)	Mobile phase (%, v/v)	
		Phase A	Phase B
Sample	0.01	98	2
	1	40	60
	4	5	95
	6	5	95
	6.1	98	2
	8	98	2
Blank	0.01	98	2
	1	5	95
	2	5	95
	2.5	98	2
	6	98	2

3.1.2.3.2 Mass Spectrometry

Prior proceeding to biological samples analysis, a method development was performed in order to adjust various instrumental parameters, such as the electrospray ionization (ESI) and the declustering potential conditions, and also to establish an ideal collision energy for each compound's fragmentation, concerning an optimized performance of the analytical method.

This method development consisted in a direct injection into the mass spectrometer of a freshly prepared standard solution of resveratrol-3-glucuronide in a concentration of 2.0 µM, and of resveratrol-3-sulfate in a concentration of 0.22 µM. Optimized values for trans-resveratrol and internal standard, trans-resveratrol-4-hydroxyphenyl-$^{13}C_6$, were already established from a previous experiment.

An ESI turbo V™ ion spray interface operating in negative ion mode was used as the ion source. All source-dependent settings were optimized to maximize ion gain. The tuning parameters were: curtain gas (CUR), 30 psi; ion source gas 1 (GS1), 30 psi; ionic spray voltage (IS), 4,500 V; and source temperature, 450 °C. Nitrogen was used as the curtain and collision gas and air was used as the ion source gas.

To identify and monitor the analytes of interest and internal standard (resveratrol-4-hydroxyphenyl-$^{13}C_6$), the MS/MS system was operated in Multiple Reaction Monitoring (MRM) scan mode. The different values of declustering potential (DP), collision energy (CE), collision exit potential (CXP) for each MRM transmission of each analyte were automatically optimized for maximum sensitivity using Analyst® software and can be conferred on Table 3.1.2.

Table 3.1.2 MS/MS acquisition parameters for each transition of each analyte and internal standard.

Compound	Transitions (m/z) Q1	Q3	DP (eV)	CE (eV)	CXP (eV)
***Trans*-resveratrol**	226.7	142.6	-65	-36	-1
		182.5		-28	-13
		184.6		-26	-3
Resveratrol-3-sulfate	306.9	142.9	-45	-54	-9
		185.2		-44	-7
		226.8		-28	-9
Resveratrol-3-glucuronide	403.2	113.1	-65	-24	-5
		175.0		-18	-13
		227.0		-36	-1
Internal Standard	232.9	148.7	-95	-36	-9
		188.8		-26	-9
		190.8		-28	-9

Other operational parameters were established as follows: dwell time, 50 ms; entrance potential (EP), 10 eV; collision gas (CAD), 3 psi.

All data was processed using Multiquant™ 2.1.1 software (ABSciex).

3.1.3 Method Validation

The quantitative determination of a drug and respective metabolites in biological samples using analytic methodology is extremely important regarding further understanding of its pharmacokinetics, bioavailability and/or disposition. However, since only reliable and reproducible results can be satisfactory interpreted, it is essential to employ well-characterized and fully validated analytical methods conducive to yield trustworthy outcomes out of it (Shah et al., 2000).

Taking that into account, in behalf of proving that our method was adequate and our results met quality and applicability criteria, we performed a validation assessment over few parameters. Noteworthy, blank plasma and brain tissue used in validation tests were obtained from mice that did not receive *trans*-resveratrol, or any other analyte.

3.1.3.1 Recovery

To evaluate the recovery, two aliquots of 10 µL of blank plasma (each one in triplicate) were spiked either before or after extraction procedure as follows:

- One aliquot of blank plasma was spiked with 10 µL of a mix solution (containing trans-resveratrol, resveratrol-3-glucuronide, resveratrol-3-sulfate and the internal standard) and then subjected to the extraction procedure (see 3.1.1.3). At last, 100 µL of the supernatant was collected – *spiked before extraction procedure* aliquot;
- To the other aliquot was added 10 µL of 70% ACN (in order to obtain the same final volume); then the sample was subjected to the extraction procedure and, after that, 100 µL of supernatant was collected, and finally spiked with 10 µL from the very same mix solution – *spiked after extraction procedure* aliquot.

The aliquots to which the mix solution was added after the extraction procedure (the *spiked after procedure* aliquots) represent a theoretical 100% recovery from the sample. Therefore, recovery is obtained by calculating the ratio between the mean of peak areas for *spiked before extraction procedure* aliquots ($\bar{A}_{SBP}$) and the mean of peak areas for *spiked after extraction procedure* aliquots ($\bar{A}_{SAP}$), for each analyte, as defined by the following equation:

$$\%Recovery = \left({\bar{A}_{SBP}}/{\bar{A}_{SAP}} \right) * 100$$

For brain matrix, recovery tests were not performed.

3.1.3.2 Matrix Effect

Along with the recovery test, the matrix effect was also evaluated. To do so, one additional aliquot (in triplicate) of the standard mix solution was prepared with equivalent concentration to the *spiked after procedure* aliquot and used as the comparator.

The prepared mix solution, since it was not spiked into the matrix, represent a theoretical zero influence of the matrix over the obtained analytical result. Therefore, matrix effect can be defined by calculating the difference of responses between *spiked after procedure* aliquot ($\bar{A}_{SAP}$) and *standard mix solution* aliquot ($\bar{A}_{SMS}$), divided by the *standard mix solution* aliquot response, as defined by the equation:

$$ME = {(\bar{A}_{SAP} - \bar{A}_{SMS})}\Big/{\bar{A}_{SMS}}$$

Importantly, matrix can either have a positive or a negative result: the first indicating an enhancement of the obtained signal, whereas the negative meaning that matrix supresses the analyte signal. In this assessment, a zero value represents no matrix effect.

Again, for brain matrix, this parameter validation was not executed.

3.1.3.3 Linearity

To gauge the linearity of the method, blank plasma samples were spiked with known increasing concentrations of each analyte. Accordingly: for *trans*-resveratrol, we ran 9 samples with concentrations ranging from 0.025 to 1.2 µM; for resveratrol-3-glucuronide, 9 samples with concentrations comprehended between 0.005 and 0.800 µM; and for resveratrol-3-sulfate, 9 samples with concentrations encompassed between 0.001 and 0.3 µM. Each prepared aliquot was also fortified with a spiking of IS at 0.38 µM, in order to correct losses of the compound during sample preparation or injection.

To assess the linearity in brain tissue, calibration curves were obtained by similar method and concentration range of those previously described to plasma samples.

Calibration curves were constructed by plotting acquired peak areas for each sample versus respective analyte nominal concentrations.

3.2 Results and Discussion

3.2.1 Fragmentation Mass Spectra

After method optimization (described in 3.2.3), fragmentation mass spectra for each analyte was available allowing the selection of the ideal product ions (usually this choice is based on the intensity of the product ions and their m/z ratio).

Fragmentation mass spectra of *trans*-resveratrol had the most intense peak for a compound with m/z of 227, which in fact correspond to the intact *trans*-resveratrol molecule. All other peaks observed in the spectra register the intensity of ion products resulting from the fragmentation of the *trans*-resveratrol molecule. From all of them, the chosen to monitor *trans*-resveratrol were those with m/z of 185, 183 and 143 (Figure 3.2.1).

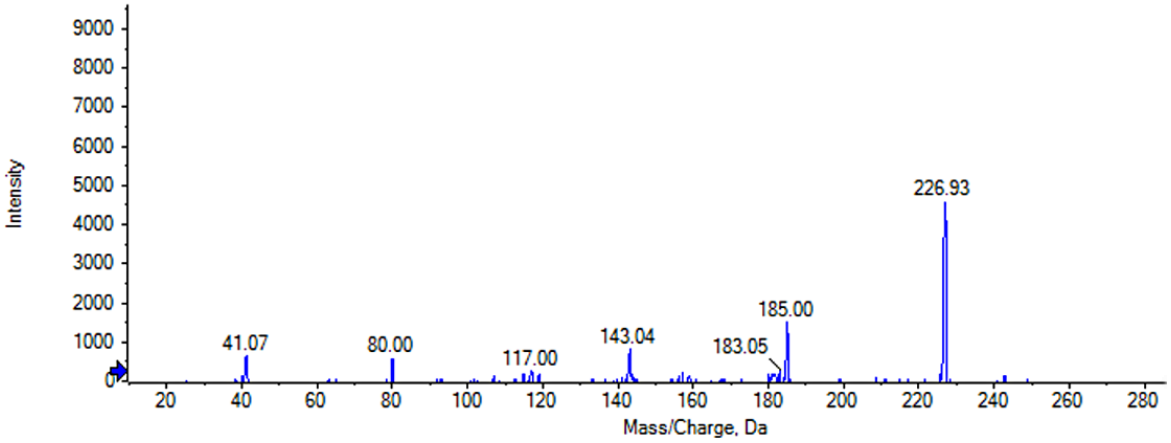

Figure 3.2.1 Mean fragmentation mass spectra of* trans-*resveratrol. CE ramped from -124 to -14V.

For resveratrol-3-glucuronide, the most intense peak was again the non-fragmented molecule (m/z, 404). Fragments with m/z of 227, 175 and 113 were the three chosen to monitor this analyte (Figure 3.2.2).

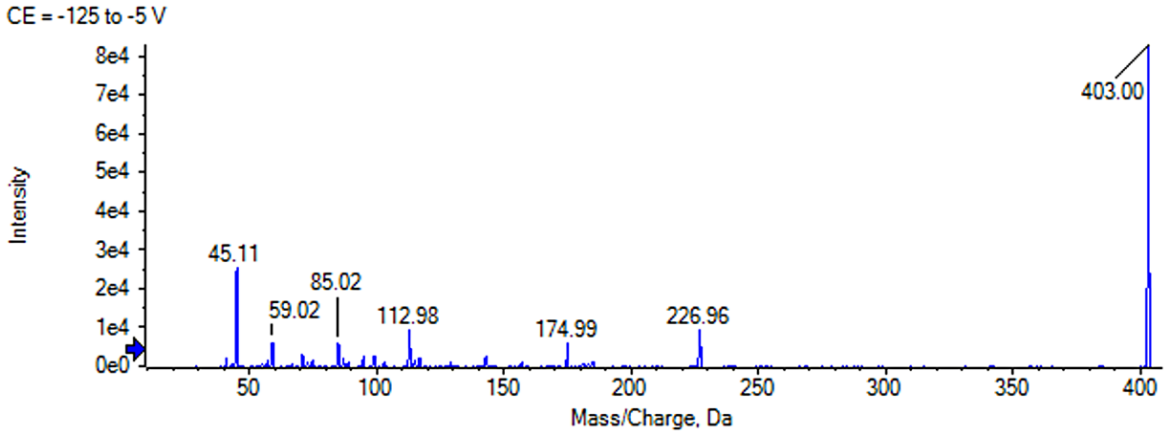

Figure 3.2.2 Mean fragmentation mass spectra of resveratrol-3-sulfate. CE ramped from -125 to -5V.

Regarding resveratrol-3-sulfate, the peak for the intact molecule (m/z, 330) was observed with the highest signal intensity. The chosen fragments to monitor this molecule were the ones with corresponding m/z of 227, 185 and 143 (Figure 3.2.3).

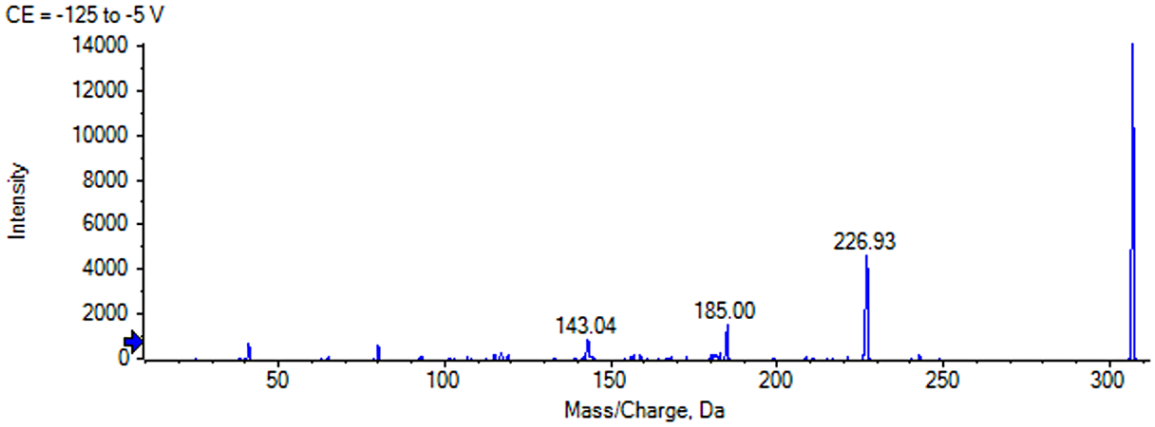

Figure 3.2.3 Mean fragmentation mass spectra of resveratrol-3-glucuronide. CE ramped from -125 to -5V.

Fragmentation spectrum obtained for the internal standard was similar to that of *trans*-resveratrol. In fact, this was predictable since the only thing that distinct the two molecules is that the carbons from one phenol ring are substituted by carbon-13 isotopes in the IS molecule, making a subtle difference - yet detectable by mass spectrometry, - in the values of molecular weight. The most intense peak was verified for the intact molecule (m/z, 232). The fragments with corresponding m/z of 190, 189 and 149 were chosen to monitor the internal standard in further analysis (Figure 3.2.4).

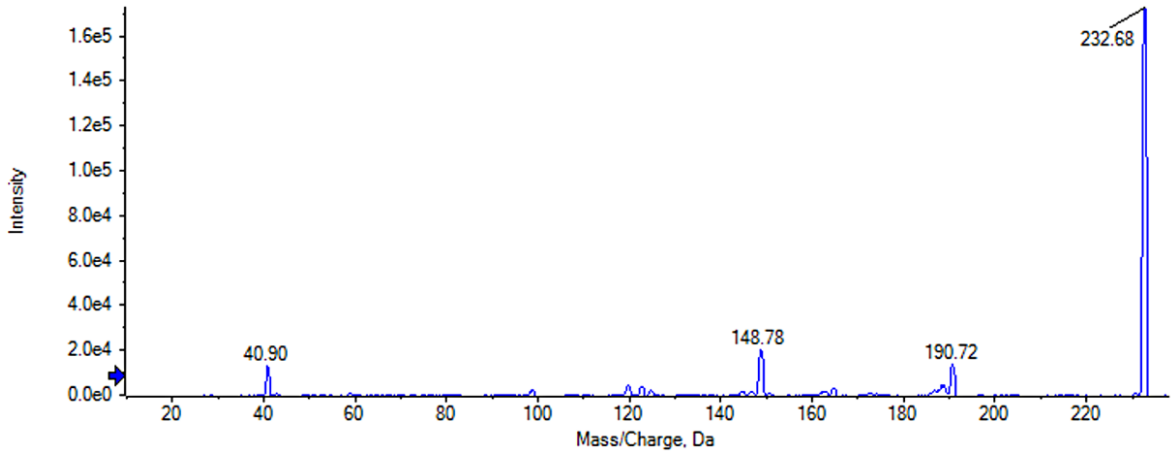

Figure 3.2.4 Mean fragmentation mass spectra of internal standard. CE ramped from -128 to -5V.

3.2.2 Method Validation

3.2.2.1 Recovery

The extraction recovery of the analytes was conducted in mice plasma samples by comparing the peak areas (in triplicate) of the stock analytes added before extraction procedure, to the peak areas of the stock analytes added to an already prepared sample, using the same concentrations for each analyte. Of note, recovery was only assessed for a single concentration. In Figure 3.2.5 are presented representative spectra with peak areas for *trans*-resveratrol and resveratrol-3-glucuronide. Similar chromatographic spectra were obtained for the other two analytes (data not shown).

Trans-resveratrol

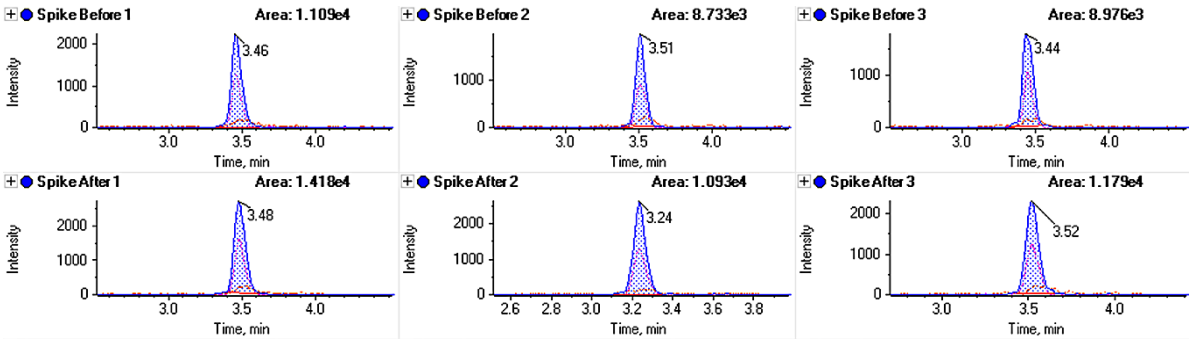

Resveratrol-3-glucuronide

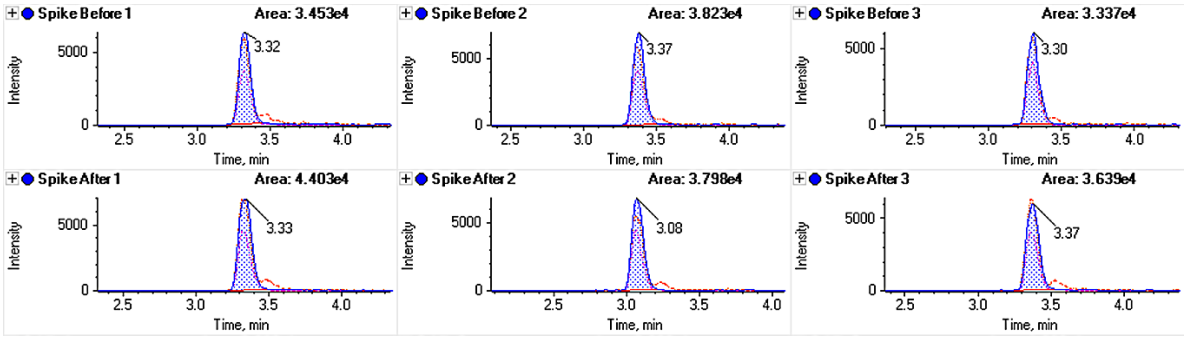

Figure 3.2.5 Recovery assessment for trans-resveratrol (first two lines) and resveratrol-3-glucuronide (third and fourth line).

The extraction recoveries were estimated ranging between 74.90% and 89.64%. Importantly, these values are within acceptable criteria established for this type of analysis (70-120%). All data obtained is shown in Table 3.2.1.

Table 3.2.1 Recovery of analytes in plasma samples.

	Sample	*Trans*-resveratrol	Resv-3-gluc	Resv-3-sulf	Internal Standard
Spike Before (peak area)	#1	11093.65	34532.05	305335.30	24281.53
	#2	8733.26	38225.93	286472.03	18870.20
	#3	8976.46	33368.92	288082.56	19768.58
	Mean	9601.12	35375.64	293296.63	20973.44
Spike After (peak area)	#1	14177.06	44034.94	358996.20	35936.56
	#2	10933.42	37975.09	307276.82	22247.73
	#3	11791.60	36388.68	339334.31	25821.35
	Mean	12300.69	39466.24	335202.44	28001.88
	% Recovery	78.05	89.64	87.50	74.90

Resv: resveratrol; gluc: glucuronide; sulf: sulfate

3.2.2.2 Matrix Effect

Matrix effect was evaluated by correlating the peak areas obtained for each analyte when added to a sample extract with those obtained for the same analytes in the same concentrations when prepared directly in a pure mobile phase solution.

Analytical responses for resveratrol-3-sulfate and for internal standard are displayed below, in Figure 3.2.6. Similar spectres were acquired for the other analytes, yet not being presented here.

Resveratrol-3-sulfate

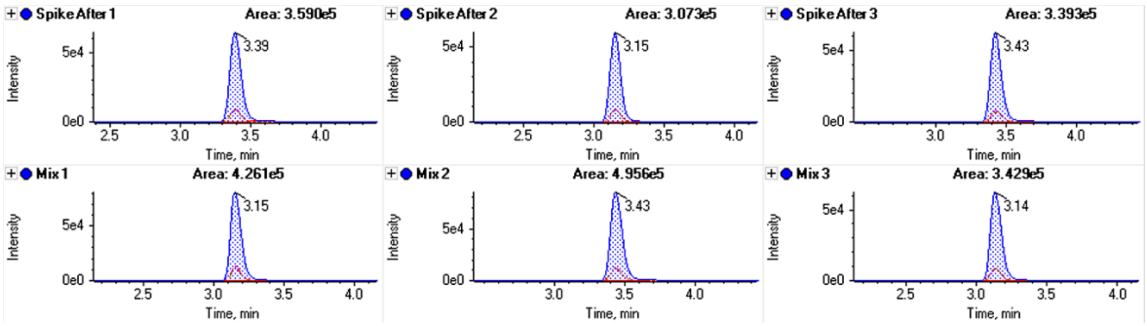

Internal Standard

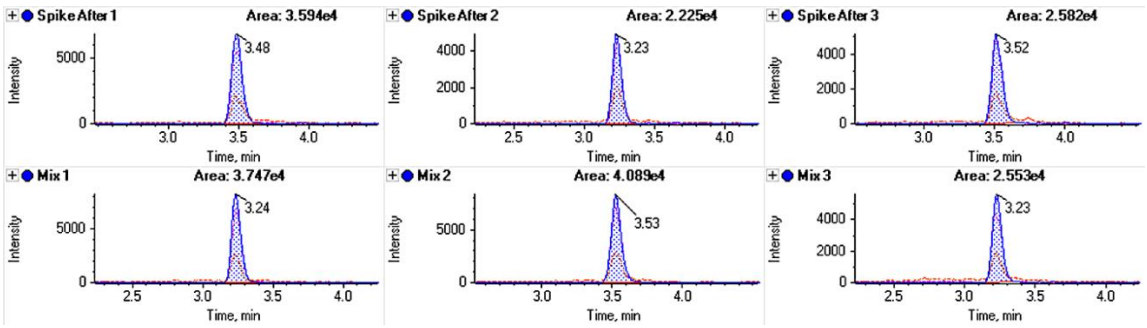

Figure 3.2.6 Matrix effect assessment for resveratrol-3-sulfate (first two lines) and internal standard (third and fourth line). Only one assay, in triplicate and in one concentration, was performed.

Overall, plasma matrix effect (Table 3.2.2) was within acceptable values, rounding 20% of signal suppression for *trans*-resveratrol, resveratrol-3-sulfate and internal standard. Plasma matrix had higher impact over resveratrol-3-glucuronide, where 33.57% signal suppression was observed.

Table 3.2.2 Plasma matrix effect.

	Sample	*Trans*-resveratrol	Resv-3-glucuronide	Resv-3-sulfate	IS
Spike Before (peak area)	#1	14177,06	44034,94	358996,20	35936,56
	#2	10933,42	37975,09	307276,82	22247,73
	#3	11791,60	36388,68	339334,31	25821,35
	Mean	12300,69	39466,24	335202,44	28001,88
Standard Mix (peak area)	#1	15619,40	63083,06	426104,31	37471,32
	#2	18192,45	68884,10	495633,17	40885,76
	#3	13381,70	46275,62	342922,35	25531,67
	Mean	15731,18	59414,26	421553,27	34629,58
	% Matrix Effect	**-21,81**	**-33,57**	**-20,48**	**-19,14**

IS: Internal standard.

3.2.2.3 Linearity

3.2.2.3.1 Analysis of Linearity in Plasma Samples

In plasma, linearity was assessed by plotting obtained areas against respective standard nominal concentration for each sample. Calibration curves were produced using a linear regression weighted 1/x and coefficient of determination, r^2, was calculated. Calibration curves for *trans*-resveratrol, resveratrol-3-glucuronide and resveratrol-3-sulfate are displayed in Figure 3.2.7, Figure 3.2.8 and Figure 3.2.9, respectively.

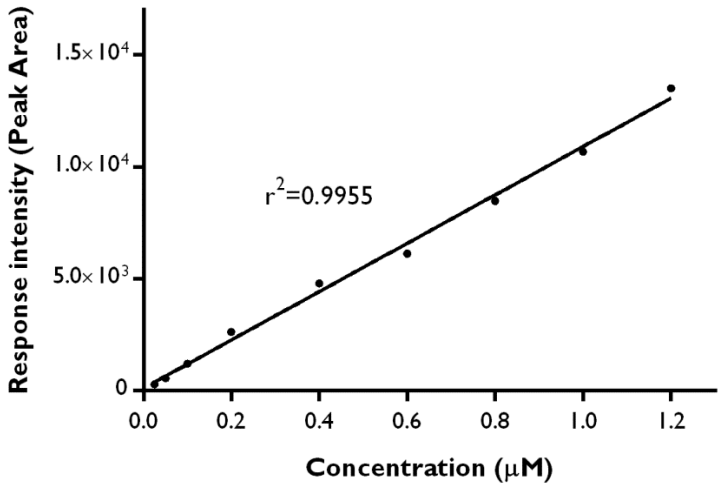

Figure 3.2.7 Calibration curve for trans-resveratrol, in plasma.

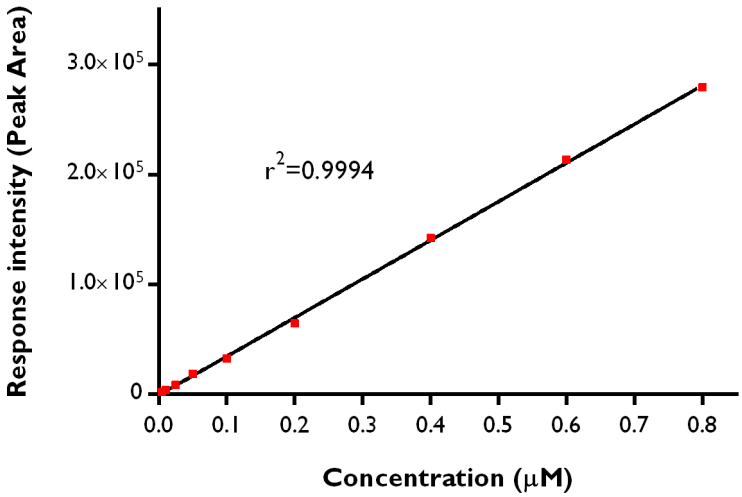

Figure 3.2.8 Calibration curve for resveratrol-3-glucuronide, in plasma.

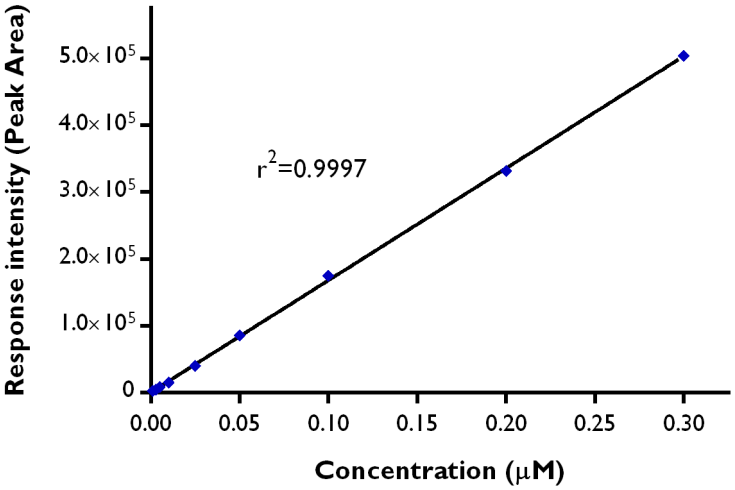

Figure 3.2.9 Calibration curve for resveratrol-3-sulfate, in plasma.

Overall, considering that all r^2 values were greater than 0.995 (Figures 3.2.7-3.2.9), calibration curves show satisfactory linearity over the concentration range stipulated for each analyte.

3.2.2.3.2 Analysis of Linearity in Brain Samples

In brain samples, linearity was assessed by plotting the result from the ratio between analyte/internal standard peak areas, versus nominal concentration of each stock analyte. Again, calibration curves were produced using a linear regression weighted 1/x and r^2 was

calculated. Importantly, calibrators with accuracy below 80% or above 120% were excluded, in order to achieve a more reliable curve. Obtained calibration curves for *trans*-resveratrol, resveratrol-3-glucuronide and resveratrol-3-sulfate, in brain samples, are represented in Figure 3.2.10, Figure 3.2.11 and Figure 3.2.12, respectively.

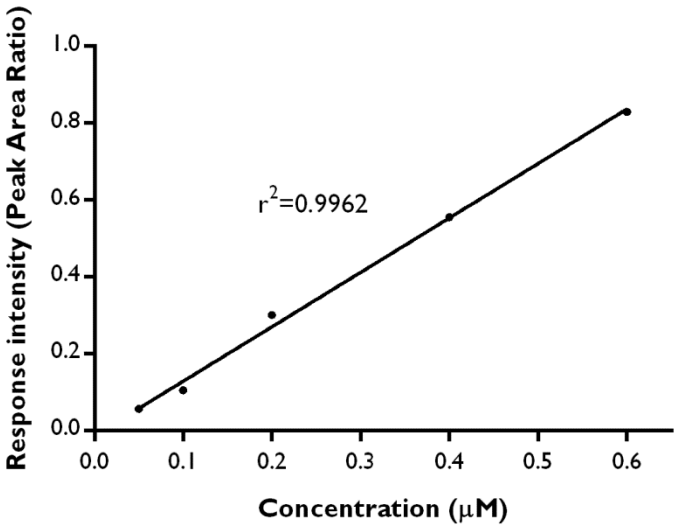

Figure 3.2.10 Calibration curve for* trans-*resveratrol, in brain samples.

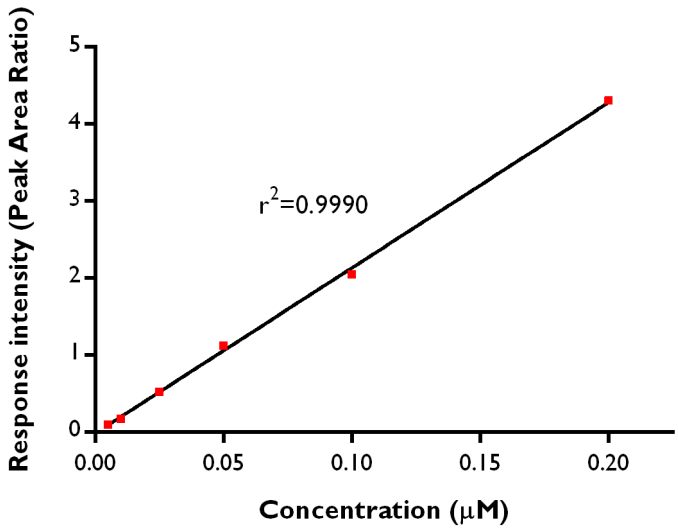

Figure 3.2.11 Calibration curve for resveratrol-3-glucuronide, in brain samples.

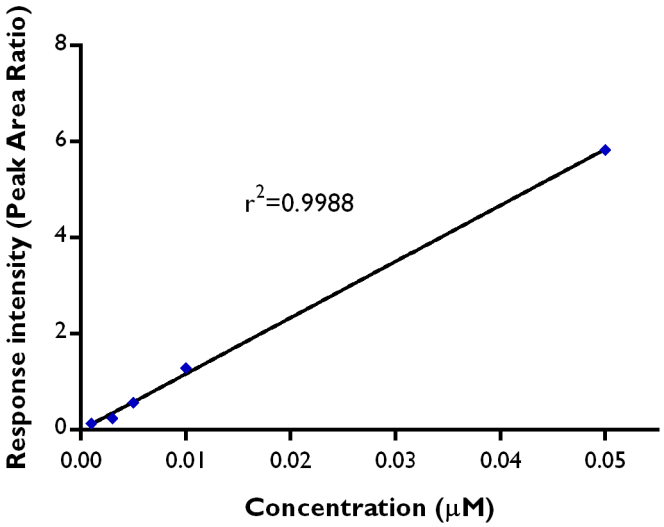

Figure 3.2.12 Calibration curve for resveratrol-3-sulfate, in brain samples.

As coefficient of determination (r^2) values were always greater than 0.995, revealing a good fit between data and regression line, we assume that linearity for all calibration curves was suitable.

3.2.4 Resveratrol and Metabolites Quantification

3.2.4.1 Analytes Levels in Plasma Samples

Mean plasma concentration versus time profiles for *trans*-resveratrol and its metabolites is portrayed in Figure 3.2.13.

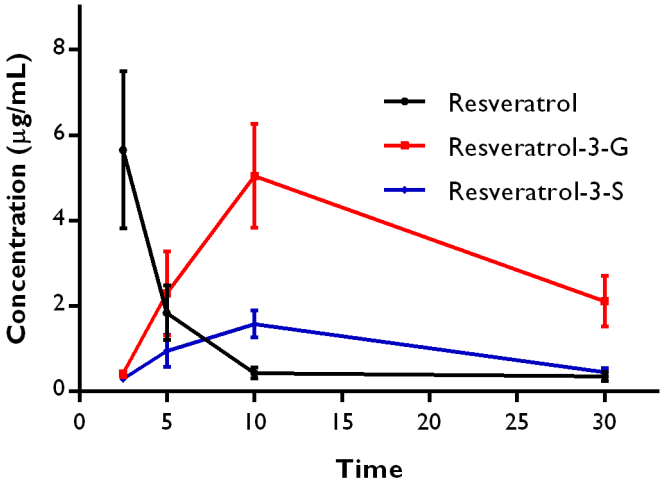

Figure 3.2.13 Plasmatic concentrations of the three analytes after i.p. administration of 10 mg/kg of trans-resveratrol. Results are expressed as mean ± standard error of the mean (SEM).

Results for the first time-point samples show that *trans*-resveratrol aglycone is the main compound in plasma, being present in a concentration of 5.65 ± 1.84 μg.mL^{-1} (mean ± SEM, n=6). At this time, concentrations of the metabolites were residual: resveratrol-3-glucuronide displayed was present at 0.42 ± 0.09 μg.mL^{-1} (n=6), whereas resveratrol-3-sulfate was estimated at 0.29 ± 0.03 μg.mL^{-1} (n=6) (Figure 3.2.13).

In the second time-point (t=5 mins), *trans*-resveratrol concentration decreased abruptly. On the contrary, metabolites concentrations increased by approximately 5-(glucuronide) and 3-fold (sulfate). Concentration values for *trans*-resveratrol, resveratrol-3-glucuronide and resveratrol-3-sulfate were, at this time, 1.84 ± 0.63 μg.mL^{-1} (n=4), 2.30 ± 0.99 μg.mL^{-1} (n=4) and 0.95 ± 0.37 μg.mL^{-1} (n=4), respectively (Figure 3.2.13).

Samples collected 10 minutes post *trans*-resveratrol administration revealed peaks for maximum concentrations (C_{max}) for the two conjugated metabolites. By that time, both resveratrol-3-glucuronide (5.05 ± 0.63 μg.mL^{-1}, n=4) and resveratrol-3-sulfate (1.58 ± 0.32 μg.mL^{-1}, n=4) were at higher concentrations than the parent compound (0.43 ± 0.12 μg.mL^{-1}, n=2). Worth mentioning, from the 4 analysed samples, 2 peak areas for *trans*-resveratrol were considered outliers and, therefore, excluded from analysis.

At the last evaluated time-point, all analyte concentrations were considerably dropping. Noteworthy, the two metabolites were detectable and quantifiable in all samples. Contrariwise, *trans*-resveratrol was only quantifiable in three out of the five samples, including one which obtained result was considered an outlier. Analytes concentrations were calculated as follows: *trans*-resveratrol was present in plasma at 0.36 ± 0.10 μg.mL^{-1} (n=2); resveratrol-3-glucuronide at 2.11 ± 0.59 μg.mL^{-1} (n=5); and resveratrol-3-sulfate at 0.45 ± 0.10 μg.mL^{-1} (n=5).

Table 3.2.3 Analytes concentrations in plasma.

	Time-points			
	2.5 min	5 min	10 min	30 min
***Trans*-resveratrol**	5.65 ± 1.84	1.84 ± 0.63	0.43 ± 0.13	0.36 ± 0.10
Resveratrol-3-glucuronide	0.42 ± 0.09	2.30 ± 0.99	5.05 ± 1.22	2.11 ± 0.59
Resveratrol-3-sulfate	0.29 ± 0.03	0.95 ± 0.37	1.58 ± 0.32	0.45 ± 0.10

Data displayed is the mean ± SEM. Concentration unit is μg.mL^{-1}.

Results obtained from the assessment of area under the curve (AUC) demonstrate that systemic exposure of resveratrol-3-glucuronide is approximately 4-fold greater compared to that of *trans*-resveratrol: 1.556 $\mu g.h.mL^{-1}$ and 0.383 $\mu g.h.mL^{-1}$ for each, respectively (Table 3.2.4). Remarkably, resveratrol-3-sulfate displayed also a greater systemic exposure (0.403 $\mu g.h.mL^{-1}$) through the analysed time window (t=0.5h) than *trans*-resveratrol.

Table 3.2.4 Values for $AUC_{0-0.5}$, C_{max} e t_{max} parameters.

Dose and vehicle	Analyte	$AUC_{0-0.5}$	C_{max}	t_{max}
10 $mg.kg^{-1}$ DMSO in saline solution (25/75, v/v)	*Trans*-resv	0.383	5.65 ± 1.84	-
	Resv-3-gluc	1.556	5.05 ± 1.22	10
	Resv-3-sulf	0.403	1.58 ± 0.32	10

AUC unit is $\mu g.h.mL^{-1}$. C_{max} unit is $\mu g.mL^{-1}$. T_{max} unit is minutes.
DMSO: dimethyl sulfoxide; resv: resveratrol; gluc: glucuronide; sulf: sulfate.

Previous results are comparable with the results we here present for *trans*-resveratrol and resveratrol-3-sulfate (Table 3.2.5). Of note, both publications from Kapetanovic and colleagues, and Marier and colleagues' evaluate larger time windows of exposure comparing to what we performed in this study, therefore comprehending a second peak of concentrations (due to enterohepatic recirculation), which justifies greater exposures for both *trans*-resveratrol (and resveratrol-3-glucuronide) achieved in their studies.

Table 3.2.5 AUC values available in literature.

Reference	Dose and vehicle	Analyte	AUC_{0-t}	
Das et al., 2008	10 $mg.kg^{-1}$ Sodium salt solution	*Trans*-resv	0.533	(t=2h)
Kapetanovic et al., 2010	15 $mg.kg^{-1}$	*Trans*-resv	0.906	(t=∞)
Marier et al., 2002	15 $mg.kg^{-1}$ 20% hydroxypropyl-cyclodextrin in saline solution (20/80 v/v)	*Trans*-resv	1.260	(t=8h)
		Resv-3-gluc	8.788	

Resv: resveratrol; gluc: glucuronide.

Altogether, results from our study suggest that *trans*-resveratrol suffers from rapid and very extensive metabolism: at 5 minutes post-administration, glucuronide metabolite was already present at greater concentrations than the parent compound and in the 10' time-point, *trans*-resveratrol existed in a ratio of 1/12 comparing to its conjugated glucuronide derivative. Moreover, at this time-point, concentrations for the sulfate conjugate were also greater than those observed for *trans*-resveratrol. Regarding AUC, *trans*-resveratrol, from the three assessed analytes, is the one with lower exposure extent over the evaluated time window (t=0.5h). Although half-life or mean residence time parameters have not been investigated, we can still report *trans*-resveratrol is quickly cleared from systemic circulation considering that its concentrations were only residual by 30 minutes post-administration. From the three analytes, resveratrol-3-glucuronide is apparently the one with greater values for residence time within systemic circulation.

3.2.4.2 Analytes Quantification in Brain Samples

Brain concentration-time profiles of i.p. administered *trans*-resveratrol are represented in figure 3.2.14.

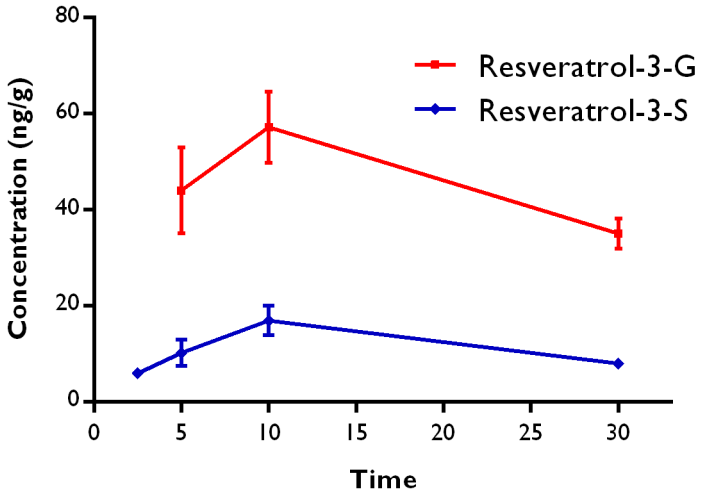

Figure 3.2.14 Brain tissue concentrations of detected analytes after i.p. administration of 10 mg/kg of trans-resveratrol. Results are expressed as mean ± SEM. Concentrations are given as ng of analyte per g of brain tissue.

From all samples, *trans*-resveratrol was within the range of quantifiable concentrations in one sample only (from the 5 minute time-point). Anyway, since that sample's concentration was notably high, we speculate that it may come from an irregularity of the method or be the result of contamination, therefore it was excluded.

At 2.5 minutes, only one sample for resveratrol-3-sulfate achieved quantifiable values of concentration (5.98 $ng.g^{-1}$), whereas the other four samples were detectable but have not reached quantifiable values. Peculiarly, resveratrol-3-glucuronide was not detected in any of the five samples.

Resveratrol-3-sulfate was detected at a quantifiable concentration in each of the samples collected 5 minutes after administration, displaying a mean concentration of 10.20 ± 2.75 $ng.g^{-1}$ (n=5), at this time-point. On its turn, and although being detected in every sample from this time-point, resveratrol-3-glucuronide only reach quantifiable concentration in two out of the five available. Mean concentration for this molecule was calculated at 44.00 ± 8.96 $ng.g^{-1}$ (n=2).

In a similar way to plasma samples, metabolites concentration in brain peaked at 10 minutes post-administration. By this time, concentrations for resveratrol-3-sulfate and resveratrol-3-glucuronide were determined at 17.00 ± 3.06 (n=6) and 57.2 ± 8.96 $ng.g^{-1}$ (n=3), respectively. Three of the evaluated samples did not reach quantifiable values for resveratrol-3-glucuronide, while resveratrol-3-sulfate was detected and quantified in all six samples.

Thirty minutes after administration, the quantity of the two analytes, in brain, decreased, being at 8.04 ± 1.15 (n=4) and 35.10 ± 3.12 $ng.g^{-1}$ (n=3), sulfate and glucuronide metabolites, respectively. Here, two samples did not reach a quantifiable concentration plateau for resveratrol-3-sulfate, whereas the glucuronide metabolite was detected but unquantifiable in three samples.

Table 3.2.6 Analytes quantification in brain tissue.

	Time-points			
	2.5 min	5 min	10 min	30 min
***Trans*-resveratrol**	ND/UNQ	UNQ	UNQ	ND
Resveratrol-3-glucuronide	ND	44.0 ± 8.96	57.2 ± 7.38	35.1 ± 3.12
Resveratrol-3-sulfate	5.98	10.2 ± 2.75	17.0 ± 3.06	8.04 ± 1.15

Data displayed is given in mean ± SEM. Concentration unit is ng per g of tissue ($ng.g^{-1}$). ND: not detected; UNQ: unquantified/below lowest level of quantification.

Similar to what was found in plasma samples, resveratrol-3-glucuronide is the most available compound at brain level, reaching maximum concentrations in this tissue 10

minutes after administration, coinciding with what was found for systemic circulation. Resveratrol-3-sulfate follows an identical pattern, yet at concentration levels 3/4-times lower. Notably, the parent compound does not reach quantifiable concentrations at brain in any of the analysed time-point, being completely undetected at 30 minutes post-administration.

3.3 Conclusion

In the present chapter, we optimized analytical conditions for *trans*-resveratrol quantification in plasma and brain matrices of mice.

Our results, despite scarce, clearly demonstrate *trans*-resveratrol's rapid metabolism and very limited exposure extent, displaying lower values for AUC than both glucuronide (approximately 4-fold) and sulfate metabolites. Within brain tissue, *trans*-resveratrol exhibited very low bioavailability – none of the samples reached quantifiable values (0.05 ng/g of tissue) and, at 30 minutes after administration, no trace of the compound was even detected. On the contrary, both metabolites were detected and quantified in this organ, presenting maximum concentrations 10 minutes post-administration. Furthermore, we can verify that, in mice, resveratrol's glucuronidation metabolism is more relevant, comparing to sulfation, as levels for the first conjugate are greater than those of resveratrol-3-sulfate.

Due to sample size, we could not evaluate differences between wild-type and transgenic animals.

Taking advantage of what was already done in this project, it would be interesting to redesign a similar assessment, setting up more time-points and expanding the sample size. Also, it would be relevant to perform a complete pharmacokinetic assessment, including parameters such as clearance, half-life, mean residence time and volume of distribution for each compound.

Concluding Remarks

With this work, we have created a strong groundwork for others to succeed with similar purposes.

We have explored epidemiologic and clinical aspects of MJD, exploring scales and questionnaires, which are effective and user-friendly tools that produce useful and reliable outcomes. Also, from medical examination reports, we described clinical symptomatology. Moreover, we have observed and reported some interesting correlations that certainly constitute an important bottom line to further prospective analysis. Finally, from our cohort, we gathered an interesting pool of patients which may apply the criteria for a potential upcoming clinical trial.

From our preclinical assessment, we have developed a methodology to quantify *trans*-resveratrol and major metabolites in rodents. Further, we characterized the concentration vs. time evolution in both plasma and brain matrices, for all three analytes. Despite scarce, our results proved that resveratrol is rapidly and extensively metabolized, existing only barely in systemic circulation few minutes after being administrated.

Altogether, we have here created a steppingstone for further investigation with the scope of achieving a pharmacological therapy for a fatal disease that is lacking one.

References

Cover photograph: Gilbert, Guillaume. 'slow pace'. 2016.

Acquaviva, R., A. Russo, A. Campisi, V. Sorrenti, C. Di Giacomo, M. L. Barcellona, M. Avitabile, and A. Vanella. 2002. 'Antioxidant activity and protective effect on DNA cleavage of resveratrol', *J Food Sci*, 67: 137-41.

Aggarwal, B. B., S. Shishodia, S. K. Sandur, M. K. Pandey, and G. Sethi. 2006. 'Inflammation and cancer: how hot is the link?', *Biochem Pharmacol*, 72: 1605-21.

Ahmad, K. A., M. V. Clement, and S. Pervaiz. 2003. 'Pro-oxidant activity of low doses of resveratrol inhibits hydrogen peroxide-induced apoptosis', *Apoptosis: From Signaling Pathways to Therapeutic Tools*, 1010: 365-73.

Albrecht, M., M. Golatta, U. Wullner, and T. Lengauer. 2004. 'Structural and functional analysis of ataxin-2 and ataxin-3', *Eur J Biochem*, 271: 3155-70.

Almeida, L., M. Vaz-da-Silva, A. Falcao, E. Soares, R. Costa, A. I. Loureiro, C. Fernandes-Lopes, J. F. Rocha, T. Nunes, L. Wright, and P. Soares-da-Silva. 2009. 'Pharmacokinetic and safety profile of trans-resveratrol in a rising multiple-dose study in healthy volunteers', *Mol Nutr Food Res*, 53 Suppl 1: S7-15.

Amor, S., L. A. N. Peferoen, D. Y. S. Vogel, M. Breur, P. van der Valk, D. Baker, and J. M. van Noort. 2014. 'Inflammation in neurodegenerative diseases-an update', *Immunology*, 142: 151-66.

Amri, A., J. C. Chaumeil, S. Sfar, and C. Charrueau. 2012. 'Administration of resveratrol: What formulation solutions to bioavailability limitations?', *J Control Release*, 158: 182-93.

Antony, P. M., S. Mantele, P. Mollenkopf, J. Boy, R. H. Kehlenbach, O. Riess, and T. Schmidt. 2009. 'Identification and functional dissection of localization signals within ataxin-3', *Neurobiol Dis*, 36: 280-92.

Araujo, J., P. Breuer, S. Dieringer, S. Krauss, S. Dorn, K. Zimmermann, A. Pfeifer, T. Klockgether, U. Wuellner, and B. O. Evert. 2011. 'FOXO4-dependent upregulation of superoxide dismutase-2 in response to oxidative stress is impaired in spinocerebellar ataxia type 3', *Hum Mol Genet*, 20: 2928-41.

Ardrey, R. E. 2003. *Liquid chromatography-mass spectrometry : an introduction* (J. Wiley: New York).

Arrasate, M., S. Mitra, E. S. Schweitzer, M. R. Segal, and S. Finkbeiner. 2004. 'Inclusion body formation reduces levels of mutant huntingtin and the risk of neuronal death', *Nature*, 431: 805-10.

Asensi, M., I. Medina, A. Ortega, J. Carretero, M. C. Bano, E. Obrador, and J. M. Estrela. 2002. 'Inhibition of cancer growth by resveratrol is related to its low bioavailability', *Free Radic Biol Med*, 33: 387-98.

Barger, J. L., T. Kayo, T. D. Pugh, T. A. Prolla, and R. Weindruch. 2008. 'Short-term consumption of a resveratrol-containing nutraceutical mixture mimics gene expression of long-term caloric restriction in mouse heart', *Exp Gerontol*, 43: 859-66.

Bauer, J. H., S. Goupil, G. B. Garber, and S. L. Helfand. 2004. 'An accelerated assay for the identification of lifespan-extending interventions in Drosophila melanogaster', *Proc Natl Acad Sci U S A*, 101: 12980-5.

Baur, J. A., K. J. Pearson, N. L. Price, H. A. Jamieson, C. Lerin, A. Kalra, V. V. Prabhu, J. S. Allard, G. Lopez-Lluch, K. Lewis, P. J. Pistell, S. Poosala, K. G. Becker, O. Boss, D. Gwinn, M. Wang, S. Ramaswamy, K. W. Fishbein, R. G. Spencer, E. G. Lakatta, D. Le Couteur, R. J. Shaw, P. Navas, P. Puigserver, D. K. Ingram, R. de Cabo, and D. A. Sinclair. 2006. 'Resveratrol improves health and survival of mice on a high-calorie diet', *Nature*, 444: 337-42.

Berke, S. J., Y. Chai, G. L. Marrs, H. Wen, and H. L. Paulson. 2005. 'Defining the role of ubiquitin-interacting motifs in the polyglutamine disease protein, ataxin-3', *J Biol Chem*, 280: 32026-34.

Berke, S. J., F. A. Schmied, E. R. Brunt, L. M. Ellerby, and H. L. Paulson. 2004. 'Caspase-mediated proteolysis of the polyglutamine disease protein ataxin-3', *J Neurochem*, 89: 908-18.

Bettencourt, C., and M. Lima. 2011. 'Machado-Joseph Disease: from first descriptions to new perspectives', *Orphanet J Rare Dis*, 6: 35.

Bettencourt, C., C. Santos, T. Kay, J. Vasconcelos, and M. Lima. 2008. 'Analysis of segregation patterns in Machado-Joseph disease pedigrees', *J Hum Genet*, 53: 920-3.

Bettencourt, C., C. Santos, R. Montiel, C. Costa Mdo, P. Cruz-Morales, L. R. Santos, N. Simoes, T. Kay, J. Vasconcelos, P. Maciel, and M. Lima. 2010. 'Increased transcript diversity: novel splicing variants of Machado-Joseph disease gene (ATXN3)', *Neurogenetics*, 11: 193-202.

Bevivino, A. E., and P. J. Loll. 2001. 'An expanded glutamine repeat destabilizes native ataxin-3 structure and mediates formation of parallel beta -fibrils', *Proc Natl Acad Sci U S A*, 98: 11955-60.

Bezprozvanny, I. 2009. 'Calcium signaling and neurodegenerative diseases', *Trends Mol Med*, 15: 89-100.

Bi, X. L., J. Y. Yang, Y. X. Dong, J. M. Wang, Y. H. Cui, T. Ikeshima, Y. Q. Zhao, and C. F. Wu. 2005. 'Resveratrol inhibits nitric oxide and TNF-alpha production by lipopolysaccharide-activated microglia', *Int Immunopharmacol*, 5: 185-93.

Bichelmeier, U., T. Schmidt, J. Hubener, J. Boy, L. Ruttiger, K. Habig, S. Poths, M. Bonin, M. Knipper, W. J. Schmidt, J. Wilbertz, H. Wolburg, F. Laccone, and O. Riess. 2007. 'Nuclear localization of ataxin-3 is required for the manifestation of symptoms in SCA3: in vivo evidence', *Journal of Neuroscience*, 27: 7418-28.

Birben, E., U. M. Sahiner, C. Sackesen, S. Erzurum, and O. Kalayci. 2012. 'Oxidative stress and antioxidant defense', *World Allergy Organ J*, 5: 9-19.

Boocock, D. J., G. E. Faust, K. R. Patel, A. M. Schinas, V. A. Brown, M. P. Ducharme, T. D. Booth, J. A. Crowell, M. Perloff, A. J. Gescher, W. P. Steward, and D. E. Brenner. 2007a. 'Phase I dose escalation pharmacokinetic study in healthy volunteers of resveratrol, a potential cancer chemopreventive agent', *Cancer Epidemiol Biomarkers Prev*, 16: 1246-52.

Boocock, D. J., K. R. Patel, G. E. Faust, D. P. Normolle, T. H. Marczylo, J. A. Crowell, D. E. Brenner, T. D. Booth, A. Gescher, and W. P. Steward. 2007b. 'Quantitation of trans-resveratrol and detection of its metabolites in human plasma and urine by high performance liquid chromatography', *J Chromatogr B Analyt Technol Biomed Life Sci*, 848: 182-7.

Braga-Neto, P., J. L. Pedroso, H. Alessi, L. A. Dutra, A. C. Felicio, T. Minett, P. Weisman, R. F. Santos-Galduroz, P. H. Bertolucci, A. A. Gabbai, and O. G. Barsottini. 2012. 'Cerebellar cognitive affective syndrome in Machado Joseph disease: core clinical features', *Cerebellum*, 11: 549-56.

Brown, V. A., K. R. Patel, M. Viskaduraki, J. A. Crowell, M. Perloff, T. D. Booth, G. Vasilinin, A. Sen, A. M. Schinas, G. Piccirilli, K. Brown, W. P. Steward, A. J. Gescher, and D. E. Brenner. 2010. 'Repeat dose study of the cancer chemopreventive agent resveratrol in healthy volunteers: safety, pharmacokinetics, and effect on the insulin-like growth factor axis', *Cancer Res*, 70: 9003-11.

Burkon, A., and V. Somoza. 2008. 'Quantification of free and protein-bound trans-resveratrol metabolites and identification of trans-resveratrol-C/O-conjugated diglucuronides - two novel resveratrol metabolites in human plasma', *Mol Nutr Food Res*, 52: 549-57.

Burnett, B., F. Li, and R. N. Pittman. 2003. 'The polyglutamine neurodegenerative protein ataxin-3 binds polyubiquitylated proteins and has ubiquitin protease activity', *Hum Mol Genet*, 12: 3195-205.

Burns, J., T. Yokota, H. Ashihara, M. E. Lean, and A. Crozier. 2002. 'Plant foods and herbal sources of resveratrol', *J Agric Food Chem*, 50: 3337-40.

Buysse, D. J., C. F. Reynolds, 3rd, T. H. Monk, S. R. Berman, and D. J. Kupfer. 1989. 'The Pittsburgh Sleep Quality Index: a new instrument for psychiatric practice and research', *Psychiatry Res*, 28: 193-213.

Calamini, B., K. Ratia, M. G. Malkowski, M. Cuendet, J. M. Pezzuto, B. D. Santarsiero, and A. D. Mesecar. 2010. 'Pleiotropic mechanisms facilitated by resveratrol and its metabolites', *Biochem J*, 429: 273-82.

Camey, S., L. B. Jardim, C. Kieling, J. A. Saute, and A. Vigo. 2010. 'A prospective study of SCA3 gait ataxia described through a Markovian method', *Neuroepidemiology*, 34: 163-70.

Cao, D., M. Wang, X. Qiu, D. Liu, H. Jiang, N. Yang, and R. M. Xu. 2015. 'Structural basis for allosteric, substrate-dependent stimulation of SIRT1 activity by resveratrol', *Genes Dev*, 29: 1316-25.

Cecchin, C. R., A. P. Pires, C. R. Rieder, T. L. Monte, I. Silveira, T. Carvalho, M. L. Saraiva-Pereira, J. Sequeiros, and L. B. Jardim. 2007a. 'Depressive symptoms in Machado-Joseph disease (SCA3) patients and their relatives', *Community Genet*, 10: 19-26.

Cecchin, D., F. Lumachi, F. Marino, R. Stramare, U. Basso, G. Grassetto, and F. Bui. 2007b. 'Thyroid C-cell hyperplasia shown by combined In-111 pentetreotide, Tc-99m pertechnetate, and Tc-99m MIBI scintigraphy', *Clin Nucl Med*, 32: 378-9.

Chalkiadaki, A., and L. Guarente. 2012. 'Sirtuins mediate mammalian metabolic responses to nutrient availability', *Nat Rev Endocrinol*, 8: 287-96.

Chan, W. K., and A. B. Delucchi. 2000. 'Resveratrol, a red wine constituent, is a mechanism-based inactivator of cytochrome P450 3A4', *Life Sci*, 67: 3103-12.

Chen, S., V. Berthelier, J. B. Hamilton, B. O'Nuallain, and R. Wetzel. 2002. 'Amyloid-like features of polyglutamine aggregates and their assembly kinetics', *Biochemistry*, 41: 7391-9.

Chen, W., L. Rezaizadehnajafi, and M. Wink. 2013. 'Influence of resveratrol on oxidative stress resistance and life span in Caenorhabditis elegans', *J Pharm Pharmacol*, 65: 682-8.

Chen, X., T. S. Tang, H. Tu, O. Nelson, M. Pook, R. Hammer, N. Nukina, and I. Bezprozvanny. 2008. 'Deranged calcium signaling and neurodegeneration in spinocerebellar ataxia type 3', *Journal of Neuroscience*, 28: 12713-24.

Chou, A. H., T. H. Yeh, Y. L. Kuo, Y. C. Kao, M. J. Jou, C. Y. Hsu, S. R. Tsai, A. Kakizuka, and H. L. Wang. 2006. 'Polyglutamine-expanded ataxin-3 activates mitochondrial apoptotic pathway by upregulating Bax and downregulating Bcl-xL', *Neurobiol Dis*, 21: 333-45.

Chou, A. H., T. H. Yeh, P. Ouyang, Y. L. Chen, S. Y. Chen, and H. L. Wang. 2008. 'Polyglutamine-expanded ataxin-3 causes cerebellar dysfunction of SCA3 transgenic mice by inducing transcriptional dysregulation', *Neurobiol Dis*, 31: 89-101.

Chow, H. H., L. L. Garland, C. H. Hsu, D. R. Vining, W. M. Chew, J. A. Miller, M. Perloff, J. A. Crowell, and D. S. Alberts. 2010. 'Resveratrol modulates drug- and carcinogen-metabolizing enzymes in a healthy volunteer study', *Cancer Prev Res (Phila)*, 3: 1168-75.

Chow, S. E., Y. C. Hshu, J. S. Wang, and J. K. Chen. 2007. 'Resveratrol attenuates oxLDL-stimulated NADPH oxidase activity and protects endothelial cells from oxidative functional damages', *J Appl Physiol (1985)*, 102: 1520-7.

Chung, M. I., C. M. Teng, K. L. Cheng, F. N. Ko, and C. N. Lin. 1992. 'An antiplatelet principle of Veratrum formosanum', Planta Med, 58: 274-6.

Coimbra, M., B. Isacchi, L. van Bloois, J. S. Torano, A. Ket, X. Wu, F. Broere, J. M. Metselaar, C. J. Rijcken, G. Storm, R. Bilia, and R. M. Schiffelers. 2011. 'Improving solubility and chemical stability of natural compounds for medicinal use by incorporation into liposomes', Int J Pharm, 416: 433-42.

Costa Mdo, C., and H. L. Paulson. 2012. 'Toward understanding Machado-Joseph disease', Prog Neurobiol, 97: 239-57.

Cottart, C. H., V. Nivet-Antoine, C. Laguillier-Morizot, and J. L. Beaudeux. 2010. 'Resveratrol bioavailability and toxicity in humans', *Mol Nutr Food Res*, 54: 7-16.

Coutinho, P., and C. Andrade. 1978. 'Autosomal dominant system degeneration in Portuguese families of the Azores Islands. A new genetic disorder involving cerebellar, pyramidal, extrapyramidal and spinal cord motor functions', *Neurology*, 28: 703-9.

Coutinho, P., L. Ruano, J. L. Loureiro, V. T. Cruz, J. Barros, A. Tuna, C. Barbot, J. Guimaraes, I. Alonso, I. Silveira, J. Sequeiros, J. Marques Neves, P. Serrano, and M. C. Silva. 2013. 'Hereditary ataxia and spastic paraplegia in Portugal: a population-based prevalence study', *JAMA Neurol*, 70: 746-55.

Crowell, J. A., P. J. Korytko, R. L. Morrissey, T. D. Booth, and B. S. Levine. 2004. 'Resveratrol-associated renal toxicity', *Toxicol Sci*, 82: 614-9.

Cunha-Santos, J., J. Duarte-Neves, V. Carmona, L. Guarente, L. Pereira de Almeida, and C. Cavadas. 2016. 'Caloric restriction blocks neuropathology and motor deficits in Machado-Joseph disease mouse models through SIRT1 pathway', *Nat Commun*, 7: 11445.

D'Abreu, A., M. C. Franca, Jr., H. L. Paulson, and I. Lopes-Cendes. 2010. 'Caring for Machado-Joseph disease: current understanding and how to help patients', *Parkinsonism Relat Disord*, 16: 2-7.

Dass, Chhabil. 2007. *Fundamentals of contemporary mass spectrometry* (Wiley-Interscience: Hoboken, N.J.).

de la Lastra, C. A., and I. Villegas. 2007. 'Resveratrol as an antioxidant and pro-oxidant agent: mechanisms and clinical implications', *Biochem Soc Trans*, 35: 1156-60.

Dixon, R. A., and N. L. Paiva. 1995. 'Stress-Induced Phenylpropanoid Metabolism', *Plant Cell*, 7: 1085-97.

Donaldson, K. M., W. Li, K. A. Ching, S. Batalov, C. C. Tsai, and C. A. Joazeiro. 2003. 'Ubiquitin-mediated sequestration of normal cellular proteins into polyglutamine aggregates', *Proc Natl Acad Sci U S A*, 100: 8892-7.

Doss-Pepe, E. W., E. S. Stenroos, W. G. Johnson, and K. Madura. 2003. 'Ataxin-3 interactions with rad23 and valosin-containing protein and its associations with ubiquitin chains and the proteasome are consistent with a role in ubiquitin-mediated proteolysis', *Mol Cell Biol*, 23: 6469-83.

Drusedau, M., J. C. Dreesen, C. De Die-Smulders, K. Hardy, M. Bras, J. C. Dumoulin, J. L. Evers, H. J. Smeets, J. P. Geraedts, and J. Herbergs. 2004. 'Preimplantation genetic diagnosis of spinocerebellar ataxia 3 by (CAG)(n) repeat detection', *Mol Hum Reprod*, 10: 71-5.

du Montcel, S. T., P. Charles, P. Ribai, C. Goizet, A. Le Bayon, P. Labauge, L. Guyant-Marechal, S. Forlani, C. Jauffret, N. Vandenberghe, K. N'Guyen, I. Le Ber, D. Devos, C. M. Vincitorio, M. U. Manto, F. Tison, D. Hannequin, M. Ruberg, A. Brice, and A. Durr. 2008. 'Composite cerebellar functional severity score: validation of a quantitative score of cerebellar impairment', *Brain*, 131: 1352-61.

Dudley, J., S. Das, S. Mukherjee, and D. K. Das. 2009. 'Resveratrol, a unique phytoalexin present in red wine, delivers either survival signal or death signal to the ischemic myocardium depending on dose', *J Nutr Biochem*, 20: 443-52.

Durcan, T. M., M. Kontogiannea, T. Thorarinsdottir, L. Fallon, A. J. Williams, A. Djarmati, T. Fantaneanu, H. L. Paulson, and E. A. Fon. 2011. 'The Machado-Joseph disease-associated mutant form of ataxin-3 regulates parkin ubiquitination and stability', *Hum Mol Genet*, 20: 141-54.

Durr, A., G. Stevanin, G. Cancel, C. Duyckaerts, N. Abbas, O. Didierjean, H. Chneiweiss, A. Benomar, O. Lyon-Caen, J. Julien, M. Serdaru, C. Penet, Y. Agid, and A. Brice. 1996. 'Spinocerebellar ataxia 3 and Machado-Joseph disease: clinical, molecular, and neuropathological features', *Ann Neurol*, 39: 490-9.

Evert, B. O., J. Araujo, A. M. Vieira-Saecker, R. A. de Vos, S. Harendza, T. Klockgether, and U. Wullner. 2006. 'Ataxin-3 represses transcription via chromatin binding, interaction with histone deacetylase 3, and histone deacetylation', *Journal of Neuroscience*, 26: 11474-86.

Evert, B. O., I. R. Vogt, C. Kindermann, L. Ozimek, R. A. de Vos, E. R. Brunt, I. Schmitt, T. Klockgether, and U. Wullner. 2001. 'Inflammatory genes are upregulated in expanded ataxin-3-expressing cell lines and spinocerebellar ataxia type 3 brains', *Journal of Neuroscience*, 21: 5389-96.

Evert, B. O., I. R. Vogt, A. M. Vieira-Saecker, L. Ozimek, R. A. de Vos, E. R. Brunt, T. Klockgether, and U. Wullner. 2003. 'Gene expression profiling in ataxin-3 expressing cell lines reveals distinct effects of normal and mutant ataxin-3', *J Neuropathol Exp Neurol*, 62: 1006-18.

Freeman, W., and Z. Wszolek. 2005. 'Botulinum toxin type A for treatment of spasticity in spinocerebellar ataxia type 3 (Machado-Joseph disease)', *Mov Disord*, 20: 644.

Friedman, J. H., H. H. Fernandez, and L. R. Sudarsky. 2003. 'REM behavior disorder and excessive daytime somnolence in Machado-Joseph disease (SCA-3)', *Mov Disord*, 18: 1520-2.

Frozza, R. L., A. Bernardi, K. Paese, J. B. Hoppe, T. da Silva, A. M. Battastini, A. R. Pohlmann, S. S. Guterres, and C. Salbego. 2010. 'Characterization of trans-resveratrol-loaded lipid-core nanocapsules and tissue distribution studies in rats', *J Biomed Nanotechnol*, 6: 694-703.

Frye, R. A. 2000. 'Phylogenetic classification of prokaryotic and eukaryotic Sir2-like proteins', *Biochem Biophys Res Commun*, 273: 793-8.

Gatchel, J. R., and H. Y. Zoghbi. 2005. 'Diseases of unstable repeat expansion: mechanisms and common principles', *Nat Rev Genet*, 6: 743-55.

Globas, C., S. T. du Montcel, L. Baliko, S. Boesch, C. Depondt, S. DiDonato, A. Durr, A. Filla, T. Klockgether, C. Mariotti, B. Melegh, M. Rakowicz, P. Ribai, R. Rola, T. Schmitz-Hubsch, S. Szymanski, D. Timmann, B. P. Van de Warrenburg, P. Bauer, and L. Schols. 2008. 'Early symptoms in spinocerebellar ataxia type 1, 2, 3, and 6', *Mov Disord*, 23: 2232-8.

Goldberg, D. M., J. Yan, and G. J. Soleas. 2003. 'Absorption of three wine-related polyphenols in three different matrices by healthy subjects', *Clin Biochem*, 36: 79-87.

Gonzalez-Zaldivar, Y., Y. Vazquez-Mojena, J. M. Laffita-Mesa, L. E. Almaguer-Mederos, R. Rodriguez-Labrada, G. Sanchez-Cruz, R. Aguilera-Rodriguez, T. Cruz-Marino, N. Canales-Ochoa, P. MacLeod, and L. Velazquez-Perez. 2015. 'Epidemiological, clinical, and molecular characterization of Cuban families with spinocerebellar ataxia type 3/Machado-Joseph disease', *Cerebellum Ataxias*, 2: 1.

Goti, D., S. M. Katzen, J. Mez, N. Kurtis, J. Kiluk, L. Ben-Haiem, N. A. Jenkins, N. G. Copeland, A. Kakizuka, A. H. Sharp, C. A. Ross, P. R. Mouton, and V. Colomer. 2004. 'A mutant ataxin-3 putative-cleavage fragment in brains of Machado-Joseph disease patients and transgenic mice is cytotoxic above a critical concentration', *Journal of Neuroscience*, 24: 10266-79.

Goto, J., M. Watanabe, Y. Ichikawa, S. B. Yee, N. Ihara, K. Endo, S. Igarashi, Y. Takiyama, C. Gaspar, P. Maciel, S. Tsuji, G. A. Rouleau, and I. Kanazawa. 1997. 'Machado-Joseph disease gene products carrying different carboxyl termini', *Neurosci Res*, 28: 373-7.

Gu, W., H. Ma, K. Wang, M. Jin, Y. Zhou, X. Liu, G. Wang, and Y. Shen. 2004. 'The shortest expanded allele of the MJD1 gene in a Chinese MJD kindred with autonomic dysfunction', *Eur Neurol*, 52: 107-11.

Guo, Y. J., S. Y. Dong, X. X. Cui, Y. Feng, T. Liu, M. Yin, S. H. Kuo, E. K. Tan, W. J. Zhao, and Y. C. Wu. 2016. 'Resveratrol alleviates MPTP-induced motor impairments and pathological changes by autophagic degradation of alpha-synuclein via SIRT1-deacetylated LC3', *Mol Nutr Food Res*, 60: 2161-75.

Haacke, A., F. U. Hartl, and P. Breuer. 2007. 'Calpain inhibition is sufficient to suppress aggregation of polyglutamine-expanded ataxin-3', *J Biol Chem*, 282: 18851-6.

Haigis, M. C., and D. A. Sinclair. 2010. 'Mammalian sirtuins: biological insights and disease relevance', *Annu Rev Pathol*, 5: 253-95.

Hao, J., J. Zhao, S. Zhang, T. Tong, Q. Zhuang, K. Jin, W. Chen, and H. Tang. 2016. 'Fabrication of an ionic-sensitive in situ gel loaded with resveratrol nanosuspensions intended for direct nose-to-brain delivery', *Colloids Surf B Biointerfaces*, 147: 376-86.

Harris, G. M., K. Dodelzon, L. Gong, P. Gonzalez-Alegre, and H. L. Paulson. 2010. 'Splice isoforms of the polyglutamine disease protein ataxin-3 exhibit similar enzymatic yet different aggregation properties', *PLoS One*, 5: e13695.

Hershko, A., and A. Ciechanover. 1998. 'The ubiquitin system', *Annu Rev Biochem*, 67: 425-79.

Hoche, F., K. Seidel, E. R. Brunt, G. Auburger, L. Schols, K. Burk, R. A. de Vos, W. den Dunnen, I. Bechmann, R. Egensperger, C. Van Broeckhoven, K. Gierga, T. Deller, and U. Rub. 2008. 'Involvement of the auditory brainstem system in spinocerebellar ataxia type 2 (SCA2), type 3 (SCA3) and type 7 (SCA7)', *Neuropathol Appl Neurobiol*, 34: 479-91.

Hoffmann, Edmond de, and Vincent Stroobant. 2007. *Mass spectrometry : principles and applications* (J. Wiley: Chichester, England ; Hoboken, NJ).

Hoshino, J., E. J. Park, T. P. Kondratyuk, L. Marler, J. M. Pezzuto, R. B. van Breemen, S. Mo, Y. Li, and M. Cushman. 2010. 'Selective synthesis and biological evaluation of sulfate-conjugated resveratrol metabolites', *J Med Chem*, 53: 5033-43.

Howitz, K. T., K. J. Bitterman, H. Y. Cohen, D. W. Lamming, S. Lavu, J. G. Wood, R. E. Zipkin, P. Chung, A. Kisielewski, L. L. Zhang, B. Scherer, and D. A. Sinclair. 2003. 'Small molecule activators of sirtuins extend Saccharomyces cerevisiae lifespan', *Nature*, 425: 191-6.

Huang, Z. M., C. L. He, A. Yang, Y. Zhang, X. J. Han, J. Yin, and Q. Wu. 2006. 'Encapsulating drugs in biodegradable ultrafine fibers through co-axial electrospinning', *J Biomed Mater Res A*, 77: 169-79.

Hubbard, B. P., A. P. Gomes, H. Dai, J. Li, A. W. Case, T. Considine, T. V. Riera, J. E. Lee, S. Y. E, D. W. Lamming, B. L. Pentelute, E. R. Schuman, L. A. Stevens, A. J. Ling, S. M. Armour, S. Michan, H. Zhao, Y. Jiang, S. M. Sweitzer, C. A. Blum, J. S. Disch, P. Y. Ng, K. T. Howitz, A. P. Rolo, Y. Hamuro, J. Moss, R. B. Perni, J. L. Ellis, G. P. Vlasuk, and D. A. Sinclair. 2013. 'Evidence for a common mechanism of SIRT1 regulation by allosteric activators', *Science*, 339: 1216-9.

Ichikawa, Y., J. Goto, M. Hattori, A. Toyoda, K. Ishii, S. Y. Jeong, H. Hashida, N. Masuda, K. Ogata, F. Kasai, M. Hirai, P. Maciel, G. A. Rouleau, Y. Sakaki, and I. Kanazawa. 2001. 'The genomic structure and expression of MJD, the Machado-Joseph disease gene', *J Hum Genet*, 46: 413-22.

Igarashi, S., Y. Takiyama, G. Cancel, E. A. Rogaeva, H. Sasaki, A. Wakisaka, Y. X. Zhou, H. Takano, K. Endo, K. Sanpei, M. Oyake, H. Tanaka, G. Stevanin, N. Abbas, A. Durr, E. I. Rogaev, R. Sherrington, T. Tsuda, M. Ikeda, E. Cassa, M. Nishizawa, A. Benomar, J. Julien, J. Weissenbach, G. X. Wang, Y. Agid, P. H. St George-Hyslop, A. Brice, and S. Tsuji. 1996. 'Intergenerational instability of the CAG repeat of the gene for Machado-Joseph disease (MJD1) is affected by the genotype of the normal chromosome: implications for the molecular mechanisms of the instability of the CAG repeat', *Hum Mol Genet*, 5: 923-32.

Ikeda, H., M. Yamaguchi, S. Sugai, Y. Aze, S. Narumiya, and A. Kakizuka. 1996. 'Expanded polyglutamine in the Machado-Joseph disease protein induces cell death in vitro and in vivo', *Nat Genet*, 13: 196-202.

Ilg, W., A. J. Bastian, S. Boesch, R. G. Burciu, P. Celnik, J. Claassen, K. Feil, R. Kalla, I. Miyai, W. Nachbauer, L. Schols, M. Strupp, M. Synofzik, J. Teufel, and D. Timmann. 2014. 'Consensus paper: management of degenerative cerebellar disorders', *Cerebellum*, 13: 248-68.

Imai, S., C. M. Armstrong, M. Kaeberlein, and L. Guarente. 2000. 'Transcriptional silencing and longevity protein Sir2 is an NAD-dependent histone deacetylase', *Nature*, 403: 795-800.

Imbert, G., F. Saudou, G. Yvert, D. Devys, Y. Trottier, J. M. Garnier, C. Weber, J. L. Mandel, G. Cancel, N. Abbas, A. Durr, O. Didierjean, G. Stevanin, Y. Agid, and A. Brice. 1996. 'Cloning of the gene for spinocerebellar ataxia 2 reveals a locus with high sensitivity to expanded CAG/glutamine repeats', *Nat Genet*, 14: 285-91.

Invernizzi, G., F. A. Aprile, A. Natalello, A. Ghisleni, A. Penco, A. Relini, S. M. Doglia, P. Tortora, and M. E. Regonesi. 2012. 'The relationship between aggregation and toxicity of polyglutamine-containing ataxin-3 in the intracellular environment of Escherichia coli', *PLoS One*, 7: e51890.

Jang, M., L. Cai, G. O. Udeani, K. V. Slowing, C. F. Thomas, C. W. Beecher, H. H. Fong, N. R. Farnsworth, A. D. Kinghorn, R. G. Mehta, R. C. Moon, and J. M. Pezzuto. 1997. 'Cancer chemopreventive activity of resveratrol, a natural product derived from grapes', *Science*, 275: 218-20.

Jardim, L. B., M. L. Pereira, I. Silveira, A. Ferro, J. Sequeiros, and R. Giugliani. 2001a. 'Machado-Joseph disease in South Brazil: clinical and molecular characterization of kindreds', *Acta Neurol Scand*, 104: 224-31.

———. 2001b. 'Neurologic findings in Machado-Joseph disease: relation with disease duration, subtypes, and (CAG)n', *Arch Neurol*, 58: 899-904.

Jeong, H., D. E. Cohen, L. B. Cui, A. Supinski, J. N. Savas, J. R. Mazzulli, J. R. Yates, L. Bordone, L. Guarente, and D. Krainc. 2012. 'Sirt1 mediates neuroprotection from mutant huntingtin by activation of the TORC1 and CREB transcriptional pathway', *Nat Med*, 18: 159-65.

Jiang, M., J. Wang, J. Fu, L. Du, H. Jeong, T. West, L. Xiang, Q. Peng, Z. Hou, H. Cai, T. Seredenina, N. Arbez, S. Zhu, K. Sommers, J. Qian, J. Zhang, S. Mori, X. W. Yang, K. L. Tamashiro, S. Aja, T. H. Moran, R. Luthi-Carter, B. Martin, S. Maudsley, M. P. Mattson, R. H. Cichewicz, C. A. Ross, D. M. Holtzman, D. Krainc, and W. Duan. 2011. 'Neuroprotective role of Sirt1 in mammalian models of Huntington's disease through activation of multiple Sirt1 targets', *Nat Med*, 18: 153-8.

Johri, A., and M. F. Beal. 2012. 'Mitochondrial dysfunction in neurodegenerative diseases', *J Pharmacol Exp Ther*, 342: 619-30.

Jose, S., S. S. Anju, T. A. Cinu, N. A. Aleykutty, S. Thomas, and E. B. Souto. 2014. 'In vivo pharmacokinetics and biodistribution of resveratrol-loaded solid lipid nanoparticles for brain delivery', *Int J Pharm*, 474: 6-13.

Juan, M. E., M. P. Vinardell, and J. M. Planas. 2002. 'The daily oral administration of high doses of trans-resveratrol to rats for 28 days is not harmful', *J Nutr*, 132: 257-60.

Jung, J., K. Xu, D. Lessing, and N. M. Bonini. 2009. 'Preventing Ataxin-3 protein cleavage mitigates degeneration in a Drosophila model of SCA3', *Hum Mol Genet*, 18: 4843-52.

Kaga, S., L. Zhan, M. Matsumoto, and N. Maulik. 2005. 'Resveratrol enhances neovascularization in the infarcted rat myocardium through the induction of thioredoxin-1, heme oxygenase-1 and vascular endothelial growth factor', *J Mol Cell Cardiol*, 39: 813-22.

Kaldas, M. I., U. K. Walle, and T. Walle. 2003. 'Resveratrol transport and metabolism by human intestinal Caco-2 cells', *J Pharm Pharmacol*, 55: 307-12.

Kanai, K., S. Kuwabara, K. Arai, J. Y. Sung, K. Ogawara, and T. Hattori. 2003. 'Muscle cramp in Machado-Joseph disease: altered motor axonal excitability properties and mexiletine treatment', *Brain*, 126: 965-73.

Kawaguchi, Y., T. Okamoto, M. Taniwaki, M. Aizawa, M. Inoue, S. Katayama, H. Kawakami, S. Nakamura, M. Nishimura, I. Akiguchi, and et al. 1994. 'CAG expansions in a novel gene for Machado-Joseph disease at chromosome 14q32.1', *Nat Genet*, 8: 221-8.

Kim, D., M. D. Nguyen, M. M. Dobbin, A. Fischer, F. Sananbenesi, J. T. Rodgers, I. Delalle, J. A. Baur, G. Sui, S. M. Armour, P. Puigserver, D. A. Sinclair, and L. H. Tsai. 2007. 'SIRT1 deacetylase protects against neurodegeneration in models for Alzheimer's disease and amyotrophic lateral sclerosis', *EMBO J*, 26: 3169-79.

Klockgether, T., R. Ludtke, B. Kramer, M. Abele, K. Burk, L. Schols, O. Riess, F. Laccone, S. Boesch, I. Lopes-Cendes, A. Brice, R. Inzelberg, N. Zilber, and J. Dichgans. 1998. 'The natural history of degenerative ataxia: a retrospective study in 466 patients', *Brain*, 121 (Pt 4): 589-600.

Kristl, J., K. Teskac, C. Caddeo, Z. Abramovic, and M. Sentjurc. 2009. 'Improvements of cellular stress response on resveratrol in liposomes', *Eur J Pharm Biopharm*, 73: 253-9.

Kroenke, K., R. L. Spitzer, and J. B. Williams. 2001. 'The PHQ-9: validity of a brief depression severity measure', *J Gen Intern Med*, 16: 606-13.

la Porte, C., N. Voduc, G. Zhang, I. Seguin, D. Tardiff, N. Singhal, and D. W. Cameron. 2010. 'Steady-State pharmacokinetics and tolerability of trans-resveratrol 2000 mg twice daily with food, quercetin and alcohol (ethanol) in healthy human subjects', *Clin Pharmacokinet*, 49: 449-54.

Laco, M. N., C. R. Oliveira, H. L. Paulson, and A. C. Rego. 2012. 'Compromised mitochondrial complex II in models of Machado-Joseph disease', *Biochim Biophys Acta*, 1822: 139-49.

Lagouge, M., C. Argmann, Z. Gerhart-Hines, H. Meziane, C. Lerin, F. Daussin, N. Messadeq, J. Milne, P. Lambert, P. Elliott, B. Geny, M. Laakso, P. Puigserver, and J. Auwerx. 2006. 'Resveratrol improves mitochondrial function and protects against metabolic disease by activating SIRT1 and PGC-1alpha', *Cell*, 127: 1109-22.

Lee, I. H., L. Cao, R. Mostoslavsky, D. B. Lombard, J. Liu, N. E. Bruns, M. Tsokos, F. W. Alt, and T. Finkel. 2008. 'A role for the NAD-dependent deacetylase Sirt1 in the regulation of autophagy', *Proc Natl Acad Sci U S A*, 105: 3374-9.

Leonard, S. S., C. Xia, B. H. Jiang, B. Stinefelt, H. Klandorf, G. K. Harris, and X. Shi. 2003. 'Resveratrol scavenges reactive oxygen species and effects radical-induced cellular responses', *Biochem Biophys Res Commun*, 309: 1017-26.

Li, F., T. Macfarlan, R. N. Pittman, and D. Chakravarti. 2002. 'Ataxin-3 is a histone-binding protein with two independent transcriptional corepressor activities', *J Biol Chem*, 277: 45004-12.

Li, Y., Y. G. Shin, C. Yu, J. W. Kosmeder, W. H. Hirschelman, J. M. Pezzuto, and R. B. van Breemen. 2003. 'Increasing the throughput and productivity of Caco-2 cell permeability assays using liquid chromatography-mass spectrometry: application to resveratrol absorption and metabolism', *Comb Chem High Throughput Screen*, 6: 757-67.

Lima, L., and P. Coutinho. 1980. 'Clinical criteria for diagnosis of Machado-Joseph disease: report of a non-Azorena Portuguese family', *Neurology*, 30: 319-22.

Lindblad, K., M. L. Savontaus, G. Stevanin, M. Holmberg, K. Digre, C. Zander, H. Ehrsson, G. David, A. Benomar, E. Nikoskelainen, Y. Trottier, G. Holmgren, L. J. Ptacek, A. Anttinen, A. Brice, and M. Schalling. 1996. 'An expanded CAG repeat sequence in spinocerebellar ataxia type 7', *Genome Res*, 6: 965-71.

Liu, C. S., W. L. Cheng, S. J. Kuo, J. Y. Li, B. W. Soong, and Y. H. Wei. 2008. 'Depletion of mitochondrial DNA in leukocytes of patients with poly-Q diseases', *J Neurol Sci*, 264: 18-21.

Liu, C. S., C. S. Tsai, C. L. Kuo, H. W. Chen, C. K. Lii, Y. S. Ma, and Y. H. Wei. 2003. 'Oxidative stress-related alteration of the copy number of mitochondrial DNA in human leukocytes', *Free Radic Res*, 37: 1307-17.

Liu, G. S., Z. S. Zhang, B. Yang, and W. He. 2012. 'Resveratrol attenuates oxidative damage and ameliorates cognitive impairment in the brain of senescence-accelerated mice', *Life Sci*, 91: 872-7.

Liu, H., X. Li, G. Ning, S. Zhu, X. Ma, X. Liu, C. Liu, M. Huang, I. Schmitt, U. Wullner, Y. Niu, C. Guo, Q. Wang, and T. S. Tang. 2016. 'The Machado-Joseph Disease Deubiquitinase Ataxin-3 Regulates the Stability and Apoptotic Function of p53', *PLoS Biol*, 14: e2000733.

Lo, R. Y., K. P. Figueroa, S. M. Pulst, S. Perlman, G. Wilmot, C. Gomez, J. Schmahmann, H. Paulson, V. G. Shakkottai, S. Ying, T. Zesiewicz, K. Bushara, M. Geschwind, G. Xia, J. T. Yu, L. E. Lee, T. Ashizawa, S. H. Subramony, and S. H. Kuo. 2016. 'Depression and clinical progression in spinocerebellar ataxias', *Parkinsonism Relat Disord*, 22: 87-92.

Lu, D. L., D. J. Ding, W. J. Yan, R. R. Li, F. Dai, Q. Wang, S. S. Yu, Y. Li, X. L. Jin, and B. Zhou. 2013. 'Influence of glucuronidation and reduction modifications of resveratrol on its biological activities', *Chembiochem*, 14: 1094-104.

Lu, X., L. Ma, L. Ruan, Y. Kong, H. Mou, Z. Zhang, Z. Wang, J. M. Wang, and Y. Le. 2010. 'Resveratrol differentially modulates inflammatory responses of microglia and astrocytes', *J Neuroinflammation*, 7: 46.

Lu, Z., B. Cheng, Y. Hu, Y. Zhang and G. Zou. 2009. 'Complexation of resveratrol with cyclodextrins: Solubility and antioxidant activity', *Food Chemistry*, 113: 17-20.

Lu, Z., Y. Zhang, H. Liu, J. Yuan, Z. Zheng, and G. Zou. 2007. 'Transport of a cancer chemopreventive polyphenol, resveratrol: interaction with serum albumin and hemoglobin', *J Fluoresc*, 17: 580-7.

MacCarrone, M., T. Lorenzon, P. Guerrieri, and A. F. Agro. 1999. 'Resveratrol prevents apoptosis in K562 cells by inhibiting lipoxygenase and cyclooxygenase activity', *Eur J Biochem*, 265: 27-34.

Macedo-Ribeiro, S., L. Cortes, P. Maciel, and A. L. Carvalho. 2009. 'Nucleocytoplasmic shuttling activity of ataxin-3', *PLoS One*, 4: e5834.

Maciel, P., M. C. Costa, A. Ferro, M. Rousseau, C. S. Santos, C. Gaspar, J. Barros, G. A. Rouleau, P. Coutinho, and J. Sequeiros. 2001. 'Improvement in the molecular diagnosis of Machado-Joseph disease', *Arch Neurol*, 58: 1821-7.

Maier-Salamon, A., B. Hagenauer, M. Wirth, F. Gabor, T. Szekeres, and W. Jager. 2006. 'Increased transport of resveratrol across monolayers of the human intestinal Caco-2 cells is mediated by inhibition and saturation of metabolites', *Pharm Res*, 23: 2107-15.

Mao, Y., F. Senic-Matuglia, P. P. Di Fiore, S. Polo, M. E. Hodsdon, and P. De Camilli. 2005. 'Deubiquitinating function of ataxin-3: insights from the solution structure of the Josephin domain', *Proc Natl Acad Sci U S A*, 102: 12700-5.

Marier, J. F., P. Vachon, A. Gritsas, J. Zhang, J. P. Moreau, and M. P. Ducharme. 2002. 'Metabolism and disposition of resveratrol in rats: extent of absorption, glucuronidation, and enterohepatic recirculation evidenced by a linked-rat model', *J Pharmacol Exp Ther*, 302: 369-73.

Maruyama, H., S. Nakamura, Z. Matsuyama, T. Sakai, M. Doyu, G. Sobue, M. Seto, M. Tsujihata, T. Oh-i, T. Nishio, and et al. 1995. 'Molecular features of the CAG repeats and clinical manifestation of Machado-Joseph disease', *Hum Mol Genet*, 4: 807-12.

Masino, L., V. Musi, R. P. Menon, P. Fusi, G. Kelly, T. A. Frenkiel, Y. Trottier, and A. Pastore. 2003. 'Domain architecture of the polyglutamine protein ataxin-3: a globular domain followed by a flexible tail', *FEBS Lett*, 549: 21-5.

Matilla-Duenas, A. 2012. 'Machado-Joseph disease and other rare spinocerebellar ataxias', *Adv Exp Med Biol*, 724: 172-88.

Mende-Mueller, L. M., T. Toneff, S. R. Hwang, M. F. Chesselet, and V. Y. Hook. 2001. 'Tissue-specific proteolysis of Huntingtin (htt) in human brain: evidence of enhanced levels of N- and C-terminal htt fragments in Huntington's disease striatum', *Journal of Neuroscience*, 21: 1830-7.

Menzies, F. M., J. Huebener, M. Renna, M. Bonin, O. Riess, and D. C. Rubinsztein. 2010. 'Autophagy induction reduces mutant ataxin-3 levels and toxicity in a mouse model of spinocerebellar ataxia type 3', *Brain*, 133: 93-104.

Merry, D. E., Y. Kobayashi, C. K. Bailey, A. A. Taye, and K. H. Fischbeck. 1998. 'Cleavage, aggregation and toxicity of the expanded androgen receptor in spinal and bulbar muscular atrophy', *Hum Mol Genet*, 7: 693-701.

Mizushima, N. 2007. 'Autophagy: process and function', *Genes Dev*, 21: 2861-73.

Montie, H. L., R. G. Pestell, and D. E. Merry. 2011. 'SIRT1 modulates aggregation and toxicity through deacetylation of the androgen receptor in cell models of SBMA', *Journal of Neuroscience*, 31: 17425-36.

Morselli, E., L. Galluzzi, O. Kepp, A. Criollo, M. C. Maiuri, N. Tavernarakis, F. Madeo, and G. Kroemer. 2009. 'Autophagy mediates pharmacological lifespan extension by spermidine and resveratrol', *Aging (Albany NY)*, 1: 961-70.

Moussa, C., M. Hebron, X. Huang, J. Ahn, R. A. Rissman, P. S. Aisen, and R. S. Turner. 2017. 'Resveratrol regulates neuro-inflammation and induces adaptive immunity in Alzheimer's disease', *J Neuroinflammation*, 14: 1.

Murer, M. G., Q. Yan, and R. Raisman-Vozari. 2001. 'Brain-derived neurotrophic factor in the control human brain, and in Alzheimer's disease and Parkinson's disease', *Prog Neurobiol*, 63: 71-124.

Nagai, Y., T. Inui, H. A. Popiel, N. Fujikake, K. Hasegawa, Y. Urade, Y. Goto, H. Naiki, and T. Toda. 2007. 'A toxic monomeric conformer of the polyglutamine protein', *Nat Struct Mol Biol*, 14: 332-40.

Nair, A. B., and S. Jacob. 2016. 'A simple practice guide for dose conversion between animals and human', *J Basic Clin Pharm*, 7: 27-31.

Nakamura, K., S. Y. Jeong, T. Uchihara, M. Anno, K. Nagashima, T. Nagashima, S. Ikeda, S. Tsuji, and I. Kanazawa. 2001. 'SCA17, a novel autosomal dominant cerebellar ataxia caused by an expanded polyglutamine in TATA-binding protein', *Hum Mol Genet*, 10: 1441-8.

Nam, J. B., J. H. Ryu, J. W. Kim, I. S. Chang, and K. D. Suh. 2005. 'Stabilization of resveratrol immobilized in monodisperse cyano-functionalized porous polymeric microspheres', *Polymer*, 46: 8956-63.

Nandagopal, R., and S. G. Moorthy. 2004. 'Dramatic levodopa responsiveness of dystonia in a sporadic case of spinocerebellar ataxia type 3', *Postgrad Med J*, 80: 363-5.

Nascimento-Ferreira, I., C. Nobrega, A. Vasconcelos-Ferreira, I. Onofre, D. Albuquerque, C. Aveleira, H. Hirai, N. Deglon, and L. Pereira de Almeida. 2013. 'Beclin 1 mitigates motor and neuropathological deficits in genetic mouse models of Machado-Joseph disease', *Brain*, 136: 2173-88.

Nascimento-Ferreira, I., T. Santos-Ferreira, L. Sousa-Ferreira, G. Auregan, I. Onofre, S. Alves, N. Dufour, V. F. Colomer Gould, A. Koeppen, N. Deglon, and L. Pereira de Almeida. 2011. 'Overexpression of the autophagic beclin-1 protein clears mutant ataxin-3 and alleviates Machado-Joseph disease', *Brain*, 134: 1400-15.

Nemoto, S., M. M. Fergusson, and T. Finkel. 2005. 'SIRT1 functionally interacts with the metabolic regulator and transcriptional coactivator PGC-1{alpha}', *J Biol Chem*, 280: 16456-60.

Nicastro, G., L. Masino, V. Esposito, R. P. Menon, A. De Simone, F. Fraternali, and A. Pastore. 2009. 'Josephin domain of ataxin-3 contains two distinct ubiquitin-binding sites', *Biopolymers*, 91: 1203-14.

Nicastro, G., R. P. Menon, L. Masino, P. P. Knowles, N. Q. McDonald, and A. Pastore. 2005. 'The solution structure of the Josephin domain of ataxin-3: structural determinants for molecular recognition', *Proc Natl Acad Sci U S A*, 102: 10493-8.

Nunes, T., L. Almeida, J. F. Rocha, A. Falcao, C. Fernandes-Lopes, A. I. Loureiro, L. Wright, M. Vaz-da-Silva, and P. Soares-da-Silva. 2009. 'Pharmacokinetics of trans-resveratrol following repeated administration in healthy elderly and young subjects', *J Clin Pharmacol*, 49: 1477-82.

Orr, H. T., M. Y. Chung, S. Banfi, T. J. Kwiatkowski, Jr., A. Servadio, A. L. Beaudet, A. E. McCall, L. A. Duvick, L. P. Ranum, and H. Y. Zoghbi. 1993. 'Expansion of an unstable trinucleotide CAG repeat in spinocerebellar ataxia type 1', *Nat Genet*, 4: 221-6.

Orrenius, S., B. Zhivotovsky, and P. Nicotera. 2003. 'Regulation of cell death: the calcium-apoptosis link', *Nat Rev Mol Cell Biol*, 4: 552-65.

Padiath, Q. S., A. K. Srivastava, S. Roy, S. Jain, and S. K. Brahmachari. 2005. 'Identification of a novel 45 repeat unstable allele associated with a disease phenotype at the MJD1/SCA3 locus', *Am J Med Genet B Neuropsychiatr Genet*, 133B: 124-6.

Park, S. J., F. Ahmad, A. Philp, K. Baar, T. Williams, H. Luo, H. Ke, H. Rehmann, R. Taussig, A. L. Brown, M. K. Kim, M. A. Beaven, A. B. Burgin, V. Manganiello, and J. H. Chung. 2012. 'Resveratrol ameliorates aging-related metabolic phenotypes by inhibiting cAMP phosphodiesterases', *Cell*, 148: 421-33.

Park, S. K., K. Kim, G. P. Page, D. B. Allison, R. Weindruch, and T. A. Prolla. 2009. 'Gene expression profiling of aging in multiple mouse strains: identification of aging biomarkers and impact of dietary antioxidants', *Aging Cell*, 8: 484-95.

Patel, K. R., C. Andreadi, R. G. Britton, E. Horner-Glister, A. Karmokar, S. Sale, V. A. Brown, D. E. Brenner, R. Singh, W. P. Steward, A. J. Gescher, and K. Brown. 2013. 'Sulfate metabolites provide an intracellular pool for resveratrol generation and induce autophagy with senescence', *Sci Transl Med*, 5: 205ra133.

Paul, B., I. Masih, J. Deopujari, and C. Charpentier. 1999. 'Occurrence of resveratrol and pterostilbene in age-old darakchasava, an ayurvedic medicine from India', *J Ethnopharmacol*, 68: 71-6.

Paulson, H. 1993. 'Spinocerebellar Ataxia Type 3.' in R. A. Pagon, M. P. Adam, H. H. Ardinger, S. E. Wallace, A. Amemiya, L. J. H. Bean, T. D. Bird, N. Ledbetter, H. C. Mefford, R. J. H. Smith and K. Stephens (eds.), *GeneReviews(R)* (Seattle (WA)).

Paulson, H. L., S. S. Das, P. B. Crino, M. K. Perez, S. C. Patel, D. Gotsdiner, K. H. Fischbeck, and R. N. Pittman. 1997a. 'Machado-Joseph disease gene product is a cytoplasmic protein widely expressed in brain', *Ann Neurol*, 41: 453-62.

Paulson, H. L., M. K. Perez, Y. Trottier, J. Q. Trojanowski, S. H. Subramony, S. S. Das, P. Vig, J. L. Mandel, K. H. Fischbeck, and R. N. Pittman. 1997b. 'Intranuclear inclusions of expanded polyglutamine protein in spinocerebellar ataxia type 3', *Neuron*, 19: 333-44.

Peng, H., H. Xiong, J. Li, M. Xie, Y. Liu, C. Bai and L. Chen. 2010. 'Vanillin cross-linked chitosan microspheres for controlled release of resveratrol', *Food Chemistry*, 121: 23-28.

Perez, M. K., H. L. Paulson, S. J. Pendse, S. J. Saionz, N. M. Bonini, and R. N. Pittman. 1998. 'Recruitment and the role of nuclear localization in polyglutamine-mediated aggregation', *J Cell Biol*, 143: 1457-70.

Pirola, L., and S. Frojdo. 2008. 'Resveratrol: one molecule, many targets', *IUBMB Life*, 60: 323-32.

Piver, B., F. Berthou, Y. Dreano, and D. Lucas. 2001. 'Inhibition of CYP3A, CYP1A and CYP2E1 activities by resveratrol and other non volatile red wine components', *Toxicol Lett*, 125: 83-91.

Pozzi, C., M. Valtorta, G. Tedeschi, E. Galbusera, V. Pastori, A. Bigi, S. Nonnis, E. Grassi, and P. Fusi. 2008. 'Study of subcellular localization and proteolysis of ataxin-3', *Neurobiol Dis*, 30: 190-200.

Price, N. L., A. P. Gomes, A. J. Ling, F. V. Duarte, A. Martin-Montalvo, B. J. North, B. Agarwal, L. Ye, G. Ramadori, J. S. Teodoro, B. P. Hubbard, A. T. Varela, J. G. Davis, B. Varamini, A. Hafner, R. Moaddel, A. P. Rolo, R. Coppari, C. M. Palmeira, R. de Cabo, J. A. Baur, and D. A. Sinclair. 2012. 'SIRT1 is required for AMPK activation and the beneficial effects of resveratrol on mitochondrial function', *Cell Metab*, 15: 675-90.

Pulst, S. M., A. Nechiporuk, T. Nechiporuk, S. Gispert, X. N. Chen, I. Lopes-Cendes, S. Pearlman, S. Starkman, G. Orozco-Diaz, A. Lunkes, P. DeJong, G. A. Rouleau, G. Auburger, J. R. Korenberg, C. Figueroa, and S. Sahba. 1996. 'Moderate expansion of a normally biallelic trinucleotide repeat in spinocerebellar ataxia type 2', *Nat Genet*, 14: 269-76.

Ravikumar, B., R. Duden, and D. C. Rubinsztein. 2002. 'Aggregate-prone proteins with polyglutamine and polyalanine expansions are degraded by autophagy', *Hum Mol Genet*, 11: 1107-17.

Reina, C. P., X. Zhong, and R. N. Pittman. 2010. 'Proteotoxic stress increases nuclear localization of ataxin-3', *Hum Mol Genet*, 19: 235-49.

Renaud, S. C., R. Gueguen, J. Schenker, and A. d'Houtaud. 1998. 'Alcohol and mortality in middle-aged men from eastern France', *Epidemiology*, 9: 184-8.

Renaud, S., and M. de Lorgeril. 1992. 'Wine, alcohol, platelets, and the French paradox for coronary heart disease', *Lancet*, 339: 1523-6.

Rius, C., M. Abu-Taha, C. Hermenegildo, L. Piqueras, J. M. Cerda-Nicolas, A. C. Issekutz, L. Estan, J. Cortijo, E. J. Morcillo, F. Orallo, and M. J. Sanz. 2010. 'Trans- but not cis-resveratrol impairs angiotensin-II-mediated vascular inflammation through inhibition of NF-kappaB activation and peroxisome proliferator-activated receptor-gamma upregulation', *J Immunol*, 185: 3718-27.

Ross, C. A., and M. A. Poirier. 2005. 'Opinion: What is the role of protein aggregation in neurodegeneration?', *Nat Rev Mol Cell Biol*, 6: 891-8.

Rotches-Ribalta, M., C. Andres-Lacueva, R. Estruch, E. Escribano, and M. Urpi-Sarda. 2012. 'Pharmacokinetics of resveratrol metabolic profile in healthy humans after moderate consumption of red wine and grape extract tablets', *Pharmacol Res*, 66: 375-82.

Ruano, L., C. Melo, M. C. Silva, and P. Coutinho. 2014. 'The global epidemiology of hereditary ataxia and spastic paraplegia: a systematic review of prevalence studies', *Neuroepidemiology*, 42: 174-83.

Rub, U., E. R. Brunt, R. A. de Vos, D. Del Turco, K. Del Tredici, K. Gierga, C. Schultz, E. Ghebremedhin, K. Burk, G. Auburger, and H. Braak. 2004. 'Degeneration of the central vestibular system in spinocerebellar ataxia type 3 (SCA3) patients and its possible clinical significance', *Neuropathol Appl Neurobiol*, 30: 402-14.

Rub, U., E. R. Brunt, D. Del Turco, R. A. de Vos, K. Gierga, H. Paulson, and H. Braak. 2003a. 'Guidelines for the pathoanatomical examination of the lower brain stem in ingestive and

swallowing disorders and its application to a dysphagic spinocerebellar ataxia type 3 patient', *Neuropathol Appl Neurobiol*, 29: 1-13.

Rub, U., E. R. Brunt, and T. Deller. 2008. 'New insights into the pathoanatomy of spinocerebellar ataxia type 3 (Machado-Joseph disease)', *Curr Opin Neurol*, 21: 111-6.

Rub, U., E. R. Brunt, E. Petrasch-Parwez, L. Schols, D. Theegarten, G. Auburger, K. Seidel, C. Schultz, K. Gierga, H. Paulson, C. van Broeckhoven, T. Deller, and R. A. de Vos. 2006. 'Degeneration of ingestion-related brainstem nuclei in spinocerebellar ataxia type 2, 3, 6 and 7', *Neuropathol Appl Neurobiol*, 32: 635-49.

Rub, U., D. Del Turco, K. Del Tredici, R. A. de Vos, E. R. Brunt, G. Reifenberger, C. Seifried, C. Schultz, G. Auburger, and H. Braak. 2003b. 'Thalamic involvement in a spinocerebellar ataxia type 2 (SCA2) and a spinocerebellar ataxia type 3 (SCA3) patient, and its clinical relevance', *Brain*, 126: 2257-72.

Rub, U., K. Seidel, I. Ozerden, K. Gierga, E. R. Brunt, L. Schols, R. A. de Vos, W. den Dunnen, C. Schultz, G. Auburger, and T. Deller. 2007. 'Consistent affection of the central somatosensory system in spinocerebellar ataxia type 2 and type 3 and its significance for clinical symptoms and rehabilitative therapy', *Brain Res Rev*, 53: 235-49.

Sakai, T., and H. Kawakami. 1996. 'Machado-Joseph disease: A proposal of spastic paraplegic subtype', *Neurology*, 46: 846-7.

Sanpei, K., H. Takano, S. Igarashi, T. Sato, M. Oyake, H. Sasaki, A. Wakisaka, K. Tashiro, Y. Ishida, T. Ikeuchi, R. Koide, M. Saito, A. Sato, T. Tanaka, S. Hanyu, Y. Takiyama, M. Nishizawa, N. Shimizu, Y. Nomura, M. Segawa, K. Iwabuchi, I. Eguchi, H. Tanaka, H. Takahashi, and S. Tsuji. 1996. 'Identification of the spinocerebellar ataxia type 2 gene using a direct identification of repeat expansion and cloning technique, DIRECT', *Nat Genet*, 14: 277-84.

Sasaki, H., A. Wakisaka, T. Fukazawa, K. Iwabuchi, T. Hamada, A. Takada, E. Mukai, T. Matsuura, T. Yoshiki, and K. Tashiro. 1995. 'CAG repeat expansion of Machado-Joseph disease in the Japanese: analysis of the repeat instability for parental transmission, and correlation with disease phenotype', *J Neurol Sci*, 133: 128-33.

Scaglione, K. M., E. Zavodszky, S. V. Todi, S. Patury, P. Xu, E. Rodriguez-Lebron, S. Fischer, J. Konen, A. Djarmati, J. Peng, J. E. Gestwicki, and H. L. Paulson. 2011. 'Ube2w and ataxin-3 coordinately regulate the ubiquitin ligase CHIP', *Mol Cell*, 43: 599-612.

Scherzed, W., E. R. Brunt, H. Heinsen, R. A. de Vos, K. Seidel, K. Burk, L. Schols, G. Auburger, D. Del Turco, T. Deller, H. W. Korf, W. F. den Dunnen, and U. Rub. 2012. 'Pathoanatomy of cerebellar degeneration in spinocerebellar ataxia type 2 (SCA2) and type 3 (SCA3)', *Cerebellum*, 11: 749-60.

Scherzinger, E., R. Lurz, M. Turmaine, L. Mangiarini, B. Hollenbach, R. Hasenbank, G. P. Bates, S. W. Davies, H. Lehrach, and E. E. Wanker. 1997. 'Huntingtin-encoded polyglutamine expansions form amyloid-like protein aggregates in vitro and in vivo', *Cell*, 90: 549-58.

Schmidt, T., G. B. Landwehrmeyer, I. Schmitt, Y. Trottier, G. Auburger, F. Laccone, T. Klockgether, M. Volpel, J. T. Epplen, L. Schols, and O. Riess. 1998. 'An isoform of ataxin-3 accumulates in the nucleus of neuronal cells in affected brain regions of SCA3 patients', *Brain Pathol*, 8: 669-79.

Schmitt, I., M. Linden, H. Khazneh, B. O. Evert, P. Breuer, T. Klockgether, and U. Wuellner. 2007. 'Inactivation of the mouse Atxn3 (ataxin-3) gene increases protein ubiquitination', *Biochem Biophys Res Commun*, 362: 734-9.

Schmitz-Hubsch, T., S. T. du Montcel, L. Baliko, J. Berciano, S. Boesch, C. Depondt, P. Giunti, C. Globas, J. Infante, J. S. Kang, B. Kremer, C. Mariotti, B. Melegh, M. Pandolfo, M. Rakowicz, P. Ribai, R. Rola, L. Schols, S. Szymanski, B. P. van de Warrenburg, A. Durr, T. Klockgether, and R. Fancellu. 2006. 'Scale for the assessment and rating of ataxia: development of a new clinical scale', *Neurology*, 66: 1717-20.

Schols, L., J. Haan, O. Riess, G. Amoiridis, and H. Przuntek. 1998. 'Sleep disturbance in spinocerebellar ataxias: is the SCA3 mutation a cause of restless legs syndrome?', *Neurology*, 51: 1603-7.

Schols, L., A. M. Vieira-Saecker, S. Schols, H. Przuntek, J. T. Epplen, and O. Riess. 1995. 'Trinucleotide expansion within the MJD1 gene presents clinically as spinocerebellar ataxia and occurs most frequently in German SCA patients', *Hum Mol Genet*, 4: 1001-5.

Schulz, J. B., J. Borkert, S. Wolf, T. Schmitz-Hubsch, M. Rakowicz, C. Mariotti, L. Schols, D. Timmann, B. van de Warrenburg, A. Durr, M. Pandolfo, J. S. Kang, A. G. Mandly, T. Nagele, M. Grisoli, R. Boguslawska, P. Bauer, T. Klockgether, and T. K. Hauser. 2010. 'Visualization, quantification and correlation of brain atrophy with clinical symptoms in spinocerebellar ataxia types 1, 3 and 6', *Neuroimage*, 49: 158-68.

Seidel, K., W. F. den Dunnen, C. Schultz, H. Paulson, S. Frank, R. A. de Vos, E. R. Brunt, T. Deller, H. H. Kampinga, and U. Rub. 2010. 'Axonal inclusions in spinocerebellar ataxia type 3', *Acta Neuropathol*, 120: 449-60.

Seidel, K., S. Siswanto, E. R. Brunt, W. den Dunnen, H. W. Korf, and U. Rub. 2012. 'Brain pathology of spinocerebellar ataxias', *Acta Neuropathol*, 124: 1-21.

Sequeiros, J., P. Maciel, F. Taborda, S. Ledo, J. C. Rocha, A. Lopes, F. Reto, A. M. Fortuna, M. Rousseau, M. Fleming, P. Coutinho, G. A. Rouleau, and C. S. Jorge. 1998. 'Prenatal diagnosis of Machado-Joseph disease by direct mutation analysis', *Prenat Diagn*, 18: 611-7.

Shah, V. P., K. K. Midha, J. W. Findlay, H. M. Hill, J. D. Hulse, I. J. McGilveray, G. McKay, K. J. Miller, R. N. Patnaik, M. L. Powell, A. Tonelli, C. T. Viswanathan, and A. Yacobi. 2000. 'Bioanalytical method validation--a revisit with a decade of progress', *Pharm Res*, 17: 1551-7.

Shao, J., and M. I. Diamond. 2007. 'Polyglutamine diseases: emerging concepts in pathogenesis and therapy', *Hum Mol Genet*, 16 Spec No. 2: R115-23.

Shi, G., L. Rao, H. Yu, H. Xiang, H. Yang, and R. Ji. 2008. 'Stabilization and encapsulation of photosensitive resveratrol within yeast cell', *Int J Pharm*, 349: 83-93.

Shibata-Hamaguchi, A., C. Ishida, K. Iwasa, and M. Yamada. 2009. 'Prevalence of spinocerebellar degenerations in the Hokuriku district in Japan', *Neuroepidemiology*, 32: 176-83.

Simonian, N. A., and J. T. Coyle. 1996. 'Oxidative stress in neurodegenerative diseases', *Annu Rev Pharmacol Toxicol*, 36: 83-106.

Soleas, G. J., J. Yan, and D. M. Goldberg. 2001a. 'Measurement of trans-resveratrol, (+)-catechin, and quercetin in rat and human blood and urine by gas chromatography with mass selective detection', *Methods Enzymol*, 335: 130-45.

———. 2001b. 'Ultrasensitive assay for three polyphenols (catechin, quercetin and resveratrol) and their conjugates in biological fluids utilizing gas chromatography with mass selective detection', *J Chromatogr B Biomed Sci Appl*, 757: 161-72.

Soong, B., C. Cheng, R. Liu, and D. Shan. 1997. 'Machado-Joseph disease: clinical, molecular, and metabolic characterization in Chinese kindreds', *Ann Neurol*, 41: 446-52.

Spanier, G., H. Xu, N. Xia, S. Tobias, S. Deng, L. Wojnowski, U. Forstermann, and H. Li. 2009. 'Resveratrol reduces endothelial oxidative stress by modulating the gene expression of superoxide dismutase 1 (SOD1), glutathione peroxidase 1 (GPx1) and NADPH oxidase subunit (Nox4)', *J Physiol Pharmacol*, 60 Suppl 4: 111-6.

Sparvoli, F., C. Martin, A. Scienza, G. Gavazzi, and C. Tonelli. 1994. 'Cloning and molecular analysis of structural genes involved in flavonoid and stilbene biosynthesis in grape (Vitis vinifera L.)', *Plant Mol Biol*, 24: 743-55.

Storey, E. 2014. 'Genetic cerebellar ataxias', *Semin Neurol*, 34: 280-92.

Sudarsky, L., and P. Coutinho. 1995. 'Machado-Joseph disease', *Clin Neurosci*, 3: 17-22.

Suite, N. D., J. Sequeiros, and G. M. McKhann. 1986. 'Machado-Joseph disease in a Sicilian-American family', *J Neurogenet*, 3: 177-82.

Tait, D., M. Riccio, A. Sittler, E. Scherzinger, S. Santi, A. Ognibene, N. M. Maraldi, H. Lehrach, and E. E. Wanker. 1998. 'Ataxin-3 is transported into the nucleus and associates with the nuclear matrix', *Hum Mol Genet*, 7: 991-7.

Takahashi, T., S. Katada, and O. Onodera. 2010. 'Polyglutamine diseases: where does toxicity come from? what is toxicity? where are we going?', *J Mol Cell Biol*, 2: 180-91.

Takahashi, Y., M. Kanai, T. Taminato, S. Watanabe, C. Matsumoto, T. Araki, T. Okamoto, M. Ogawa, and M. Murata. 2016. 'Compound heterozygous intermediate MJD alleles cause cerebellar ataxia with sensory neuropathy', *Neurol Genet*, 3: e123.

Takiyama, Y., S. Igarashi, E. A. Rogaeva, K. Endo, E. I. Rogaev, H. Tanaka, R. Sherrington, K. Sanpei, Y. Liang, M. Saito, and et al. 1995. 'Evidence for inter-generational instability in the CAG repeat in the MJD1 gene and for conserved haplotypes at flanking markers amongst Japanese and Caucasian subjects with Machado-Joseph disease', *Hum Mol Genet*, 4: 1137-46.

Takiyama, Y., M. Nishizawa, H. Tanaka, S. Kawashima, H. Sakamoto, Y. Karube, H. Shimazaki, M. Soutome, K. Endo, S. Ohta, and et al. 1993. 'The gene for Machado-Joseph disease maps to human chromosome 14q', *Nat Genet*, 4: 300-4.

Taroni, F., and S. DiDonato. 2004. 'Pathways to motor incoordination: the inherited ataxias', *Nat Rev Neurosci*, 5: 641-55.

Tellone, E., A. Galtieri, A. Russo, B. Giardina, and S. Ficarra. 2015. 'Resveratrol: A Focus on Several Neurodegenerative Diseases', *Oxidative Medicine and Cellular Longevity*, 2015: 392169.

Trela, B. C., and A. L. Waterhouse. 1996. 'Resveratrol: Isomeric molar absorptivities and stability', *Journal of Agricultural and Food Chemistry*, 44: 1253-57.

Trottier, Y., G. Cancel, I. An-Gourfinkel, Y. Lutz, C. Weber, A. Brice, E. Hirsch, and J. L. Mandel. 1998. 'Heterogeneous intracellular localization and expression of ataxin-3', *Neurobiol Dis*, 5: 335-47.

Tsai, S. H., S. Y. Lin-Shiau, and J. K. Lin. 1999. 'Suppression of nitric oxide synthase and the down-regulation of the activation of NFkappaB in macrophages by resveratrol', *Br J Pharmacol*, 126: 673-80.

Tsuji, S., O. Onodera, J. Goto, M. Nishizawa, and Diseases Study Group on Ataxic. 2008. 'Sporadic ataxias in Japan--a population-based epidemiological study', *Cerebellum*, 7: 189-97.

Um, J. H., S. J. Park, H. Kang, S. Yang, M. Foretz, M. W. McBurney, M. K. Kim, B. Viollet, and J. H. Chung. 2010. 'AMP-activated protein kinase-deficient mice are resistant to the metabolic effects of resveratrol', *Diabetes*, 59: 554-63.

Valdecantos, M. P., P. Perez-Matute, P. Quintero, and J. A. Martinez. 2010. 'Vitamin C, resveratrol and lipoic acid actions on isolated rat liver mitochondria: all antioxidants but different', *Redox Report*, 15: 207-16.

Valenzano, D. R., E. Terzibasi, T. Genade, A. Cattaneo, L. Domenici, and A. Cellerino. 2006. 'Resveratrol prolongs lifespan and retards the onset of age-related markers in a short-lived vertebrate', *Curr Biol*, 16: 296-300.

van Alfen, N., R. J. Sinke, M. J. Zwarts, A. Gabreels-Festen, P. Praamstra, B. P. Kremer, and M. W. Horstink. 2001. 'Intermediate CAG repeat lengths (53,54) for MJD/SCA3 are associated with an abnormal phenotype', *Ann Neurol*, 49: 805-7.

van de Warrenburg, B. P., R. J. Sinke, C. C. Verschuuren-Bemelmans, H. Scheffer, E. R. Brunt, P. F. Ippel, J. A. Maat-Kievit, D. Dooijes, N. C. Notermans, D. Lindhout, N. V. Knoers, and H. P. Kremer. 2002. 'Spinocerebellar ataxias in the Netherlands: prevalence and age at onset variance analysis', *Neurology*, 58: 702-8.

Vaz-da-Silva, M., A. I. Loureiro, A. Falcao, T. Nunes, J. F. Rocha, C. Fernandes-Lopes, E. Soares, L. Wright, L. Almeida, and P. Soares-da-Silva. 2008. 'Effect of food on the pharmacokinetic profile of trans-resveratrol', *Int J Clin Pharmacol Ther*, 46: 564-70.

Vian, M. A., V. Tomao, S. Gallet, P. O. Coulomb, and J. M. Lacombe. 2005. 'Simple and rapid method for cis- and trans-resveratrol and piceid isomers determination in wine by high-performance liquid chromatography using chromolith columns', *J Chromatogr A*, 1085: 224-9.

Vitaglione, P., S. Sforza, G. Galaverna, C. Ghidini, N. Caporaso, P. P. Vescovi, V. Fogliano, and R. Marchelli. 2005. 'Bioavailability of trans-resveratrol from red wine in humans', *Mol Nutr Food Res*, 49: 495-504.

Walle, T., F. Hsieh, M. H. DeLegge, J. E. Oatis, Jr., and U. K. Walle. 2004. 'High absorption but very low bioavailability of oral resveratrol in humans', *Drug Metab Dispos*, 32: 1377-82.

Wang, G., K. Ide, N. Nukina, J. Goto, Y. Ichikawa, K. Uchida, T. Sakamoto, and I. Kanazawa. 1997. 'Machado-Joseph disease gene product identified in lymphocytes and brain', *Biochem Biophys Res Commun*, 233: 476-9.

Wang, G., N. Sawai, S. Kotliarova, I. Kanazawa, and N. Nukina. 2000. 'Ataxin-3, the MJD1 gene product, interacts with the two human homologs of yeast DNA repair protein RAD23, HHR23A and HHR23B', *Hum Mol Genet*, 9: 1795-803.

Weber, J. J., A. S. Sowa, T. Binder, and J. Hubener. 2014. 'From pathways to targets: understanding the mechanisms behind polyglutamine disease', *Biomed Res Int*, 2014: 701758.

Wellington, C. L., L. M. Ellerby, C. A. Gutekunst, D. Rogers, S. Warby, R. K. Graham, O. Loubser, J. van Raamsdonk, R. Singaraja, Y. Z. Yang, J. Gafni, D. Bredesen, S. M. Hersch, B. R. Leavitt, S. Roy, D. W. Nicholson, and M. R. Hayden. 2002. 'Caspase cleavage of mutant huntingtin precedes neurodegeneration in Huntington's disease', *Journal of Neuroscience*, 22: 7862-72.

Wellington, C. L., L. M. Ellerby, A. S. Hackam, R. L. Margolis, M. A. Trifiro, R. Singaraja, K. McCutcheon, G. S. Salvesen, S. S. Propp, M. Bromm, K. J. Rowland, T. Zhang, D. Rasper, S. Roy, N. Thornberry, L. Pinsky, A. Kakizuka, C. A. Ross, D. W. Nicholson, D. E. Bredesen, and M. R. Hayden. 1998. 'Caspase cleavage of gene products associated with triplet expansion disorders generates truncated fragments containing the polyglutamine tract', *J Biol Chem*, 273: 9158-67.

Wenzel, E., and V. Somoza. 2005. 'Metabolism and bioavailability of trans-resveratrol', *Mol Nutr Food Res*, 49: 472-81.

Wilder-Smith, E., E. K. Tan, H. Y. Law, Y. Zhao, I. Ng, and M. C. Wong. 2003. 'Spinocerebellar ataxia type 3 presenting as an L-DOPA responsive dystonia phenotype in a Chinese family', *J Neurol Sci*, 213: 25-8.

Williams, L. D., G. A. Burdock, J. A. Edwards, M. Beck, and J. Bausch. 2009. 'Safety studies conducted on high-purity trans-resveratrol in experimental animals', *Food Chem Toxicol*, 47: 2170-82.

Winborn, B. J., S. M. Travis, S. V. Todi, K. M. Scaglione, P. Xu, A. J. Williams, R. E. Cohen, J. Peng, and H. L. Paulson. 2008. 'The deubiquitinating enzyme ataxin-3, a polyglutamine disease protein, edits Lys63 linkages in mixed linkage ubiquitin chains', *J Biol Chem*, 283: 26436-43.

Wood, J. G., B. Rogina, S. Lavu, K. Howitz, S. L. Helfand, M. Tatar, and D. Sinclair. 2004. 'Sirtuin activators mimic caloric restriction and delay ageing in metazoans', *Nature*, 430: 686-9.

Xia, N., A. Daiber, A. Habermeier, E. I. Closs, T. Thum, G. Spanier, Q. Lu, M. Oelze, M. Torzewski, K. J. Lackner, T. Munzel, U. Forstermann, and H. Li. 2010. 'Resveratrol reverses endothelial nitric-oxide synthase uncoupling in apolipoprotein E knockout mice', *J Pharmacol Exp Ther*, 335: 149-54.

Yamada, M., S. Hayashi, S. Tsuji, and H. Takahashi. 2001. 'Involvement of the cerebral cortex and autonomic ganglia in Machado-Joseph disease', *Acta Neuropathol*, 101: 140-4.

Yamada, M., T. Sato, S. Tsuji, and H. Takahashi. 2008. 'CAG repeat disorder models and human neuropathology: similarities and differences', *Acta Neuropathol*, 115: 71-86.

Yamada, M., C. F. Tan, C. Inenaga, S. Tsuji, and H. Takahashi. 2004. 'Sharing of polyglutamine localization by the neuronal nucleus and cytoplasm in CAG-repeat diseases', *Neuropathol Appl Neurobiol*, 30: 665-75.

Yao, Y., J. Li, Y. Niu, J. Q. Yu, L. Yan, Z. H. Miao, X. X. Zhao, Y. J. Li, W. X. Yao, P. Zheng, and W. Q. Li. 2015. 'Resveratrol inhibits oligomeric Abeta-induced microglial activation via NADPH oxidase', *Mol Med Rep*, 12: 6133-9.

Ye, K., C. B. Ji, X. W. Lu, Y. H. Ni, C. L. Gao, X. H. Chen, Y. P. Zhao, G. X. Gu, and X. R. Guo. 2010. 'Resveratrol attenuates radiation damage in Caenorhabditis elegans by preventing oxidative stress', *J Radiat Res*, 51: 473-9.

Yeh, T. H., C. S. Lu, Y. H. Chou, C. C. Chong, T. Wu, N. H. Han, and R. S. Chen. 2005. 'Autonomic dysfunction in Machado-Joseph disease', *Arch Neurol*, 62: 630-6.

Yeung, F., J. E. Hoberg, C. S. Ramsey, M. D. Keller, D. R. Jones, R. A. Frye, and M. W. Mayo. 2004. 'Modulation of NF-kappaB-dependent transcription and cell survival by the SIRT1 deacetylase', *EMBO J*, 23: 2369-80.

Yoshizawa, T., K. Nakamagoe, T. Ueno, K. Furusho, and S. Shoji. 2004. 'Early vestibular dysfunction in Machado-Joseph disease detected by caloric test', *J Neurol Sci*, 221: 109-11.

Yu, C., Y. G. Shin, A. Chow, Y. Li, J. W. Kosmeder, Y. S. Lee, W. H. Hirschelman, J. M. Pezzuto, R. G. Mehta, and R. B. van Breemen. 2002. 'Human, rat, and mouse metabolism of resveratrol', *Pharm Res*, 19: 1907-14.

Yu, X., and G. Li. 2012. 'Effects of resveratrol on longevity, cognitive ability and aging-related histological markers in the annual fish Nothobranchius guentheri', *Exp Gerontol*, 47: 940-9.

Yu, Y. C., C. L. Kuo, W. L. Cheng, C. S. Liu, and M. Hsieh. 2009. 'Decreased antioxidant enzyme activity and increased mitochondrial DNA damage in cellular models of Machado-Joseph disease', *J Neurosci Res*, 87: 1884-91.

Zarse, K., S. Schmeisser, M. Birringer, E. Falk, D. Schmoll, and M. Ristow. 2010. 'Differential effects of resveratrol and SRT1720 on lifespan of adult Caenorhabditis elegans', *Horm Metab Res*, 42: 837-9.

Zawacki, T. M., J. Grace, J. H. Friedman, and L. Sudarsky. 2002. 'Executive and emotional dysfunction in Machado-Joseph disease', *Mov Disord*, 17: 1004-10.

Zhao, Y., E. K. Tan, H. Y. Law, C. S. Yoon, M. C. Wong, and I. Ng. 2002. 'Prevalence and ethnic differences of autosomal-dominant cerebellar ataxia in Singapore', *Clin Genet*, 62: 478-81.

Zhuchenko, O., J. Bailey, P. Bonnen, T. Ashizawa, D. W. Stockton, C. Amos, W. B. Dobyns, S. H. Subramony, H. Y. Zoghbi, and C. C. Lee. 1997. 'Autosomal dominant cerebellar ataxia (SCA6) associated with small polyglutamine expansions in the alpha 1A-voltage-dependent calcium channel', *Nat Genet*, 15: 62-9.

Zoghbi, H. Y., and H. T. Orr. 2000. 'Glutamine repeats and neurodegeneration', *Annu Rev Neurosci*, 23: 217-47.